DEPARTMENT OF CIVIL ENGINEERING AND ARCHITECTURE
PH.D. COURSE IN DEFENCE AGAINST NATURAL RISKS AND ECOLOGICAL TRANSITION OF BUILT ENVIRONMENT
CYCLE XXXVIII

---

**THESIS**

# NEW TECHNOLOGY FOR THERMAL DESORPTION FEEDING WITH CONCENTRATING SOLAR POWER (CSP) SYSTEM

*PhD student: Enrico Licitra*

Tutor: *Prof. Eng. Gabriele Freni*
*Full Professor – University of Enna 'Kore'*

Co-Tutors: *Prof. Eng. Gaetano Di Bella*
*Full Professor – University of Enna 'Kore'*

*Dr. Hatem Saadaoui*
*Deputy General Manager & Chief Scientist – Haemers Technologies*

---

Academic Year 2024/2025

# INDEX

# List of Figures

# List of Tables

# Acknowledgements

At the conclusion of this doctoral experience, I would first like to express my deepest gratitude to my family, to whom I dedicate this work. From them, I have learned the true meaning of sacrifice and the value of hard work, principles that have guided and sustained me throughout these years and without which this achievement would not have been possible.

I am sincerely grateful to my tutor, Prof. Gabriele Freni, and co-tutor, Prof. Gaetano Di Bella, for the guidance, expertise, and trust they have offered me over the past three years. Their invaluable insights and the opportunities they provided have greatly shaped both my academic growth and personal development.

A heartfelt thank-you goes to Icaro Ecology for the opportunities granted to me and for believing in my potential throughout the development of this research project. Without their trust and support, I would not have had access to the key opportunities that ultimately enabled this project to take shape.

I am equally indebted to Haemers Technologies, and in particular to Hatem, co-tutor of this thesis project, whose essential support and expertise were fundamental during my months of research experience in Brussels. He proved to be an outstanding man and a remarkably knowledgeable professional, someone from whom I can only learn and continue to grow, both professionally and personally.

I would also like to thank all the people who have been close to me and with whom I have shared important moments over these three years, Ignazio, with which we also faced this path together, Giorgio, colleagues, friends, and all those who contributed, in different ways, to making this journey meaningful and enriching.

Finally, my deepest gratitude goes to my girlfriend Martina, who has stood by my side, even from afar and throughout every stage of this journey. Her constant presence, understanding, and support during both the challenging and the joyful moments have been invaluable, and I am grateful to her.

# Summary

This PhD thesis work reports the research activities focused on the evaluation of Thermal Desorption (TD) as a remediation technology for contaminated soils and sediments, with a particular emphasis on the integration of renewable energy sources into the process. Laboratory investigations demonstrated that TD is highly effective even in matrices with significant hydrocarbons contamination, achieving regulatory compliance within optimized low-temperature operating conditions. In parallel, the study explored the potential of biochar derived from biomass pyrolysis as a sustainable adsorbent material useful to manage the desorbed pollutants, highlighting its promising performance as an alternative to conventional activated carbon in Vapour Treatment Units.

The second core activity of the thesis involved advanced numerical modelling and simulation, performed through computational fluid dynamics (CFD) using Ansys Fluent and customizing simulation through User-Defined Functions (UDFs), to design a renewable-driven TD system. The proposed configuration studied, in reference to the specific coordinates of Gela (CL, Italy), was based on the coupling of a concentrating solar power (CSP) system, specifically the parabolic trough collectors (PTCs) and Therminol-VP1 as heat transfer fluid (HTF), with conduction heating tubes, drawing inspiration from existing industrial TD solutions to remediate hydrocarbon contaminated solid matrix, while extending the approach to renewable integration. The modelling approach required several simplifying assumptions to manage the complexity of the heat transfer processes involved, but it successfully demonstrated the feasibility of replacing conventional fossil-based energy inputs with solar thermal energy. Furthermore, the study investigated an alternative scenario in which the same heating tube was repurposed as a Borehole Thermal Energy Storage (BTES) system, underscoring the dual applicability of the design for both remediation and geothermal storage as site reuse option.

The overall results confirm that TD, when combined with solar thermal technologies, can be considered a viable and sustainable remediation strategy. The simulations indicate that a scalable design is technically achievable, while the preliminary economic assessment highlights the potential competitiveness of such systems if supported by optimized design and future cost reductions. This research thus provides a foundational contribution to advancing TD towards pilot-scale and large-scale applications powered by renewable energy, addressing both the energy intensity and environmental footprint of conventional thermal treatments that usually involves the use of fossil fuels.

***Keywords***: Thermal Desorption; Concentrating Solar System; Thermal Conductive Heating; Ansys Fluent; Hydrocarbons; Computational Fluid Dynamic; Thermal Solar Energy; Geothermal Storage System; Sustainable Remediation Strategies.

# Sommario

In questa tesi di dottorato vengono riportate le attività di ricerca incentrate sulla valutazione del Desorbimento Termico (DT) come tecnologia di bonifica di suoli e sedimenti contaminati, con particolare attenzione all'integrazione di fonti energetiche rinnovabili nel processo. Indagini di laboratorio hanno dimostrato che il DT è altamente efficace anche in matrici con significativa contaminazione da idrocarburi, rispettando i requisiti normativi in condizioni operative ottimizzate a bassa temperatura. Parallelamente, lo studio ha esplorato il potenziale di biochar derivato dalla pirolisi di biomasse, utilizzato come materiale adsorbente sostenibile per gestire gli inquinanti desorbiti, evidenziandone le prestazioni promettenti come alternativa ai convenzionali carboni attivi nelle Unità di Trattamento dei Vapori.

La seconda parte della tesi ha riguardato attività di modellazione numerica avanzata e simulazione, eseguite mediante fluidodinamica computazionale (CFD) con Ansys Fluent e tramite personalizzazione delle simulazioni mediante User-Defined Functions (UDF), per progettare un sistema di DT alimentato da fonti rinnovabili. La configurazione proposta, studiata con riferimento alle coordinate geografiche specifiche di Gela (CL, Italia), si basa sull'accoppiamento di un sistema energetico con solare a concentrazione, in particolare i collettori parabolici lineari e Therminol-VP1 come fluido termovettore, con tubi di riscaldamento conduttivo, traendo ispirazione da soluzioni industriali esistenti di DT per la bonifica di matrici solide contaminate da idrocarburi, ma estendendo al contempo l'approccio all'integrazione di energie rinnovabili. La fase di modellazione ha richiesto diverse ipotesi semplificative per gestire la complessità dei processi di trasferimento di calore coinvolti, ma ha dimostrato con successo la fattibilità per la sostituzione dei sistemi energetici convenzionali e di origine fossile con sistemi ad energia solare termica. Inoltre, è stato studiato uno scenario alternativo in cui il medesimo tubo di riscaldamento è stato riutilizzato come sistema geotermico "Borehole Thermal Energy Storage" (BTES), evidenziando la doppia applicabilità del modello configurato sia per la bonifica sia per lo stoccaggio geotermico come opzione di riutilizzo del sito.

I risultati finali confermano che il DT, se combinato con tecnologie solari termiche, può essere considerato una strategia di bonifica valida e sostenibile. Le simulazioni indicano che una soluzione progettuale scalabile è tecnicamente realizzabile, mentre la valutazione economica preliminare evidenzia la potenziale competitività di tali sistemi se supportati da un progetto ottimizzato e da futuri abbattimenti dei costi. Questa ricerca fornisce quindi un contributo fondamentale all'avanzamento del DT verso applicazioni in scala pilota e in larga scala alimentate da energie rinnovabili, ottimizzando sia l'intensità energetica sia l'impatto ambientale dei trattamenti termici convenzionali che solitamente implicano l'uso di combustibili fossili.

***Parole chiave***: Desorbimento Termico; Solare a Concentrazione; Riscaldamento termico conduttivo; Ansys Fluent; Idrocarburi; Fluidodinamica Computazionale; Energia solare termica; Sistemi di stoccaggio geotermico; Strategie di bonifica sostenibile

# Chapter 1 - Introduction

The increasing interest in the state of contamination of soils and sediments at a global level has highlighted the need to implement international and community strategies, aimed at restoring environmental matrices due to contamination by various type of pollutants: organic, inorganic, recalcitrant, persistent, etc.. (Zhao et al., 2019). A polluted environment (soil, sediment, water, or air) is a medium in which the concentration of harmful substances, whether of anthropogenic or natural origin, exceeds a threshold value, leading to an alteration of its physical or chemical properties and posing risk for human health, the environment, or ecosystem. Several countries have adopted policies aimed at identifying best practices to remediate different type of contaminated sites. In Italy for example, Measure 2, Component 4 (M2C4) of the PNRR (National Recovery and Resilience Plan) for the implementation of investment 3.4 (Reclamation of the "soil of orphan sites") and 3.5 (Restoration and protection of the seabed and marine habitats) represents a further signal to face the problem of contamination (*Decreto-legge del 24/02/2023 n. 13 - Disposizioni urgenti per l'attuazione del Piano nazionale di ripresa e resilienza (PNRR) e del Piano nazionale degli investimenti complementari al PNRR (PNC), nonche' per l'attuazione delle politiche di coesione e della politica agricola comune*, 2023). According to the ISPRA-SNPA (Sistema Nazionale per la Protezione dell'Ambiente, National System for Environmental Protection) report, as of December 2020 nearly 35.000 contaminated sites were formally under remediation procedures, which, when measured in area, translated into approximately 75.000 hectares, equivalent to 0,25% of Italy's national territory (ISPRA-SNPA, 2021).

Across Europe, soil and sediment contamination remains a widespread legacy of past and ongoing human activities. The European Commission's Joint Research Centre (JRC) most recent continent-wide stock-take (based on the 2016–2018 data call) estimated around 2,8 million sites where polluting activities have taken or are taking place. The waste sector (municipal and industrial) and industrial/commercial activities remain the dominant contributors to local contamination pressures, together accounting for roughly 70% of reported soil contamination in European datasets. Within industrial/commercial activities, metal processing, chemicals, oil industry, and energy production frequently appear as priority source groups. In soils, heavy metals (e.g., Pb, Cd, Hg, As, Cr, Ni) and mineral oil hydrocarbons are, together, the most frequently reported contaminant groups, jointly contributing on the order of 60% of cases (Panagos et al., 2013; Payá Pérez and Rodríguez Eugenio, 2018; Welsch et al., 2025). In North-East Atlantic, OSPAR's 2023 Quality Status Report documents stability or declines for many hazardous substances in sediments and biota across assessed areas; in marine and transitional sediments, the document corroborates the prominence of metals, PAHs, PCBs, organotin and the rising policy focus on PFAS and other emerging pollutants (Hylland and Assunção, 2022; OSPAR Commission, 2024).

Although they share many contaminants, such as petroleum hydrocarbons, chlorinated solvents, PAHs, PCBs, pesticides, metals, and PFAS, soils and sediments differ in hydraulics, biogeochemistry, and exposure pathways. Soils at terrestrial sites often present vadose-zone mass that drives vapor intrusion or leaches to groundwater; sediments sit at the land–water interface where sorbed hydrophobics can remain bioavailable to benthic organisms and move up food webs (Song et al., 2024; Welsch et al., 2025).

Soils typically become contaminated due to industrial activities, improper waste disposal, agricultural practices involving pesticides and fertilizers, atmospheric deposition, and accidental spills. These processes often lead to the accumulation of heavy metals, petroleum hydrocarbons, chlorinated solvents, and other persistent organic pollutants within the soil matrix, directly impacting terrestrial ecosystems, groundwater quality, and human health through direct exposure or food-chain

transfer. Sediments, in contrast, are primarily affected by contamination through hydrological transport. Pollutants originating from industrial discharges, urban runoff, mining residues, and atmospheric deposition tend to accumulate in riverbeds, estuaries, and marine environments. Due to their fine-grained and organic-rich nature, sediments act as sinks for hydrophobic organic contaminants such as polychlorinated biphenyls (PCBs), dioxins, and polycyclic aromatic hydrocarbons (PAHs), as well as for metals like mercury, cadmium, and lead. Unlike soils, sediments are dynamic and subject to resuspension events, dredging, or natural disturbances, which can remobilize pollutants back into the water column, thus posing renewed ecological and human health risks. The fundamental distinction lies in their environmental interfaces. Soil contamination primarily affects the vadose and saturated zones, leading to risks for agriculture, terrestrial ecosystems, and groundwater. Sediment contamination, however, is intimately linked to aquatic environments and biota, with risks of bioaccumulation and biomagnification along aquatic food webs. Furthermore, regulatory frameworks often address soils and sediments separately: soil policies tend to focus on land reclamation and reuse, while sediment legislation is more concerned with dredging operations, safe disposal, or beneficial reuse. These contrasts influence treatment technology choice (Eggleton and Thomas, 2004; Förstner and Salomons, 2010; Ribeiro and others, 2020; Pasciucco et al., 2021; Mohan Das A N, Sudeep Kumar T, 2024; Fernandes et al., 2025).

Remediation treatments can be classified according to their nature into chemical, physical, thermal and biological, applied either in situ or ex-situ and increasingly combined in "technology trains" (Li et al., 2020; Welsch et al., 2025). The selection of an appropriate remediation strategy is shaped by a combination of environmental, social, and economic considerations. In real-world applications, the decision is typically guided by the specific constraints of the site, the nature and classification of the contaminants, the time available to complete the remediation process, and the intended future use of the area (Falconi M. et al., 2025).

Sites contaminated with mineral oil and related hydrocarbons mirror Europe's dense legacy of refining, petrochemical processing, storage depots, service stations, and transport infrastructure, coupled with frequent historical releases. Thermal treatments are suitable methods for removing organic contaminants such as hydrocarbons. Among thermal treatments, Thermal Desorption (TD) has demonstrated numerous advantages, such as its high removal efficiency, the ability to address a wide spectrum of pollutants, enhanced safety during operation, relatively short treatment durations, the potential for recovering both soils and contaminants, and the avoidance of secondary pollution (Bianco et al., 2020; Li et al., 2020).

TD is an effective remediation technique for soils and sediments contaminated with volatile and semi-volatile organic compounds, such as total petroleum hydrocarbons (TPHs), polycyclic aromatic hydrocarbons (PAHs), polychlorinated biphenyls (PCBs), per- and polyfluoroalkyl substances (PFASs) and some inorganic contaminants like mercury. TD involves heating the contaminated material, either directly or indirectly, to specific temperatures for sufficient durations, promoting volatilization and removal of contaminants. The volatilized compounds are subsequently managed through vapor treatment units. On the limitations side, the process does not address non-volatile metals, requires vapor treatment units downstream of the heating system, as well as high energy consumption, commonly associated with the use of fossil fuels as heat carriers or electricity sources. This limitation is directly linked to substantial $CO_2$ emissions (Li et al., 2020; Brown et al., 2021; Cho et al., 2021; Falconi M. et al., 2024, 2025).

The reuse of soils and sediments following thermal treatment represents one of the most promising pathways toward sustainable remediation and circular resource management. Once contaminants are volatilized and either destroyed or captured, the treated material can often be safely reintegrated into the environment, allowing for the recycling of both soils and, in some cases,

recovered contaminants. From a regulatory standpoint, the key requirement for reuse is that thermally treated soils and sediments meet the environmental quality standards defined by legislation. When these conditions are satisfied, thermally treated soils can be used as backfill, construction material, or landscaping substrate, while treated sediments can be directed toward beneficial applications such as coastal protection, beach nourishment, or habitat restoration. Thermal treatment therefore acts not only as a remediation technique but also as a gateway to circular reuse, bridging the gap between waste management and secondary raw material valorisation (Falconi M. et al., 2025; US-EPA, 2025).

A key-example is Haemers Technologies, a Belgian company that patented and uses a proven TD remedial technology to remove VOCs, SVOCs, like PAHs, and mercury from soils, water, and groundwater (for this last case, and under certain conditions, TD is combined with other technologies such as multi-phase extraction, MPE, Steam injection, Hot air injection, etc..). When TD is applied without excavation and piles-arranging of contaminated soil, it is referred to in-situ thermal desorption treatment (ISTD). Haemers Technologies uses the ISTD technology (Figure 1) by installing several patented heating pipes using individual patented burner (heaters) and perforated vapor extraction tubes (using vacuum) in deep wells. These heater-vacuum wells operate to heat the contaminated soil to the target treatment temperature and extract the produced vapor from the contaminated soil. A thermal heat front advances radially outward from the wells through the adjacent soils, with most of the heat transfer occurring via thermal conduction. The spacing between wells is defined by several criteria, namely, the constituents being treated, the remedial objectives and the off-gas treatment requirements. The spacing used by Haemers Technologies usually varies between 1 and 3 m. ISTD technology can safely be used inside buildings and near infrastructure.

On the other hand, the ex-situ thermal desorption (ESTD) mode is applied after excavation of contaminated soils. The ESTD mode (or thermal pile, Figure 2) uses multi-layers of contaminated soil in which horizontal pipes, equipped with burners (heating pipes) and perforated vapor tubes, are placed. Different sizes of thermal piles can be used. The standard size has a volume of contaminated soil of 2000 $m^3$. This size of standard thermal pile requires 75 heating pipes homogenously spaced and distributed vertically in two rows separated by a row of 25 exchanger tubes. Each tube (exchanger tube and heating pipe) is accompanied by a perforated vapor tube. A total of 100 vapor tubes is used to collect the COCs vapor produced into the soil during the thermal treatment. Other tubes (thermocouple tubes, hot-sampling tubes, and pressure tubes) are also used to monitor the treatment. Four centrifugal fans are used for flue gas extraction. The thermal pile is covered by a concrete layer of about 10 cm thickness and the roof is thermally insulated

Gases and contaminants volatilized in the subsurface are extracted through the vapor extraction tubes and treated in several ways, depending on the type of contaminants initially present in the soil: reburn, condensation, vapor phase activated carbon (GAC filters), impregnated GAC or zeolite, and/or a catalytic or thermal oxidizer. All of these off-gas treatment methods reduce airborne contaminant concentrations to acceptable levels prior to be releases to the atmosphere (Jordens et al., 2023; Falconi M. et al., 2024, 2025).


**Figure 1.** Haemers Technologies ISTD plant with Vapour Treatment Unit (VTU) (Gela site, 2018)

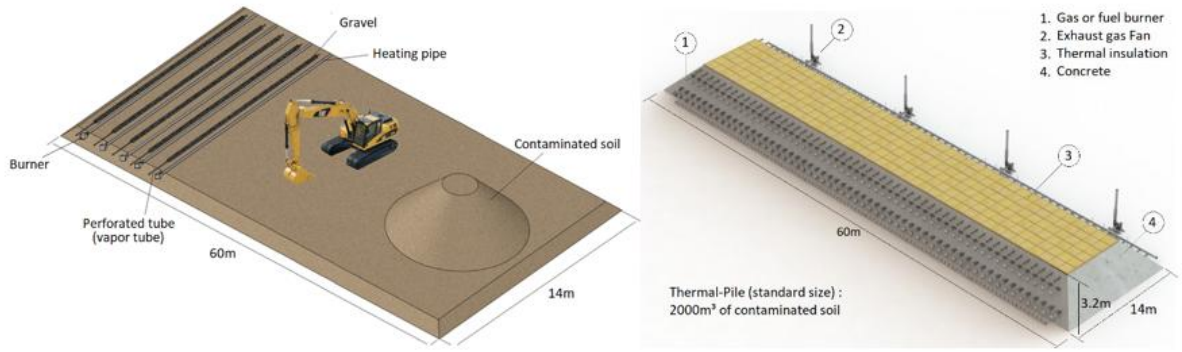


**Figure 2.** Haemers Technologies ESTD plant and thermal-pile (2000 $m^3$ of contaminated soils)

Economic and effective heat transfer into the soil is the main success factor for thermal treatment. Generally, the application of heat requires the use of energy carriers such as fuels (i.e. diesel, LPG, natural gas) or electricity. The use of gas-fired system (smart-burners) or electrical system usually may involve high energy requirement (and then consumption) that increase the final cost of the treatment, but also moves far away from that sustainable environmental criteria that need the reduction and prevention of CO2 emissions and from the alignment with the 'sustainable' policies of the European Union, as foreseen by 'The 2030 Agenda for Sustainable Development Goals' (i.e. Goal number 7: Affordable and Clean Energy). Indeed, the evaluation of CO2 emissions should not be referred only to the use of the required amount of energy during the application of remediation treatment, but it must consider the whole 'life cycle assessment', from the production to the direct use. For this reason, it is necessary to relate CO2 emissions both to the gas-fired heating system and to the electrical one.

Electrical heating systems typically have an efficiency of approximately 95%, while gas-fired systems have a lower value at the point of use about 80% efficiency in transferring energy into the soil. In the first case, electrical heating for soil achieves this efficiency level due to the direct nature of the energy conversion and due to electrons' movement through a resistor to generate heat, transferred to the soil with minimal losses; instead, the gas-fired system employs combustion process that results in some heat loss, primarily through exhaust gases. However, this comparison changes considerably taking into account the entire energy supply chain. In Europe, the average efficiency of electricity generation is around 30-40% that includes losses in power plants, possibly fossil-fuel based, and inefficiencies in transmission and distribution networks. This low value of efficiency is

largely unavoidable due to the laws of thermodynamics governing power generation and the current state of transmission technology. On the other hand, natural gas and propane have close to 95% efficiency in terms of delivery to the point of use, because these fuels are burned directly on site. This means that for every kilowatt-hour (kWh) of energy required to heat soil with electricity, approximately 3 kWh of primary energy is consumed, compared to just over 1 kWh when directly using natural gas or propane (Mneimneh et al., 2023).

Also, considering environmental impact of these heating methods, referred to CO2 emissions, it is known that in Europe electricity is produced from a blend of fossil fuels, nuclear power and renewable energy sources such as wind, solar, and hydropower system. However, marginal energy production, referred to the additional electricity needed to meet demand beyond what is supplied by renewables and nuclear, is produced by natural gas-fired plants, even in countries which have a largely renewable grid. Gas-fired plants are favoured for marginal production because they can be rapidly adjusted to meet real-time demand, unlike intermittent renewable sources. For electricity generated from fossil fuels such as coal or natural gas, emissions can range from 550 to 1100 g CO2 per kWh at the power plant. Transmission and distribution losses in Europe typically range from 1% to 13.5%, meaning that the actual CO2 emission factor for electricity delivered on-site can be even higher than at the generation point. In comparison, when natural gas is burned directly on-site for heating, its emissions are approximately 200-250 g CO2 per kWh of heat produced. Since natural gas combustion happens at the point of use, there are no significant energy conversion or transmission losses, meaning that the carbon footprint for direct heating with natural gas remains consistently lower compared to electricity, particularly when the latter comes from fossil fuel sources. Thus, it is possible to point out that between the two heating systems analysed, the gas-fired one involves higher efficiency and lower emissions than electrical heating system. Despite this and accounting for low-carbon transportation, more energy-efficient technologies, and low-carbon (particularly renewable) energy sources, further technological solutions, more innovative and sustainable, can be identified (Malode et al., 2022; Rodríguez Rodrigo et al., 2024).

To make thermal desorption less impactful in terms of CO2 emissions and to make it economically more accessible among remediation techniques, the adoption of a power system with renewable energy sources can represent a valid solution. An example could be related to solar energy, a leading renewable energy source due to its high availability, sustainability, and zero-emission profile, even if it's affected by high capital costs, spatial constraints for collector installation, and variability in solar irradiance due to climatic dependence (Singh and Chandra, 2023).

Solar energy conversion occurs via photovoltaic (PV) systems for electrical output or solar thermal collectors to include also thermal energy conversion. Considering the conversion of solar energy in thermal energy, solar thermal collectors operate by transferring incident solar radiation to a heat transfer fluid (HTF), with major configurations including flat-plate collectors (FPCs), evacuated tube collectors (ETCs), and concentrating collectors, mostly referring to concentrating parabolic collectors (CPCs). Among the CPCs, parabolic trough collectors (PTCs) stand out for their high efficiency and cost-effectiveness (Calderón et al., 2021; Anna Hammerstingl, 2024). PTCs use curved mirrors or reflectors to concentrate direct normal irradiance (DNI) onto a central absorber tube filled with thermal fluid (Figure 3). The receiver tube, often composed of stainless steel, aluminium, or copper with a selective surface coating, is enclosed in an evacuated glass envelope to minimize convective and radiative heat losses. Bellows, whose thermal expansion is very low, helps in the expansion of the absorber tube without affecting the glass cover, and provide proper vacuum in

annular space. Tracking systems are essential for maintaining optical alignment with the sun, as PTCs cannot concentrate diffuse radiation. Reflector surfaces are made of high-reflectivity materials (e.g., silvered glass, aluminium sheets) to optimize solar flux concentration (El Kouche and Ortegón Gallego, 2022; Singh and Chandra, 2023; Rodríguez Rodrigo et al., 2024; Ahmad et al., 2024).

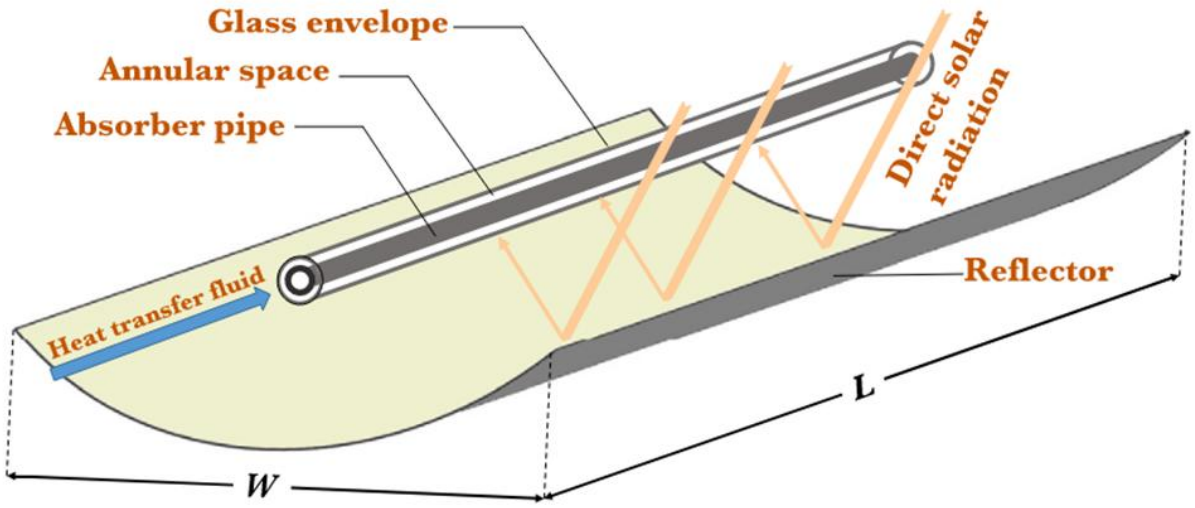


**Figure 3.** Schematic representation of PTC (source: (El Kouche and Ortegón Gallego, 2022))

Solar radiation originates from the Sun as a high-temperature, high-exergy and energy source, with an irradiance of about 63 MW/m² (S Mathew et al., 2010). Solar radiation reaching the Earth's surface spans a broad spectral range, primarily from about 280 nm in the ultraviolet (UV) region to nearly 2500 nm in the near-infrared (NIR), with the most significant fraction concentrated in the visible spectrum (400–700 nm). This distribution reflects the blackbody emission characteristics of the Sun, which has an effective surface temperature of approximately 5778 K. During its propagation through space, solar radiation travels as electromagnetic waves at the speed of light, without requiring a medium for transmission. Upon entering the Earth's atmosphere, however, its propagation is strongly influenced by interactions with atmospheric constituents, including gases, aerosols, and water vapor, which cause absorption, scattering, and reflection phenomena. Rayleigh scattering by molecules preferentially affects shorter wavelengths, explaining the blue colour of the sky, while Mie scattering by larger particles affects a broader spectral range. Absorption bands linked to ozone, carbon dioxide, and water vapor reduce the intensity at specific wavelengths, shaping the solar spectrum observed at ground level (Li et al., 2012; Thuillier et al., 2022). These processes determine both the direct and diffuse components of solar irradiance, which are critical for the design and performance evaluation of solar energy systems.

PTCs are of great importance because of their applicability. In recent years, a lot of research has been performed for all kinds of solar receivers. The preliminary design of a PTC systems consists of applying an approach based on modelling and simulation (M&S) tools, providing detailed information on fluid behaviour and thermal distribution without the need for physical experiments, reducing costs and design time. It also allows to study extreme or difficult-to-reproduce conditions in a laboratory, thus relying on Computational Fluid Dynamic (CFD). CFD is the simulation of fluids

engineering systems using modelling and numerical methods to analyse and solve fluid dynamics problems, instead of "build&test". This approach is based on the use of CFD software, such as Ansys Fluent, to examine the suitability and efficiency of the system. (S Mathew et al., 2010; Akbarzadeh and Valipour, 2018; Bellos and Tzivanidis, 2018a; Yılmaz and Mwesigye, 2018; Sandá et al., 2019; Abed and Afgan, 2020; El Kouche and Ortegón Gallego, 2022; Munawwar Khalil, 2023; Singh and Chandra, 2023; Mohan Das A N, Sudeep Kumar T, 2024).

Currently, there are no technological solutions that combine TD application with the use of renewable energy source, specifically the solar source to supply the energy required for the solid matrix decontamination. The objectives of this thesis work refer to the evaluation of the effectiveness of thermal desorption as a remediation technique for contaminated solid matrices, and to the identification of the technological characteristics that allow TD to be implemented via power supply with a renewable energy source. In particular, the efficiency of the heat treatment (in the range of Low Temperature Thermal Desorption) was investigated through experimental activities conducted with laboratory-scale plant on marine sediments that presented different levels of hydrocarbon contamination. Once the efficiency of the reclamation treatment had been verified, a real TD plant and process was taken as a reference, specifically the one patented by the company Haemers Technologies SA (Bruxelles, Belgium) and also used in the Italian context by Icaro Ecology S.p.A. For technological innovation, among concentrated solar power systems, the PTC has been investigated. Instead of the expensive build&test approach, preliminary design of the PTC was conducted via modelling and simulation (M&S) tools. Numerical and modelling evaluations had the aim of identifying the necessary efficiencies for the application of TD, hypothesized for the in-situ configuration, with process characteristics of the Belgian company's existing technology. Taking advantage of the conversion of solar energy into thermal energy via heat transfer fluid, different design conditions were studied and referred to favourable geographical coordinates for the exploitation of the renewable source.

Solar energy convertible in thermal energy was georeferenced to real data via the Direct Normal Irradiance (DNI) at a specific location. DNI is the amount of solar radiation intercepted per unit area of a surface, which is held at right angles to the rays that propagate in a straight line from the sun at its instantaneous position in the sky. DNI and the efficiency of its transfer to the receiver is then a key-parameter for the design of a CSP system. To combine thermal desorption with CSP system, all design evaluations were referred to an application of remediation treatment for hydrocarbon contaminated soils, extendable to both in situ and ex situ configuration.

Further evaluations were aimed at identifying alternatives for the reuse of decontaminated site after solar powered-thermal desorption application. Specifically, reference was made to the reuse for geothermal purposes, studying a preliminary system through a modelling and simulation approach. In this way, soil acts as a thermal battery or Thermal Energy Storage (TES) system. TES systems are categorized into three types: sensible, latent, and thermochemical. Sensible Heat Storage (SHS) is the simplest method, storing heat directly within a material. Latent Heat Storage (LHS) involves using thermal energy to trigger a phase change in a material, which then releases the energy when it returns to its original state. Thermochemical Heat Storage (THS) relies on reversible chemical reactions, separating compounds and recombining them to produce heat. Among these, SHS is the most developed and widely used (Ma and Wang, 2020; Mahon et al., 2022; Buscemi et al., 2023).

Energy storage systems encompass three main stages: charging, storing, and discharging. Solar and geothermal energy are highlighted as promising solutions for reducing carbon emissions and meeting heating demands, particularly in winter. Since solar energy is inconsistent, thermal energy storage is essential to ensure a steady supply when sunlight is unavailable. By capture the heat generated by solar collectors during the sunnier months and store it for later use, this stored thermal energy is distributed during winter or cold months (Salaudeen, 2019; Vanaga et al., 2023; Bu et al., 2024; Rapti et al., 2024). The geothermal system hypothesized in this thesis work refers to Borehole Thermal Energy Storage (BTES). It involves drilling multiple boreholes into the ground and circulating a heat transfer fluid through them to deposit or extract heat. The stored heat in the soil is then used, i.e. during winter for heating purposes. This technology is highly efficient and can store large amounts of energy. BTES system deals well with the discontinuity of the solar source, compensating for this drawback. The pipes in the Borehole system may have different configurations, including single U-shaped, bent U-shaped, parallel double U-shaped or multi-U-shaped (Velraj, 2016; Fadejev et al., 2017; Buscemi et al., 2023; Anna Hammerstingl, 2024). In this work, the geometric model used for geothermal evaluations was a multi shaped U-tube.

# Chapter 2 - Legislation

## 2.1 Remediation

### 2.1.1 European Union

At the EU level there are several binding acts that together create the framework within which Member States have to regulate soil and sediments management and remediation.

If considered as waste, these solid matrices were mandatory part of the Waste Framework Directive 2006/12/EC, which to date has been repealed but is of significant importance, as it establishes basic definitions (waste, recovery, disposal), key principles (waste hierarchy, "polluter pays"), authorizations/registrations for waste operators and obligations for national waste plans. This framework was particularly relevant for soils and sediments in remediation contexts, since classification as waste determined whether disposal, recovery, or reuse operations had to follow waste law (Parliament and Council, 2006). Shifting to a life-cycle/circular-economy approach, the EU repealed 2006/12/EC and adopted Directive 2008/98/EC, effective 12 December 2010. The recast codified the five-step waste hierarchy, enabled "end-of-waste" and by-product status, strengthened prevention and producer responsibility, and kept core safeguards for human health and the environment. The Directive clarified conditions under which excavated soils and dredged sediments cease to be classified as waste. These provisions were crucial for soils and sediments, providing a legal pathway to reuse excavated or dredged materials (e.g., in construction or land reclamation) rather than classifying them as waste requiring disposal (European Union, 2008; Zecca et al., 2023). Directive (EU) 2018/851 amended the Waste Framework Directive by setting binding municipal waste recycling targets (55% by 2025; 60% by 2030; 65% by 2035), introducing minimum requirements for extended producer responsibility (EPR), and mandating separate collection for bio-waste by 31 December 2023 and for textiles and household hazardous waste by 1st January 2025. It also included rules for materials considered recycled or recovered, important in tracking dredged sediments or excavated soils in circular economy strategies (European Union, 2018).

Other important European Frameworks mainly refer to sediments rather than soils. The adoption of the Water Framework Directive (WFD, 2000/60/EC) in 2000 represented a milestone in European environmental legislation. It established a comprehensive and integrated legal framework for water protection in the European Union, introducing the river basin as the basic management unit, and setting the long-term objective of achieving at least “good ecological and chemical status” for all waters within the European Union. Although soils are not directly regulated under the WFD, the Directive has far-reaching implications for both soils and sediments. These environmental compartments act as long-term repositories of pollutants such as heavy metals, hydrophobic organic compounds, and persistent organic pollutants, which can subsequently be remobilized into aquatic systems, making soils and sediments both sinks and secondary sources of pollution. A substantial amendment to the Directive 2000/60/EC occurred through the Environmental Quality Standards (EQS) Directive (2008/105/EC), which translated the WFD’s general chemical objectives into concrete numerical thresholds. The introduction of environmental quality standards was a substantive innovation: it provided binding concentration limits against which the chemical status of water bodies had to be assessed, directly shaping sediments monitoring strategies and remediation measures (Farmer, A.M., 2012). Later amendments, most notably Directive 2013/39/EU, revised and updated

the list of priority substances, introduced stricter EQS for several pollutants, and strengthened the so-called "watch list" mechanism, which allows emerging contaminants (such as pesticides and pharmaceuticals) to be monitored at EU level (Ferrante et al., 2015).

Most recently, in line with the European Green Deal and the Zero Pollution Action Plan, the European Commission has proposed further reforms to update pollutant lists, strengthen environmental quality standards, and enhance monitoring of mixtures and micro-pollutants. By explicitly recognizing the role of sediments and biota in chemical monitoring, and by placing greater emphasis on cumulative effects, these proposals represent a significant departure from the Directive's original design, which was primarily focused on the water column. This regulatory evolution is closely aligned with the broader objectives of the 2030 Agenda for Sustainable Development. Sustainable Development Goal (SDG) 6 aims to ensure the availability and sustainable management of water and sanitation for all, while SDG 15 emphasizes the protection, restoration, and sustainable use of terrestrial ecosystems, including soils. The WFD's emphasis on integrated, ecosystem-based management contributes directly to SDG 6, particularly in its target of improving water quality by reducing pollution, eliminating dumping, and minimizing the release of hazardous chemicals. At the same time, the Directive indirectly supports SDG 15 by addressing soil degradation through its impact on water resources (Bruce and Ohlsson, 2020; Backhaus, 2023; Copetti and Erba, 2024; Singh et al., 2025).

The lack of explicit European regulation of contaminated soils has led to the Soil Monitoring Law (Soil Monitoring and Resilience Directive) proposed in July 2023 and, politically agreed in 2025 (Parliament–Council provisional deal). It represents the first comprehensive EU legal framework dedicated to the protection and sustainable management of soils. Its primary aim is to achieve and maintain healthy soils across Member States by 2050, addressing widespread degradation caused by erosion, contamination, compaction, and biodiversity loss. The directive establishes a harmonized soil monitoring system, requiring standardized assessment procedures, data collection, and sharing to support evidence-based policymaking and cross-border comparability. The Soil Monitoring Law aligns with broader European environmental goals, including the European Green Deal and the United Nations Sustainable Development Goals, marking a significant step toward integrated soil governance and resilience. It sets measures for identifying and remediating contaminated sites, ensuring that soil pollution levels do not pose risks to human health or the environment. The Soil Monitoring Law is at provisional agreement stage and will require transposition after formal adoption (Panagos et al., 2025).

### 2.1.2 Italy

Italy layers a robust, risk-based cleanup code on top of those EU obligations and adds a specialised dredging/sediment rulebook. The cornerstone is Legislative Decree 152/2006. For land-based sites, Part IV, Title V of Legislative Decree 152/2006 ("Testo Unico Ambientale") governs the identification and remediation of contaminated sites providing the overarching rules for environmental protection, including soil and sediment remediation. This decree establishes the criteria for identifying contaminated sites, the procedures for risk assessment, and the acceptable threshold concentrations for contaminants. It redefines the criteria for identifying so-called "Sites of National Interest" (introduced for the first time with law n. 426/1998), subjected to direct intervention by the Ministry for the Environment due to their scale, complexity, or relevance for public health and ecosystems. Under the Italian framework, remediation is not limited to the removal of pollutants, but

rather is guided by a risk-based approach. This approach requires that site-specific risk assessments determine the acceptable level of contamination based on current or planned land use, environmental protection goals, and human health criteria. Specifically, the Decree sets the Concentration Thresholds of Contamination (CSC) in Annex 5 (Table 1 for soil; Table 2 for groundwater), differentiated by land use: Column A for residential/green uses; Column B for industrial/commercial. Where contamination exceeds CSC values, a site-specific risk assessment determines Remediation Objectives (CSR). The procedure includes not only a risk assessment but also the emergency safety measures (MISE), operational safety measures (MISO), the Remediation Project (Progetto di Bonifica), and post-operational monitoring. Once a remediation project attains the relevant CSR (or demonstrates compliance with CSC), treated soils can typically remain in place or be reused on site under the approved design, provided that the final use is consistent with the risk framework. Liability follows the polluter-pays principle; if the liable party is unknown, the public authority may intervene with recovery mechanisms. Sediments in inland waters can fall under this part of Decree when linked to a "site" (Government, 2006).

With particular reference to sediments, two 2016 ministerial decrees regulate dredging operations and the fate of dredged sediments in marine and transitional waters. Decree 172/2016 applies to dredging in Sites of National Interest (SIN) and sets technical rules for characterisation, environmental management during works, and potential re-use or confined placement options consistent with site remediation objectives. Decree 173/2016 implements Article 109 of Legislative Decree 152/2006 for the immersion at sea of dredged materials, laying down the authorisation pathway, quality criteria, and environmental safeguards. Read together, the two decrees create a matrix in which sediments that meet quality thresholds may be allocated to beneficial uses (e.g., beach nourishment or engineering uses), while those that do not must be confined or managed as waste, are regulated with stringent monitoring and permitting (Environment, 2016a, 2016b).

In conformity with the principles outlined by European directives, the WFD and the MSFD, Italian legislation provides robust methods for classification and for the management of sediment. Among the available methodologies, the Weight of Evidence (WoE) approach has emerged as one of the most comprehensive frameworks for sediment quality assessment, as it integrates different "lines of evidence" into a unified system for decision-making. Traditionally, sediment classification based only on chemical concentrations (and the compliance with CSC) often failed to capture actual ecological risks, given that bioavailability, toxicity, and ecosystem responses can differ significantly from predicted values. The WoE framework addresses these shortcomings by combining chemical analyses, ecotoxicological bioassays, and ecological/benthic community assessments (the Lines of Evidence, LOEs) into a tiered classification system that provides a holistic evaluation of sediment quality in an integrated risk classification. In Italy, the application of WoE has been explicitly introduced through Ministerial Decrees n. 172/2016 and n. 173/2016 to regulate the management and classification of dredged materials intended for marine immersion, and to help the management decisions in Sites of National Interest. This classification ensures that the degree of contamination is linked not only to chemical exceedances, but also to actual biological and ecological relevance, thereby reducing the likelihood of misclassifying sediments that might either pose a hidden risk or be unnecessarily discarded in compliance with sustainable reuse and circular economy objectives. The WoE methodology generally identifies quality classes of sediment that guide management decisions. However, the outcome of the WoE procedure is not a simple assignment to a predefined numerical class, but rather a comprehensive evaluation of the sediment quality and its potential impact on the

environment. This process is operationalized through tools like Sediqualsoft®, developed by the Italian Environmental Protection Agency (ISPRA), which facilitates the integration of diverse data types into a cohesive classification system. It's a quantitative Weight-Of-Evidence (WOE) model developed to elaborate data from different lines of evidence (LOEs; i.e., sediment chemistry- LOE1, bioaccumulation-LOE2, biomarkers-LOE3, ecotoxicological bioassays-LOE4, and benthic communities-LOE5) in ecological risk assessment studies of contaminated or potentially contaminated sites. The comprehensive evaluation through WoE procedure turns into the assignment of a class:

- Class A: Sediments that pose minimal or no risk to the environment.
- Class B: Sediments with low environmental risk.
- Class C: Sediments with moderate environmental risk.
- Class D: Sediments with high environmental risk.
- Class E: Sediments with very high environmental risk.

These classifications guide management decisions regarding sediment disposal, reuse, or remediation strategies (d'Errico et al., 2021; Manfra et al., 2021; Commission, 2022; Miglino and Holmes, 2023; Piccardo et al., 2024).

Another important regulation is Presidential Decree 120/2017, which provides simplified procedures for the management of excavated soils and rocks. This decree reflects the Italian effort to foster a circular economy by enabling the reuse of excavated materials, provided that they meet environmental quality standards. In this way, soils and sediments that have undergone treatment can re-enter productive cycles as construction materials, backfilling materials, or other industrial applications (Government, 2017).

The concept of reusing soils and sediments that have undergone thermal remediation represents a pivotal evolution in sustainable environmental engineering. Moreover, the integration of thermal treatment technologies, such as thermal desorption, into the Italian remediation framework is particularly relevant for highly contaminated (e.g., hydrocarbons, PCBs, dioxins) matrices and due to the short treatment times required and the high efficiencies achievable. According to Italian legislation, soils or sediments treated with thermal technologies can be classified as "non-waste" if they meet the quality criteria set by Decree 152/2006 and subsequent amendments (Falciglia et al., 2020a). Despite the potential of thermal treatments, careful consideration of soil functionality remains crucial. Treatment protocols must include post-remediation assessments of properties like organic content, capacity for plant growth, and hydraulic behaviour. Engineering-focused studies revealed that treatment operating around 350°C yielded the highest reuse potential and remediation efficiency (Ding et al., 2019; Li et al., 2022).

# 2.2 Renewable energy

## 2.2.1 European Union

The energy sector plays a crucial role in driving national socio-economic development. Since the 1990s, global energy demand has risen steadily, with an average annual growth of about 1–2%. In 2021, fossil fuels still represented roughly 72% of total consumption, while renewables accounted for only 28%. In response, energy and environmental policies in advanced economies have

increasingly focused on strategies to curb and reduce carbon emissions. This international effort began with the 1992 United Nations Framework Convention on Climate Change, followed by the 1997 Kyoto Protocol, and culminated in the 2015 Paris Climate Agreement, the first universal and legally binding global climate accord. To meet its commitments under the Paris Agreement, the European Union launched the "Clean Energy Package," a comprehensive set of measures targeting three key goals for 2030: at least a 40% reduction in greenhouse gas (GHG) emissions compared with 1990 levels, a minimum 32% share of renewables in final energy use, and a 32,5% improvement in energy efficiency. Accordingly, each Member State prepared a National Integrated Energy and Climate Plan (NECP) for 2021–2030, outlining the legislative and regulatory framework to achieve these objectives (Maris and Flouros, 2021; Esposito and Romagnoli, 2023).

Alongside EU initiatives, global strategies such as the 2030 Agenda for Sustainable Development and its 17 Sustainable Development Goals (adopted in 2015) have provided an overarching framework for sustainable growth. In Europe, early legislative steps included Regulation (EC) No 1099/2008, Directive 2001/77/EC, and Directive 2003/30/EC (RED I), which promoted the uptake of renewable energy technologies, particularly in the transport sector. Within this evolving policy context, renewable energy communities (RECs) have emerged as an innovative model to accelerate the transition toward cleaner and more decentralized energy systems. RECs bring together local stakeholders to jointly develop, own, and manage renewable energy projects. Their benefits include the decentralization of energy production, which reduces transmission needs and energy losses, while enhancing system resilience, reliability, and diversity. Recognizing their potential, the European Union formally integrated energy communities into policy with Directive 2018/2001/EU (RED II). The most recent revision, Directive (EU) 2023/2413 (RED III), entered into force in November 2023, raising the binding 2030 renewable energy target to at least 42,5%, with an aspirational goal of 45%. To accelerate the transitions, Emergency Permitting Regulation (Regulation (EU) 2022/2577) creates temporary, faster permitting for renewable projects and grids, including renewables "go-to" areas, time-limits for procedures, and simplified environmental assessments for repowering. These measures aim to strengthen incentives for Member States and streamline permitting processes, which had been a major bottleneck in 2019–2022 (European Parliament, 2018; Biresselioglu et al., 2021; Moretti and Stamponi, 2023).

Beyond RED, the European Solar Strategy (2022) represents the first dedicated plan to unlock solar potential across the EU. It sets out the EU Solar Rooftop Initiative, making rooftop solar mandatory for new public and commercial buildings (by 2026–2027) and for new residential buildings (by 2029). It also addresses skills shortages in the solar industry and aims to strengthen Europe's manufacturing base, reducing dependency on non-EU supply chains. Member states are expected to support industrial solar thermal, including concentrating solar, to reach these targets. Countries with higher DNI (such as Spain, Italy, Greece, Cyprus) are seen as prime candidates for industrial CSP demonstration projects. Together, these instruments create a coherent framework that not only promotes renewables broadly, but explicitly positions solar power as a cornerstone of Europe's decarbonization pathway (Molnár et al., 2024; Müllejans, H. et al., 2020).

## 2.2.2 Italy

Legislative Decree 199/2021 represents Italy's main transposition of RED II (2018/2001), now being updated to align with RED III. It reorganised support schemes, streamlined some permits, and created the legal basis for energy communities and collective self-consumption. In compliance

with European Solar Strategy principles, Italian energy policy emphasizes solar deployment, reflecting the country's favourable irradiance and territorial potential. To support Legislative Decree 199/2021, three other pillars have been introduced:

- Decree on Renewable Energy Communities (so-called "Decreto CER") - Ministerial Decree 7 Dec 2023, No. 414: establishes a national operating premium on shared energy for community and collective self-consumption configurations (CACER) and, under the National Resilience and Recovery Plan (NRRP), a capital grant up to 40% of eligible costs for projects in municipalities;
- FER2 (Fonti Energetiche Rinnovabili), Ministerial Decree 19 June 2024 (in force August 13, 2024): a multi-technology auction-based scheme for innovative or higher-cost renewables excluded from FER1 (e.g., offshore wind, floating PV, geothermal, biogas/biomass, marine energy). The decree defines reference tariffs and competitive discounts;
- FER-X, Ministerial Decree 30 Dec 2024 and rules updated on February 2025: a bridge support for mature technologies "close to market parity" (rooftop/ground-mount PV, onshore wind, small hydro, residual-gas plants).

Italy incentive schemes are administered principally by the Gestore dei Servizi Energetici (GSE). Italian policy mixes regulatory measures (permitting simplification, grid connection rules), direct incentives and fiscal measures (IEA, 2023; D'Auria et al., 2024; Prestigiacomo et al., 2024). Key national instruments still in active use include:

- Conto Termico (thermal incentives, managed by GSE): a longstanding national support mechanism providing direct financial incentives for energy efficiency and for producing thermal energy from renewable sources (including solar thermal and other renewable heating). Conto Termico is explicitly aimed at both public administrations and private entities (including companies) and can subsidize investments that replace fossil-fuel thermal generation with renewable thermal technologies;
- Industrial decarbonisation funds and NRRP instruments: Italy, under the National Recovery and Resilience Plan, channels EU funds toward industrial decarbonisation, with a focus on renewable heat and electrification. Projects that demonstrate replacement of fossil-based thermal treatment with renewable CSP heat can potentially access these instruments.

Even if there are currently no specific decrees or directives exclusively target the use of renewable energy for soil or sediment remediation, the reference for a plant operating in that field must be industrial applications. In this context and considering TD plants are commonly powered by fossil fuels, certain regional/national measures can support renewable integration in industrial contexts, such as:

- Decreto Coesione (Decree-law No. 60/2024) that allocates funds for renewable (also thermal) energy production in industrial areas of Southern Italy;
- ASSET Decree (DL 104/2023) introduces a single authorization procedure (autorizzazione unica) to simplify permitting for renewable plants, reducing administrative barriers;
- L.D. 17/2022 establishes a tax credit for companies in Southern Italy investing in renewable energy and storage to enhance energy efficiency in their production facilities.

These legislative tools can encourage access to currently expensive technologies, e.g. concentrating solar power systems to be combined with a thermal desorption plant. CSP, particularly

parabolic-trough collectors (PTCs) can deliver renewable thermal energy instead of diesel or natural gas reducing $CO_2$ and pollutant emissions, making remediation thermal treatment more sustainable. Legislative Decree 152/2006 governs industrial installations, soil remediation, and integrated environmental authorisation (Autorizzazione Integrata Ambientale, AIA). Industrial plants that use thermal processes for soil remediation (e.g., thermal desorption) usually operate under AIA and must comply with emission limits and Best Available Techniques (BAT). A shift from fossil-fuel combustion to renewable heat generation is consistent with BAT principles and may even simplify and facilitate AIA renewal and permitting, since it reduces greenhouse gas and pollutant emissions.

# Chapter 3 – State of the Art

## 3.1 Thermal Desorption

### 3.1.1 Overview

Thermal desorption (TD) is an established remediation technology designed for the treatment of soils and sediments contaminated with volatile and semi-volatile organic pollutants and mercury, as Contaminants of Concern, COC. The process is based on the application of heat to the contaminated matrix in order to increase the vapor pressure of the contaminants and promote their transfer into the gas phase. These vapours must subsequently be captured and treated in a dedicated off-gas system, preventing their uncontrolled release into the environment. It is precisely this dual configuration, the heating stage and the gas treatment unit, that defines the process and differentiates thermal desorption from other thermal technologies such as incineration. In incineration, the destruction of contaminants occurs directly within the soil matrix at very high temperatures, whereas in TD the volatilized compounds are usually removed from the soil by a ventilation/extraction network and only subsequently oxidized, destroyed or condensed in a separate, engineered system. The U.S. Environmental Protection Agency, in its Thermal Desorption Technology Resource Guide and the Community Guide to Thermal Desorption, has emphasized the centrality of off-gas management in TD systems, noting that the effectiveness of the technology depends not only on the volatilization of contaminants but equally on the safe and efficient management of the vapor stream. Compared with incineration, thermal desorption allows a cost saving of roughly 75%, and the treated soil retains its essential characteristics for reuse (Zhao et al., 2016; Falciglia et al., 2020a; Li et al., 2022; US-EPA, 2025; Huang et al., 2025).

Referring to the technological configuration, TD can be implemented as ex-situ (ESTD) and in-situ (ISTD) systems. Ex-situ involves excavation of contaminated soils or dredging of sediments, which are then processed in thermal desorbers, such as rotary kilns or fluidized beds. This option provides strict control over process conditions and is particularly suited for large volumes of material or when soil removal is already necessary for construction purposes or for the treatment of sediments. In contrast, in-situ thermal desorption applies heat directly to the subsurface via conductive elements, steam injection, or electrical heating. The in-situ approach is advantageous when excavation is impractical or when minimizing disturbance to the site is a priority. Both ex-situ and in-situ systems require sophisticated off-gas treatment units, typically composed of condensers, scrubbers, activated carbon filters, or thermal oxidizers. The complexity of vapour treatment unit in a TD application is also depending on the mode of heat transfer employed to reach the target temperature. According to heating methods, TD can be divided in direct heating systems and indirect heating systems. In direct heating systems, combustion gases come into direct contact with the contaminated matrix, transferring heat by convection and radiation. This configuration allows rapid heating rates and is typically implemented in direct-fired rotary kilns or fluidized bed desorbers. A common example is the direct-fired rotary kiln, where burners introduce hot combustion gases directly into the rotating drum. Direct heating often produces a more complex off-gas stream, containing not only volatilized contaminants, but also combustion by-products, particulates, and potentially incomplete oxidation products, requiring robust and more expensive vapour treatment unit. In contrast, in indirect-contact thermal desorption, heat is indirectly provided by heat conduction and the contaminated matrix is not

in direct contact with the heat source. In this case, thermal energy is transferred through a physical barrier, such as the heated walls of a rotary kiln. Indirect heating reduces the risk of forming combustion by-products, providing a better process control and it doesn't require an extensive vapour treatment unit (Zhao et al., 2019; Li et al., 2020; Kristanti et al., 2022).

Thermal desorption presents a series of advantages that make it a particularly attractive option for remediation. The technology achieves very high removal efficiencies for a broad range of volatile and semi-volatile organic compounds, including petroleum hydrocarbons, polycyclic aromatic hydrocarbons (PAHs), pesticides, and chlorinated solvents. Concerning inorganic pollutants, TD has shown its effectiveness as remediation process for mercury contaminated sites. Several authors have already demonstrated the high efficiencies achievable through TD. Sierra et al., applied thermal desorption to remediate highly mercury contaminated soils through a pilot scale solar rotary kiln, obtaining mercury removal efficiencies higher than 80% (Sierra et al., 2016). Another example of the high efficiency of thermal treatment refers to soils highly contaminated by hydrocarbons (exceeding 40000 mg/kg). In particular, hydrocarbons decontamination of a mega site has been studied by Huang et al. and different TD technologies were used. One of these was the on-site Thermally-enhanced vapor extraction technology (TEVET) which included as heater system a thermal oxidizer with a propane or LPG fuel source to allow for the thermal treatment, a blower system, a vapour collection and air polishing system. Also, multi-screw thermal desorption system and rotary kiln system were employed to remediate petroleum hydrocarbon contaminated soils within the mega site. Prior to the on-site treatment, experimental activities were carried out using a bench scale system consisting of a tube furnace to evaluate the TD process parameters necessary to comply with the hydrocarbon limit concentrations. Both in the experimental activities and in the on-site treatments, high removal efficiencies were obtained always exceeding 90% hydrocarbon removal, demonstrating that TD is insensitive to contaminant concentration levels in the soil, but the factors affecting performance of thermal desorption mostly depend on contaminant type, residence time and maximum temperature in thermal treatment unit, and on site-specific characteristics, such as soil moisture, soil organic matter content and soil texture (Huang et al., 2025).

Unlike biological treatments, which rely on the activity of microorganisms and may require several months or even years to achieve significant contaminant reductions, thermal desorption can complete the remediation process within weeks or months, depending on the scale of intervention. The choice of thermal desorption over alternative technologies must therefore be guided by site-specific considerations. Compared to biological treatments, TD offers much faster remediation and is particularly indicated for contaminants that are poorly biodegradable (e.g., high molecular weight PAHs or chlorinated solvents). Compared to chemical oxidation or stabilization, TD has the advantage of removing contaminants from the solid matrix rather than transforming or immobilizing them through reactive agents, thus eliminating long-term liabilities associated with residual pollutants. Moreover, biological treatments, such as bioremediation, bioaugmentation or biostimulation, may be inefficient or even ineffective for highly chlorinated compounds, recalcitrant hydrocarbons, or environments with toxic contaminants that inhibit microbial activity; chemical treatments can target both organic and inorganic contaminants but may leave behind transformation products that are potentially toxic or unstable and the efficiency depends on the ability of chemical agents to diffuse through the solid matrix and reach target contaminants (Hullebusch et al., 2005; Pino-Herrera et al., 2017; O'Brien et al., 2018; Zhao et al., 2019; Pagnozzi et al., 2020; Anno et al., 2021; Li et al., 2022).

Nevertheless, TD is also characterized by limitations. At a scientific level, many authors and several real applications of TD have defined a classification as a function of the temperature treatment of the solid matrix. In particular, for temperatures up to 300°C reference is made to Low Temperature Thermal Desorption (LTTD), for temperatures greater than 300°C reference is made to High Temperature Thermal Desorption (HTTD). In practical applications, this temperature threshold also refers to the treatment of volatile (up to 300°C) and semi-volatile organic contaminants and mercury (>300°C) (Ding et al., 2019; Zhao et al., 2019; Zivdar et al., 2019; Falciglia et al., 2020a). This classification is closely related to energy consumption and to the alterations of soil/sediment properties due to the elevated temperatures. Energy consumption increases with the use of high temperature and energy demand is typically met with fossil fuels (e.g. diesel, natural gas) to generate the heat required, resulting in elevated operating costs and greenhouse gas (GHG) emissions, thus deviating from the sustainability principles advocated by the numerous European and Italian measures. The high GHG emissions make TD in contrast and in an opposite extreme with bioremediation, which is widely considered the most sustainable remediation technology. Chemical treatment sits between the two extremes: although faster than bioremediation, it requires substantial quantities of chemical reagents, the production and transport of which also entail environmental impacts. TD may be preferred in cases where contamination is severe, complex, or requires rapid intervention, but a change in the energy supply system would reduce the emissions generated, thus extending its field of application (O'Brien et al., 2018; Falciglia et al., 2020a; Wang et al., 2021; Kristanti et al., 2022; Chen et al., 2024; Sun et al., 2024; Liao et al., 2025).

At the same time, the use of high temperatures not only increases the energy consumption of the TD, but also compromises the properties of the treated matrix, modifying their ecological functions due to irreversible alteration of their mineral and physico-chemical structure. Specifically, at elevated temperatures soils/sediments undergo a series of structural, mineralogical, and chemical transformations that can affect their fertility, porosity, and long-term reuse potential:

- Organic matter is one of the most temperature-sensitive components of soil. Falciglia et al. 2020 observed a slight decrease in marine sediments' organic matter content when TD was applied in the range of low temperature (particularly, when temperatures were less than 240°C). Studies have shown that heating soils to 300–400 °C leads to a reduction of total organic carbon (TOC) by up to 70%, resulting in the loss of nutrient reservoirs and cation exchange capacity (CEC) reducing soil's ability to retain nutrients and metals and altering its fertility.
- Mineral fractions of soils and sediments also undergo modifications during TD. Clay minerals such as kaolinite and illite are particularly sensitive. Excessive heating or high temperatures (up to 400°C) imply dehydroxylation reactions and decomposition of mineral clay lattice structures causing irreversible changes in crystallinity.
- The reuse of solid matrix after thermal treatment is also limited by the change in its porosity, bulk density, and permeability. If moderate heating may increase porosity due to the volatilization of organics and water, at higher temperatures (>500 °C), partial sintering and agglomeration of particles can occur, leading to densification and reduced permeability. These alterations affect pollutant desorption from solid phase (then TD removal efficiency) and inhibit the reuse for agricultural purposes.
- TD also induces significant shifts in soil/sediment pH and nutrient availability. Heating accelerates the volatilization of nitrogen compounds and sulphurs. In carbonate-rich soils,

decarbonation elevates alkalinity, whereas in acidic soils combustion of organic matter can temporarily increase acidity. These chemical imbalances may reduce the potential for ecological restoration of remediated soils. Restoration of microbial function in thermally treated soils could require bioaugmentation or long recovery times.

Due to these limitations, several studies demonstrated that applying TD in the temperature range of LTTD may provide a balance between contaminant removal efficiency and preservation of soil properties (O'Brien et al., 2018; Falciglia et al., 2020a, 2020b; Leite et al., 2021; Li et al., 2022; Sun et al., 2024; Zhang et al., 2025; Liao et al., 2025).

Another critical issue for TD is the water content of the soil or sediment. High moisture levels demand additional energy to evaporate water before contaminants can be volatilized effectively, reducing process efficiency and increasing costs. Moreover, water content affects heat transfer (thermal conductivity and heat capacity), mass transport (vapour advection and diffusion), contaminant partitioning (dissolution and steam-stripping behaviour), and the kinetics of desorption. The practical consequence is that moisture control is often one of the most important aspects of TD project design. Some authors stated that contaminated soils/sediments for TD treatment should have specific moisture content in the range of 10-20 %. Due to the complexity of pollutant removal mechanisms during thermal treatment, water can act as inhibitory factor and as key factor. Water molecules are highly polar and easily occupy the adsorption sites of the solid matrix, so many contaminants can be removed from it; water rapidly evaporates during heating, implying the effect of vapour extraction and distillation to enhance the removal of contaminants, at the same time water evaporation increases the heat loss during heating process, thus increasing processing costs; also, if a large amount of water is heated and evaporated, the generated steam increases the amount of off-gases, thereby influencing the size of the required vapour treatment unit. From a physical point of view, water in porous media may be present in form of:

- free (bulk) water (water in macropores);
- capillary water (water in small pores held by capillary forces);
- bound (adsorbed) water (thin molecular layers on mineral surfaces, especially on clays and organic matter, that are held by electrostatic and hydrogen-bonding forces).

The energy required for the removal of these types of water in porous media increases passing from free water to bound water. In general, the energy required to remove 1 kg of water includes both the sensible heating from ambient temperature to the boiling/evaporation temperature and the latent heat of vaporization. At near-atmospheric pressure the latent heat of vaporization of liquid water is 2250-2260 kJ/kg. This is orders of magnitude larger on a per-kilogram basis than the latent heats of many volatile organic contaminants (VOCs) and light hydrocarbons (i.e. benzene has a enthalpy of vaporization of 395 kJ/kg); this difference in enthalpy of vaporization values and the typical site condition referred to water content and contaminant mass, mean that the heat required to evaporate water commonly exceeds the heat required to volatilize the mass of volatile organic pollutants in the solid matrix (Zhao et al., 2019; Chai et al., 2022; Zhang et al., 2022; Sun et al., 2024; Xu et al., 2024; Zhang et al., 2024).

Applying TD and providing heat to the solid matrix involves different removal mechanisms that affect both the contaminants and the water content, including evaporation and boiling (or co-boiling), hydrolysis, pyrolysis, and oxidation. At the lower temperature spectrum, evaporation and boiling are the dominant processes. Volatile and semi-volatile organic compounds (VOCs and

SVOCs) can evaporate as their vapor pressure increases with temperature, and once the boiling point of a compound is reached under the specific system pressure, it undergoes rapid phase transition to the gas phase, facilitating efficient desorption. The increase in vapor pressure with temperature for water and many DNAPLs (Dense Non-Aqueous Phase Liquids) can be approximated using the Antoine law:

$$Log_{10}(P) = A - \frac{B}{(C+T)}$$

In this equation, P represents the vapor pressure of a compound, A, B, and C are compound-specific empirical constants, and T is the temperature.

The presence of water significantly modulates removal mechanisms: moisture not only contributes to the energy balance by requiring latent heat for evaporation but also promotes the mobilization of hydrophilic contaminants via co-distillation. Indeed, when two immiscible liquids are present in the saturated or unsaturated zone, the vapor pressures of both liquids contribute to the total gas pressure. This phenomenon is known as co-boiling: since the vapor pressures of the two immiscible liquids add up, vapor formation occurs at a lower temperature (the co-boiling point) than the boiling point of either pure component individually considered. At intermediate temperature ranges, hydrolysis reactions may occur, particularly for compounds that are thermally labile or that interact with mineral and aqueous phases in the soil matrix. Hydrolysis can alter contaminant molecular structures, breaking them down into smaller, often more volatile fragments, which are then more easily desorbed. Beyond hydrolysis, pyrolysis becomes a significant removal pathway at higher temperature (from 200°C). In this stage, organic contaminants undergo thermal decomposition in the absence of oxygen, usually in an inert atmosphere using nitrogen gas and generating smaller hydrocarbons, gases (CO, $CO_2$, $CH_4$), and sometimes tar-like residues. Oxidation reactions may take place when oxygen is present, either intentionally introduced or through residual air in the treatment system. Thermal oxidation leads to the partial or complete mineralization of organic contaminants into $CO_2$, $H_2O$, and inorganic residues. This process is particularly important for reducing the risk of re-condensation or secondary contamination by degraded by-products. However, it can also contribute to the alteration of soil mineralogy, such as the decomposition of carbonates or the sintering of clay particles, with potential implications for soil structure and fertility (Xu et al., 2024; Zhang et al., 2024).

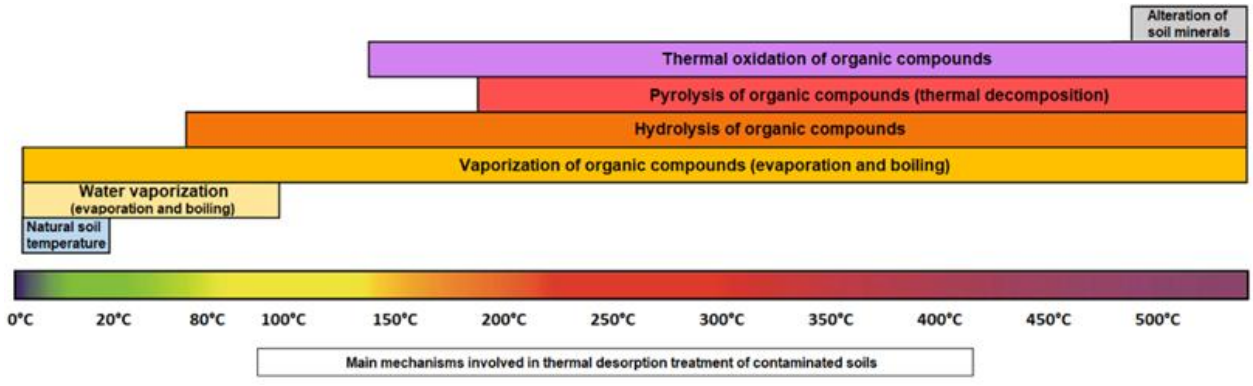


**Figure 4.** Removal mechanisms during thermal treatment of polluted soil (provided by Haemers Technologies)

Therefore, understanding these mechanisms of removal is crucial for optimizing the design and operation of thermal desorption systems. The selection of an operational temperature regime

determines both the dominant removal mechanisms and the environmental and material impacts of the treatment. Low-temperature thermal desorption (LTTD), typically operated up to 300°C, primarily exploits physical volatilization, steam-stripping and enhanced vapor-phase mass transfer to remove volatile and lighter semi-volatile organic compounds even in inert atmosphere; High-temperature thermal desorption (HTTD), generally above 300-600°C, is in the range of thermochemical decomposition pathways including pyrolysis and, when oxygen is present, oxidation reactions. These differences have direct consequences for energy demand, off-gas composition, soil alteration and long-term land usability. LTTD frequently offers clear advantages as it reduces fuel consumption and greenhouse-gas emissions for a given mass of treated soil. Many target contaminants possess sufficiently high vapor pressures at temperatures well below 300 °C (in the range of LTTD) to be transferred from the solid or aqueous phase into the gas phase when soils are heated and coupled to an effective soil-gas extraction system; the presence of water enables steam-stripping (co-distillation), whereby volatile and some semi-volatile contaminants partition into the steam phase and are carried to the vapor treatment unit. Optimized remedial designs often adopt hybrid strategies, also called treatment train, combining LTTD with chemical or biological techniques (such as thermally enhanced bioremediation) to combine the strengths of both regimes while minimizing costs and impacts (Biache et al., 2015; Falciglia et al., 2020a; Ren et al., 2020). Typical plant layouts of TD existing solutions in Europe and Italy are described in the following paragraph.

## 3.1.2 Existing technologies

Main existing technological and plant systems are strongly depending on the configuration used to apply thermal desorption: ESTD and ISTD, which definitions and general characteristics are given in the previous paragraph. While the fundamental principle is the same, heating solid matrix to volatilize organic compounds or mercury, the engineering design, process flow, and functional units differ significantly. A typical TD system consists of a thermal desorber, a vapor collection system, vapor treatment units, and a process control and monitoring system. Solids handling (excavation or dredging, charging and discharging once remediated) and the pre-treatment (screening, drying) of the polluted matrix are operations unit specifically considered for ESTD.

In ESTD applications, thermal desorber unit usually consists of a rotary kiln (indirectly heated or direct fired). It's a rotating, slightly inclined cylinder providing continuous conveyance and mixing; heat is transferred by conduction/convection from heated walls or hot gases to the solid matrix. Thermal desorber usually operates under slight negative pressure and is connected to a vapor conveyance ducting system that funnels volatilized compounds to the vapour treatment units (VTU), which can be composed of cyclones for particulate removal, multi-stage condensers (air or water cooled) to recover condensable organics and reduce vapor load, thermal oxidizers (direct fired) or catalytic oxidizers to destruct residual VOC/SVOCs, and activated carbon adsorption (fixed beds or dynamic systems) before release. Continuous emission monitoring of the specific volatile compounds, temperature monitoring and soil and product sampling ensure compliance and process monitoring and optimization (Vidonish et al., 2016; Zhao et al., 2019; Horst et al., 2021; Wang et al., 2021).

In ISTD applications, several alternative heating technologies have been applied using subsurface heating elements to heat soil. Contaminants are separated from soil and collected by the aboveground VTU. Technologies mostly used include:

- Steam Enhanced Extraction (SEE), transfers heat through convection by the water vapour or hot air injection into the contaminated area through wells. Three distinct zones are formed with increasing distance from the injection well, a steam zone, a variable temperature zone containing hot water, and an ambient temperature zone containing cool fluids;
- Electrical Resistance Heating (ERH), involves passing low-frequency (60 Hz) electrical current through subsurface. Based on Joule's law, this technology takes advantage of converting electrical energy into heat, aiming to increase temperature. Soil moisture is then converted to steam as the temperature increases, which strips the contaminants to the extraction well. In addition, a portion of the contaminants is directly vaporized as a result of an increase in their Henry's Law Constants. Moreover, heating-enhanced polishing mechanisms can occur during heating, such as hydrolysis, iron reductive dechlorination, or enhanced bioremediation;
- Thermal Conductive Heating (TCH), involves simultaneous applications of electrical or fuel-fired heaters and extraction wells. Target treatment areas are heated via thermal conduction and convection, and significant temperature gradients are created around each heater well. The highest temperature is in the immediate vicinity of the heater wells while lowest is at the midpoint between heater wells. Electricity, natural gas or diesel are common energy source for TCH; unlike ERH, in TCH the passage of current does not occur directly in the porous medium through electrodes but in local systems (such as heating pipes) that transfer heat to the ground;
- Radio-Frequency Heating (RFH), heats soil via dielectric heating. The frequency of electromagnetic waves in this treatment is generally between 1 and 27 MHz. The most common electrodes used include rod electrodes, parallel plate electrodes, and coaxial antennae.

ISTD relies on large installed electrical power (such as for ERH or electrical heaters in TCH) or on fuel for thermal burners. For electrical systems, grid integration, substations and power distribution are key cost drivers; for conductive or burner systems, fuel logistics and combustion control are essential (Ding et al., 2019; Horst et al., 2021; Wang et al., 2021; Falconi M. et al., 2025).

Several companies in Europe and Italy design and operate TD plants, as ESTD and ISTD. These include:

- TRS Group is an international thermal remediation developer whose portfolio includes electrical resistance heating (ERH), thermal conduction heating (TCH), and combined approaches for in-situ remediation. The combined technology TCH-ERH has practical implications for treating also PFAS: ERH for rapid power input and TCH for achieving higher localized temperature. TRS group has its headquarters in USA, but European market entry has been advanced through partnerships (i.e. application of TD in Belgium, Anderlecht, to remove DNAPL) (source: https://www.thermalrs.com/thermal-remediation-technology).
- Emgrisa, a Spanish company that has patented a mobile thermal desorption unit to heat soil to temperatures ranging between 90 ºC and 540 ºC. It consists of pre-treatment system, a revolving furnace where heat is applied directly or indirectly, and a gas treatment system to process particulates, condensate compounds and where the gases generated are oxidised at temperatures above 1000 ºC (source: https://www.emgrisa.es/en/publications/thermal-desorption).

- Haemers Technologies, a Belgian company patented a TD technology consisting of Smart Burners which are heating elements designed for Thermal Conductive Heating (TCH), in both in-situ and ex-situ configuration. Using small heating units (burners) connected to metal tubes put into the soil, the technology allows for the delivery of heat by conduction into the adjacent soil matrix; vapours are simultaneously extracted by a vacuum recovery network. In the different application of TD, the company used electrical-heaters or gas-fired heaters (remote-flame burners) as heating elements. In ISTD configuration heating elements and tubes are placed vertically into the soil, in ESTD configuration they are placed horizontally (source: https://haemers-technologies.com).
- Icaro Ecology, an Italian company involved as local operator/partner in large ISTD application, notably the Gela refinery project in collaboration with Haemers Technologies and with involvement from ENI. In this project, the Smart Burners technology was used to remediate the site heavily contaminated with hydrocarbons, chlorinated compounds and mercury. In that application the target temperature to achieve in the soil (in the monitoring points) was 250°C. The remediation system beyond the smart burners and heating tubes included a vapor extraction network and subsequent treatment units. Icaro Ecology is currently committed in the national context to promoting the application of TD via mobile plant, using the technology patented by Haemers Technologies (https://www.icaroecology.com/settori-di-intervento).

# 3.2 Concentrating Solar Power System

## 3.2.1 Overview

The European Solar Strategy and the European Green Deal aims to promote the use of renewable energy sources, among which solar energy has become one of the central pillars of decarbonization strategies (Molnár et al., 2024). Solar energy refers to the electromagnetic radiation emitted by the Sun that reaches the Earth's atmosphere and surface. When this radiation vector reaches ground level, it can be decomposed into components according to its path through the atmosphere: Direct Normal Irradiance (DNI), which is the component of solar radiation arriving in a straight line from the Sun, perpendicular ("normal") to the surface oriented towards the Sun; and Diffuse Horizontal Irradiance (DHI), or Diffuse Horizontal Radiation, which is that part of the radiation scattered by molecules, aerosols, clouds, and other atmospheric constituents, arriving from all directions of the sky vault (excluding the solar disk). The sum of the direct component projected onto a surface and the diffuse component gives Global Horizontal Irradiance (GHI) on a surface. Accurate knowledge of these irradiance components is critical for designing solar energy systems. Specifically, solar energy can be harnessed in two primary technical routes: the thermal route, by capturing sunlight and adsorbing and converting it into heat; and the photonic/photovoltaic route, by converting sunlight directly into electricity using semiconductor devices. From a technical point of view, photovoltaic systems are usually designed for converting Global or Diffuse Irradiance into electricity, while technologies such as concentrating solar power systems rely almost exclusively on Direct Normal Irradiance (Munawwar Khalil, 2023; Pourasl et al., 2023; Ahmad et al., 2024). The use of concentration systems is highly dependent on DNI, which intensity varies across the surface of the globe. Figure 5 shows the geographical coordinates where the annual DNI assumes higher

values, entailing a greater convenience of converting solar energy into thermal or electrical energy. North and South Africa, Australia and South America have the higher amounts of DNI; also, the southern part of Europe (such as Spain, Italy) has suitable values of DNI for the use of solar energy systems (Munawwar Khalil, 2023).

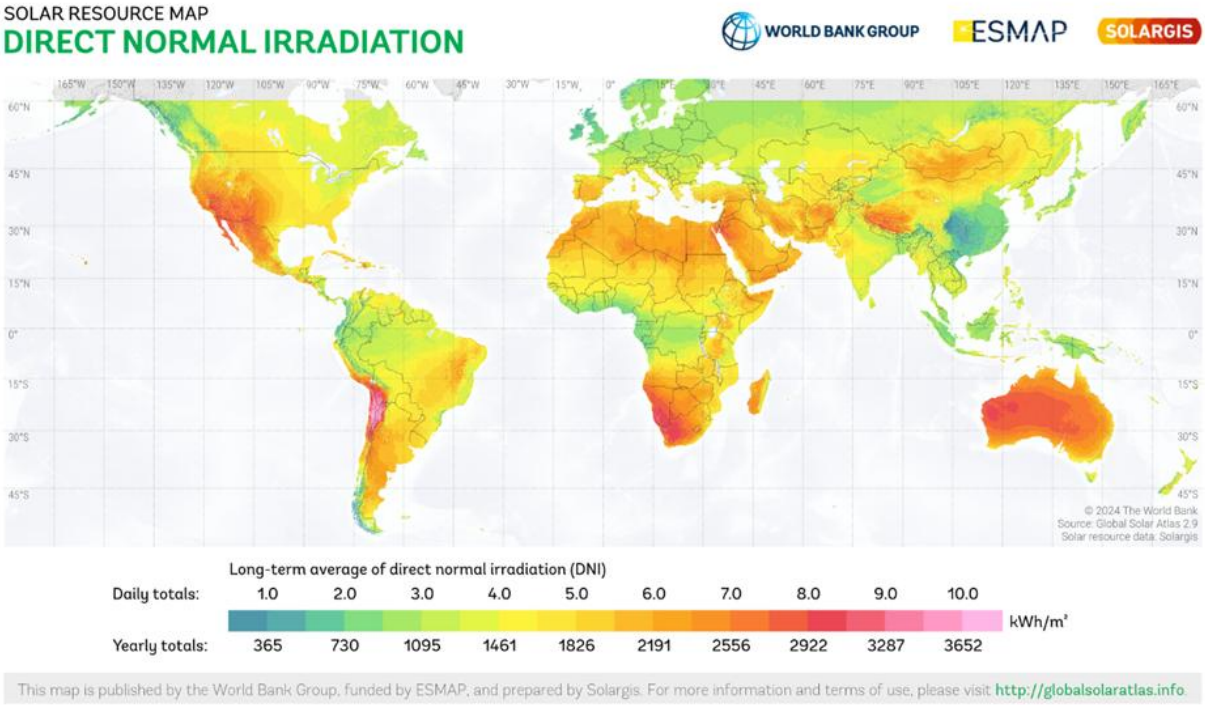


**Figure 5.** A world solar resource map of DNI (the long-term average of an annual sum and a daily sum in kWh/m$^2$). Source: Solar resource map © 2021 Solargis. (*https://solargis.com)*

Referring to concentrating solar power (CSP) technology, it focuses solar energy to produce high-temperature systems, suitable for applications like electricity generation and heat transfer process. Unlike PV and non-concentrating solar thermal systems, CSP achieves higher energy flux by concentrating a large energy surface onto a smaller one. CSP technologies (Figure 6) can be classified by the nature of their optical concentrator in terms of whether they focus onto a line (line-focusing systems) or onto a point (point-focusing systems). Line-focusing systems include parabolic trough collectors (PTCs) and linear Fresnel reflectors (LFRs). These systems concentrate incident sunlight in one dimension, with mirrors/tracks that focus light onto a receiver line (a tube), also called heating collector element (HCE) which contains the heat transfer fluid, HTF. Point-focusing systems include parabolic dish reflectors and solar power towers (central receivers using heliostat fields); these focus sunlight into a point (or small area) where very high flux densities and thus high temperatures can be reached. For CSP system, a fundamental parameter is the geometric concentration ratio, defined as the ratio of aperture area to absorber area, ranges from 10 to 150 for line-focusing systems and up to 2000 for point-focusing systems (Alami et al., 2023; Ferruzzi et al., 2023; Singh and Chandra, 2023).

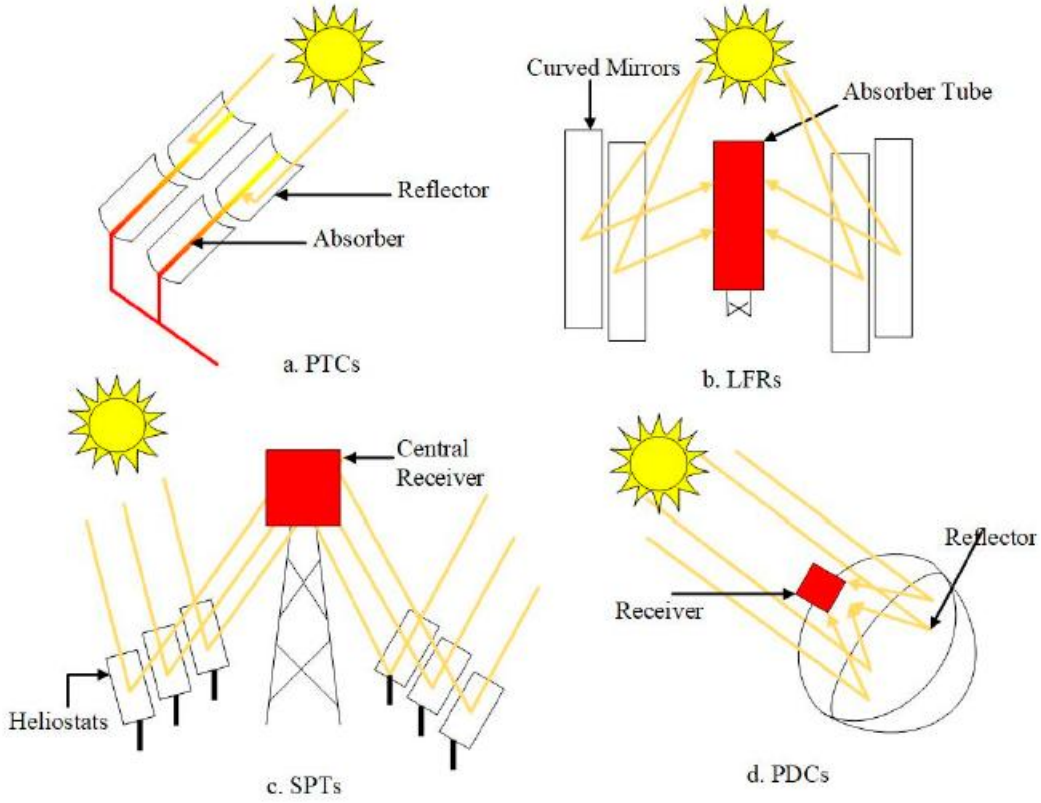


**Figure 6.** Types of CSP: a) Parabolic trough collectors (PTCs); b) linear Fresnel reflectors (LFRs); c) solar power towers (SPTs); d) parabolic dish collectors (PDCs) (Soomro et al., 2019**)**.

Parabolic Trough Collectors are among the most mature CSP technologies. A PTC uses a parabolic-shaped reflector to focus beam radiation (the DNI) onto an absorber pipe located at the focal point. Its design enables precise reflection of solar radiation onto the absorber, making it the most optically efficient among line-focusing systems. Efficiency depends on factors like reflector reflectivity, intercept factors, glass pipe transmissivity, absorber coating absorptivity, and reflector cleanliness. However, the curved mirror design increases costs compared to flat mirror systems, making economic considerations important. Key components of a PTC include its structure, mirror or reflector, receiver (glass envelope, absorber pipe, and bellow), and the working fluid that flows through the absorber pipe. The reflector or mirror in a CSP system directs incoming beam radiation to the absorber and is crucial for maintaining energy focus. Its shape (flat or curved) and material (silvered glass, aluminum, silvered polymer, or advanced solar reflective mirrors) vary based on the system design. Structural construction ensures the reflector maintains its focal point and withstands wind loads. Durability against weathering is essential, as the reflector operates outdoors and must remain effective under varying environmental conditions. The absorber pipe in a CSP system stores thermal energy and transfers it to the heat transfer fluid. It requires high thermal conductivity, robust mechanical strength to handle heat stress and pressure, and resistance to corrosion. While metals like copper, aluminum, and stainless steel are used, stainless steel could be preferred for its strength despite lower thermal conductivity. The choice of pipe depends on the heat transfer fluid, desired temperature, and pressure. A bellow connects the absorber pipe to the glass envelope, accommodating thermal expansion and providing support. However, bellows are prone to inter-granular stress corrosion cracking due to material susceptibility, environmental stress (humidity and temperature

changes), and welding-related stress (Yılmaz and Mwesigye, 2018; Kannaiyan and Bokde, 2022; Munawwar Khalil, 2023; Ahmad et al., 2024; Rodríguez Rodrigo et al., 2024).

For thermal energy-conversion, PTCs exhibit specific advantages. First of all, there is no intermediate thermodynamic cycle for electricity, avoiding Carnot limitations and cycle irreversibility, turbine losses, generator inefficiencies, etc. This means that more of the captured solar energy can be delivered as thermal energy. Second, PTCs allow more consistent integration of thermal storage compensating for the solar source's discontinuity: since the HTF is already in a fluid medium, storing heat in a molten salt or other storage medium can smooth out diurnal or transient variations. Also, cost reductions have been achieved by improving materials (mirror facets, receiver coatings, envelope materials), by optimizing geometric aspects (mirror segmentation, field layout, tracking precision), by improving thermal insulation and reducing optical losses (Bellos and Tzivanidis, 2018b; Singh and Chandra, 2023; Shokrnia et al., 2024).

Heat transfer working fluids transport thermal energy within the absorber pipe and significantly impact thermal and fluid dynamics performance. Choosing unsuitable fluids can lower outlet temperatures, reduce energy generation efficiency, and cause high-pressure drops, increasing energy usage. Each suitable fluid has its own temperature limit to be used in solar power plant and it is important not to operate beyond this value for safety and long-lasting operation. Common fluids include thermal oil, molten salt, water, gases, nanofluids and liquid metals, each with advantages and limitations depending on the application and temperature requirements:

- Thermal oils, a mixture of biphenyl and diphenyl, are widely used due to their affordability, thermal stability, low vapor pressure, and durability with proper maintenance. Disadvantages are referred to environmental contamination, danger of fire when leaks, hydrogen permeability. Thermal oils have been used in USA since the end of the 20th century, but the working temperature only reached 300°C (such as Therminol 55). New generation of thermal oils, such as Therminol VP1 and Syltherm 800, can reach 420°C. They are best suited for moderate temperature PTC systems.
- Molten salt, usually as eutectic mixtures of sodium nitrate, potassium nitrate, other nitrate or chloride salts, capable of operating at 500–600°C, enhances power plant efficiency and integrates thermal energy storage (TES) without requiring a heat exchanger between the solar field and TES. It offers high density, specific heat, thermal stability, and low vapor pressure, reducing pressure drops. It is no contamination and fire danger when leaking happens since it solidifies at ambient temperature. However, its high freezing point (around 240°C) poses challenges for long absorber pipes and fittings. Proper operation within the temperature limits is essential for safety and longevity. Disadvantages also include corrosiveness (salt mixtures can attack steel or other materials, especially at high temperature; materials selection must address corrosion, erosion, creep), higher specific viscosity at lower temperature (thus higher pumping energy especially when starting from cold or during transient operation), and sometimes chemical decomposition/stability issues at very high temperature.
- Water or pressurized water/steam can be used at lower to moderate temperature ranges. It has a lot of advantages as its heat capacity is very favourable and thermal properties are well known; heat transfer coefficients are high and operative and maintenance cost is low. For PTCs with moderate outlet temperatures, pressurized water or water with anti-freezing additives can be used. This system is not suitable for TES system since storing steam needs larger volume and condensation happens while steam transfers its energy to medium.

- Recently, compressed gases have also been considered as potential candidates for working fluids in CSP systems. They are non-flammable, environmentally safe, and capable of operating at high temperatures. However, their main drawback lies in their relatively low density (even after compression), which leads to higher pumping power requirements, low heat transfer coefficients, and significant pressure drops caused by the high velocities needed to compensate for the low density. Gases commonly used are nitrogen, carbon dioxide, air, helium, etc. In general, compressed gas is not suitable for PTC system due to high pressure drop, but it is a good fluid for solar tower.
- Nanofluids are used to enhance thermal properties. They are nano sized particles or additives (e.g. metal oxides, metals, carbon nanotubes) added to base fluids (molten salts, water, thermal oils). Studies showed that nanofluids can yield improvements in thermal efficiency, heat transfer coefficient, exergy efficiency, and reduced entropy generation in PTC configurations. Using nanofluids as HTF also imply drawbacks, such as potential stability issues due to agglomeration, settling of particles or erosion of tubes, thus increasing cost of fluid preparation or maintenance.
- Thanks to continuous progress in the field of research and development, emerging fluids have been investigated for PTC systems. Among these, silicone-based mixtures, ionic liquids, or even supercritical carbon dioxide can yield significantly higher thermodynamic efficiencies, but they still remain primarily at the research and development stage, as issues of compatibility, cost and large-scale reliability have yet to be resolved.

When selecting among these HTFs for a given PTC application, several parameters must be assessed: desired outlet temperature, continuous vs intermittent operation, need for thermal storage, ambient conditions, economic viability, safety and environmental impact. Thermal oils dominate medium-temperature industrial applications, molten salts underpin high-temperature plants with integrated storage system, water and steam remain viable for lower-temperature or niche cases, and nanofluids or advanced fluids point towards future improvements in performance (Bellos and Tzivanidis, 2018b; Olia et al., 2019; Abed et al., 2020; Giaconia et al., 2021; Kannaiyan and Bokde, 2022; Mhatre and Thakur, 2022; Alaidaros and AlZahrani, 2024; Anand and Kumar, 2024; Jebbar et al., 2024; Oketola and Mwesigye, 2024; Sathish et al., 2024).

In the design of PTC, many scientific studies today use numerical modelling as a preliminary evaluation of the process conditions to be implemented in real conditions. This approach is the basis of the design phase which is then followed by possible pilot tests. Specifically, modelling and simulation tools often allow designers to capture optical interception, conjugate heat transfer in the receiver, transient plant behaviour and control strategies before prototyping. Since these studies concern heat transfer models, they fall within the field of Computational Fluid Dynamics (CFD). CFD is a branch of fluid mechanics that uses numerical methods and algorithms to solve and analyze problems involving fluid flow. By discretizing the governing equations of fluid motion, such as the Navier–Stokes equations, continuity equation or energy equation, CFD enables the simulation of complex flow fields under realistic operating conditions. Modern CFD tools, such as ANSYS Fluent or OpenFOAM, allow researchers and engineers to capture detailed information about phenomena that would be extremely difficult or costly to obtain through experimental techniques alone. CFD has become a powerful framework for investigating heat transfer processes, since it can simultaneously resolve energy equations alongside momentum conservation. This makes it possible to study conduction, convection, and radiation in coupled systems, evaluate the thermal performance of

devices such as heat exchangers, solar collectors, and optimize geometries and operating conditions to enhance efficiency. In a recent study, Donga et al. (2025) combined SolTrace optics with 3-D ANSYS Fluent conjugate heat-transfer simulations to analyze finned absorber configurations and transient thermal fields in the design of an heating collector element of PTC (Donga et al., 2025). Javidan et al. (2023) used ANSYS Fluent to compare absorber-tube modifications (fins, turbulators, perforations) under different HTFs, including thermal oils such as Syltherm-nanofluids variants, demonstrating that simulation is key to trade off thermal efficiency gains versus oil temperature limits (Javidan et al., 2023).

# Chapter 4 - Experimental activities

The experimental work was divided in two main phases: laboratory activities to validate the high efficiencies of TD achievable to remediate the hydrocarbon contaminated solid matrix and conducted through a laboratory-scale plant, and modelling and simulation activities carried out using mathematical models and simulation software to assess the favourable conditions to implement a concentrating solar power system in a TD existing technology. This assessment was also referred to suitable geographical coordinates, and in particular in a place where exploitable solar radiation (the DNI) can guarantee the replacement of the TD power system in terms of energy contribution. Laboratory activities were conducted at the Sanitary Environmental Engineering Laboratory and at the Energy and Environment Laboratory of the University of Enna “Kore”. Modelling and simulation activities, coupled with the study of an existing thermal desorption technology, were conducted in Brussels at Haemers Technologies, a Belgian company known for having patented a particular TD process mainly based on Thermal Conductive Heating technology, as in-situ and ex-situ remediation treatment. In the following paragraphs is reported an in-depth description of both the laboratory activities, and those carried out at Haemers Technologies on the preliminary design of a TD treatment in which the energy supply comes from a Parabolic Trough Collector system.

## 4.1 Laboratory activities

As previously noted, the evaluation and validation of the high removal efficiencies achievable through thermal desorption of hydrocarbon-contaminated solid matrices were conducted at the University of Enna "Kore." The experimental activities encompassed the preparation and characterization of the contaminated matrix (before and after experimental tests), the execution of thermal desorption tests using a laboratory-scale plant, and the subsequent analysis of the results. This analysis enabled the establishment of correlations between thermal desorption removal efficiencies and the principal process parameters, namely treatment time and maximum heating temperature, defined for the specific contaminated matrix and in compliance with the national regulatory thresholds for hydrocarbons. In thermal desorption applications, and in particular, among Vapour Treatment Units (VTUs), an adsorption step on activated carbons is frequently used. For this reason, a specific phase of the experimental campaign was focused on the preliminary evaluation of an alternative adsorbent material (biochar) in compliance with the principles of the circular economy, as it is a solid waste from pyrolytic treatments.

### Material and methods

#### *4.1.1 Sediment characterization*

The solid matrix under investigation and experimental activities consisted of marine sediments collected from Sicilian port areas, which had previously been employed in other research activities (Lumia et al., 2020; Avona et al., 2022). Different sediment samples stored in a cold room were mixed to have a single homogenized sample to be characterized.

First characterization was carried out to analyse the concentration of TPHs and sediment moisture, fundamental characteristics for TD applications. Specifically, moisture was assessed using the ASTM D2216-80 method (with the AnD type-ML-50 analyser, Fig. 7), while TPHs concentration, expressed as $mg/kg_{DM}$, was assessed using the EPA 3545A method (pressurized fluid extraction) with

subsequent analysis with GC/FID. Specifically, starting from a quantity of 10,0 g of fine sediment (<2mm), previously dried in an oven at 40°C for 48 hours, the solid-liquid solvents extraction phase was carried out using the "BUCHI Speed Extractor E-916". Filters (0.45µm) were inserted at the upper and lower ends of each container to contain the sample inside it and ensure the release of only TPH, limiting the presence of impurities in the extracted solution. In particular, the extraction phase involved pressurized washing of the samples with organic solvents (acetone and n-hexane), allowing their transfer to the liquid phase. The extracted solution was loaded into the "BUCHI Syncore" evaporator, for the recovery of the pollutant and the removal of the extraction solvents. Following the solvent evaporation phase, the purification of the extracted contaminants in the liquid phase was performed using purification columns packed with "Florisil" and anhydrous sodium sulphate (Na2SO4) for their adsorbent properties towards water and inorganic substances. At the same time, using hexane, the eluate was filtered into 10 mL volumetric flasks. The purification procedure was concluded by bringing to the necessary volume with hexane. Therefore, after extraction, the necessary aliquot was taken for chromatographic analysis on the GC/FID "Agilent 6890N" (Figure 8).

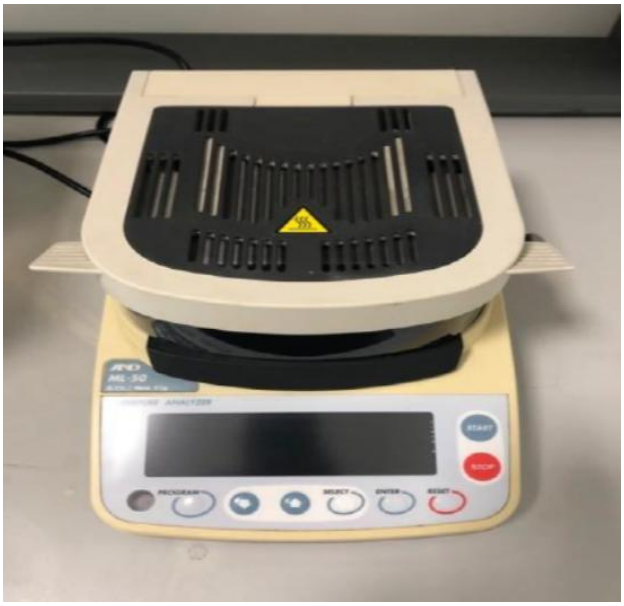

**Figure 7.** AnD mod. ML-50 moisture analyser.

**Figure 8.** GC-FID (Agilent 6890)

A granulometric analysis, assessed by ASTM D421-85 method, completed the characterization and highlighted the main presence of silt (67,3 %) and sand (29,7 %), while the clay fraction wasn't relevant (3%). Granulometric characterization and the Shepard ternary diagram (Shepard, 1954) shown in Figure 9, suggest that the sediment is sandy-silt type.

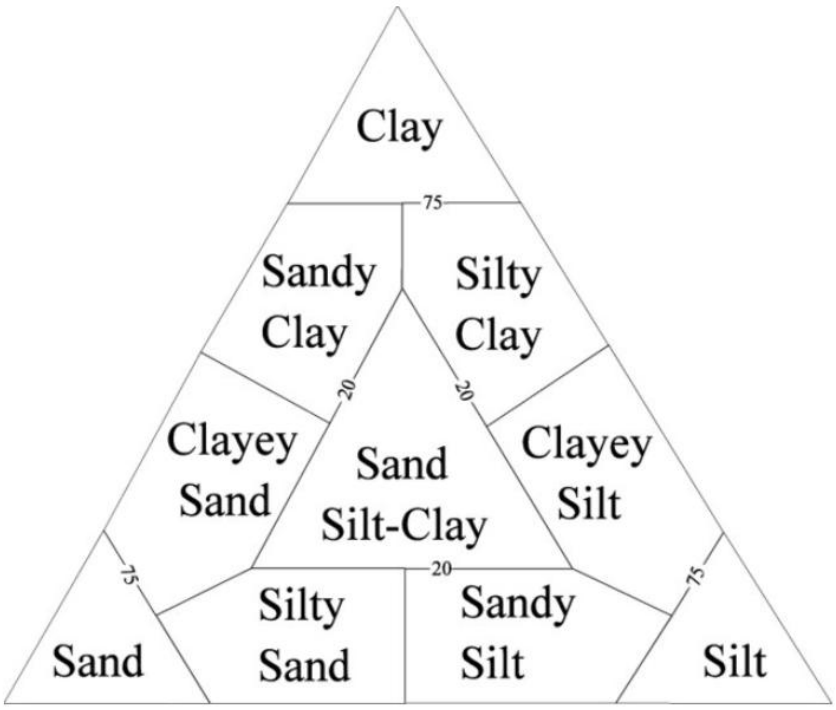


**Figure 9.** Shepard's ternary diagram for classifying sediment type.

From the results of the initial characterization, marine sediments had a hydrocarbon concentration of 787 $mg_{TPH}/kg_{DM}$, thus resulting in slightly higher than 750 $mg_{TPH}/kg_{DM}$ (Legislative

Decree n. 152/2006 threshold concentration for "sites for commercial and industrial use"). However, as several studies have demonstrated the effectiveness of TD for highly contaminated matrices (Bykova et al., 2021; Wang et al., 2023; Huang et al., 2025), it was decided to increase the hydrocarbons concentration through different artificial contaminations, by adding commercial diesel, in order to guarantee a significant TPHs contamination for the investigation. Further details of the contamination procedure are described in next paragraph.

### *4.1.2 Sediment contamination*

Before adding commercial diesel, sediment samples were sieved through a 2 mm mesh sieve, so as to proceed with fine fraction contamination. This choice, suggested by US-EPA in the document "*Thermal Desorption Technology Resource Guide*" and by several researchers, is basically depending on the strength of pollutants sorption in fine particles, thus influencing desorption dynamics under thermal treatment. In a nutshell, TD treatment of polluted fine fraction enhances contaminant removal efficiency, reduces treatment costs, and focuses remediation efforts on the portion of soil or sediment that presents the highest environmental risk (Zhao et al., 2019; Łyszczarz et al., 2021; Liu et al., 2022; US EPA and Innovation, 2022).

Hydrocarbon contamination was carried out in three distinct phases, by adding a known volume of commercial diesel (C13-C25), and a subsequent stirring phase, using a digital shaker "VWR Advanced Digital Shaker" (Figure 10) for a given contact time. In particular, in order to have different contamination levels, the sediment/diesel ratio of 500 g/80 mL (first contamination), 500 g/500 mL (second contamination) and 500 g/250 mL (third contamination) was used. Samples thus contaminated were stirred at a speed of 150 rpm for 60 days in the digital shaker. Once the mixing phase was completed, a filtration step was executed to remove the non-adsorbed diesel layer from the sediments. Finally, characterization was performed using EPA 3545A method and GC/FID analysis to evaluate the TPHs concentration obtained and the results are given in the table below.

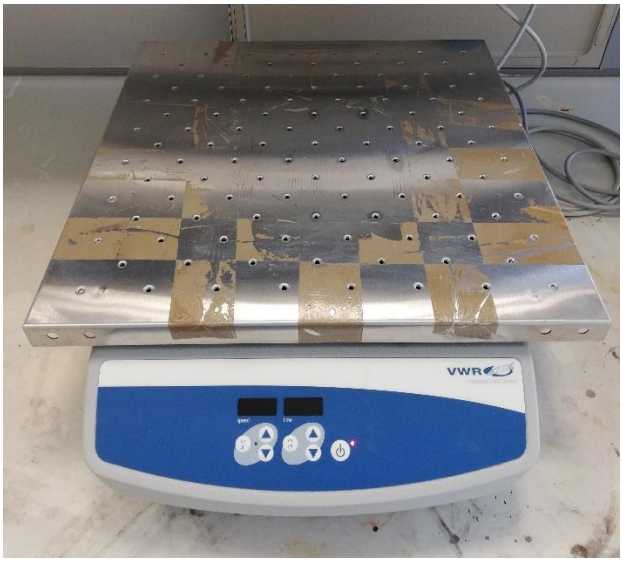


**Figure 10.** Digital shaker "VWR Advanced Digital Shaker"

**Table 1.** Characterization of artificially contaminated sediments

| | | |
|---|---|---|
| **First contamination** | | |
| Sediment mass | 500 | g |
| Total Volume of Diesel | 80 | mL |
| TPH concentration | **1336** | $mg_{TPH}/kg_{DM}$ |
| Moisture | 11,6 | % |
| **Second contamination** | | |
| Sediment mass | 500 | g |
| Total Volume of Diesel | 500 | mL |
| TPH concentration | **35011** | $mg_{TPH}/kg_{DM}$ |
| Moisture | 14,2 | % |
| **Third contamination** | | |
| Sediment mass | 500 | g |
| Total Volume of Diesel | 250 | mL |
| TPH concentration | **13182** | $mg_{TPH}/kg_{DM}$ |
| Moisture | 12,6 | % |

### *4.1.3 Experimental campaign*

As can be seen from Table 1, the contamination phase involved three distinct sediment samples with different levels of hydrocarbon contamination: low level for the first contamination, high level for the second and an intermediate contamination level for the third sample. The experimental campaign was developed in three phases, namely PHASE 1, PHASE 2 and PHASE 3, whose operating conditions are shown in Table 2. In the first two phases the performances of TD were compared as a function of the initial concentration of contamination, with the aim of evaluating the effects of the heating temperature in PHASE 1 and the sediment/heat source contact time in PHASE 2, for both low and high contamination levels (first and second contamination). The choice to proceed in this way was due to the need to identify the optimal thermal desorption process parameters for these marine sediments, which guarantee compliance with the limits established by national legislation, specifically the CSCs foreseen by Legislative Decree n. 152/2006, part IV, Table 1, columns A and B, Annex 5- Italian law, with reference to TPHs and equal to 750 $mg/kg_{DM}$ for "sites with an industrial or commercial use" (column B) and to 50 $mg/kg_{DM}$ for "sites with a residential, public, or green use" (column A).

**Table 2.** TD operating conditions during the three experimental phases

| EXPERIMENTAL PHASE | SEDIMENT MASS | TEMPERATURE | TIME OF CONTACT | GAS LINE |
|---|---|---|---|---|
| PHASE 1, 1st and 2nd contamination | 20 g | 200°C | 15 min | trap |
| | | 350°C | | |
| | | 500°C | | |
| PHASE 2, 1st and 2nd contamination | 20 g | 200°C | 10 min | trap |
| | | | 15 min | |
| | | | 20 min | |
| PHASE 3, 3rd contamination | 20 g | 200°C | 15 min | GAC + trap |
| | | | | BIOCHAR 1 + trap |
| | | | | BIOCHAR 2 + trap |

As described in the above table, thermal desorption tests carried out in PHASE 1 had the aim of evaluating removal efficiencies by varying the maximum heating temperature: 200°C, 350°C and 500°C and maintaining that temperature for a contact time of 15 minutes. Hydrocarbons removal efficiency or performance was calculated as a function of $C_0$ (initial TPHs concentration) and C (residual concentration), using the following equation:

$$RE = \frac{[(C_0 - C) \times 100]}{C_0}$$

Moreover, given that TD application in the low temperature range for hydrocarbons treatment has been proven to be convenient in several sector studies (Falciglia et al., 2011; Liu et al., 2019; Falciglia et al., 2020a; Ren et al., 2020; Park et al., 2025), and considering the results obtained (and discussed in the next chapter) in PHASE 1 of experimental campaign, during PHASE 2 the variation of contact time was related to maintaining a maximum heating temperature in the LTITD (Low Temperature Indirect Thermal Desorption) range and specifically equal to 200°C. Once in PHASE 1 and PHASE 2 the optimal heating temperature and contact time were found, these process parameters had been proposed again for the last phase, in which the focus was on the management system of pollutants desorbed from the solid matrix. During PHASE 1 and 2, energy consumption was monitored via digital wattmeter.

In the first two experimental phases, the heat treatment was coupled to a desorbed pollutant management system consisting of traps containing solvent, with the aim of condensing the off-gases downstream of the heating treatment, preventing their atmospheric dispersion. In PHASE 3, the off-gas management system involved not only condensing traps, but also the use of two innovative recovery matrices (BIOCHAR) to exploit the phenomenon of pollutants adsorption on a solid matrix, in the same way the activated carbons are usually used in real applications, thus in order to propose a simple and environmentally compatible technique for controlling gaseous discharges after thermal treatment, and to demonstrate that the re-use of these adsorbent materials is an innovative alternative to activated carbons. For these reasons, tests conducted in PHASE 3 involved the use of both biochar and granular activated carbons (GAC). More details about the setting of TD laboratory-plant and vapour treatment unit are provided in the following paragraphs.

### *4.1.4 Laboratory-scale plant and setup*

The experimental plant used to simulate Thermal Desorption was installed at the Energy and Environment Laboratory of the University of Enna “Kore”. It consists of a tubular furnace of the type (Split Furnace) with heating elements “SAFTherm SANTE FURNACE”, shown in Figure 11 and equipped with a quartz tube of 60 mm diameter and 800 mm long. The use of this type of system is widely disseminated in the literature, for example Liu et al., 2022 has conducted thermal desorption tests on contaminated soil using a quartz tube furnace (Liu et al., 2022), mostly extendable to an ex-situ treatment involving conductive heat transfer phenomena. The selection of process parameters in PHASE 1 and PHASE 2 and their experimental levels was also based on previous studies, mostly based on laboratory activities through tubular furnace in which the optimization of hydrocarbons removal performance was investigated in the same range of temperature selected in this work, and under other similar process conditions, e.g. the mass of sediment for each test, the carrier gas (Zivdar et al., 2019; Falciglia et al., 2020a; Ren et al., 2020; Sang et al., 2021).

The Split Furnace was equipped at the ends with gastight stainless-steel flanges for the control of the internal atmosphere and the flushing of specific carrier gases, specifically inert gases such as nitrogen, which allowed to maintain an inert atmosphere and to transport the desorbed fumes and vapours outside the quartz tube.

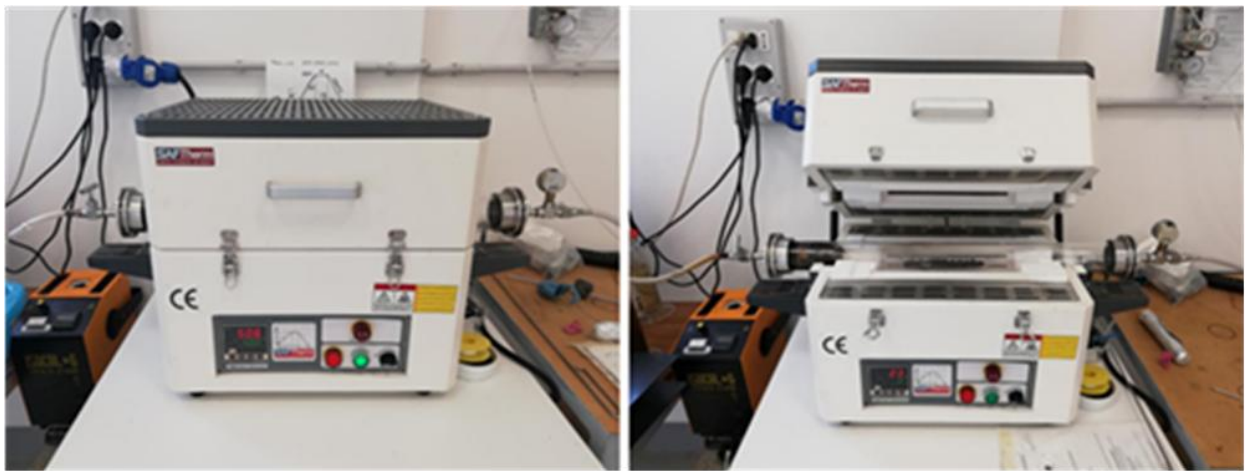

**Figure 11.** Experimental set-up SAFTherm SANTE FURNACE with 60 mm diameter quartz tube

The sediment samples (approx. 20,0 g of grain size < 2 mm with the water content shown in Table 1) were placed in the middle of the tube inside a quartz boat. From one end of the quartz tube, nitrogen was fluxed at a constant flow rate of 1,5 L/min. The opposite end of the quartz tube was appropriately connected to the off-gas recovery/management system. As previously mentioned, in PHASE 1 and PHASE 2 of experimental campaign, the system consisted of two cold traps for the condensation of VOCs (maintained at a temperature of 4°C, with a water and ice bath), containing a known volume of iso-propanol and showed in Figure 12. At the end of each test, 10 mL aliquot of iso-propanol was taken from the traps for the subsequent VOCs evaluation using the GC/MS analysis. As already mentioned in the previous paragraph, during PHASE 3, Pyrex columns packed with adsorbent material (Figure 13) were added to the traps already used in the previous phases. The traps were placed in series with the adsorption columns and each column had a net volume of approximately 0,35 L. During PHASE 1 and 2, energy consumption was monitored via digital wattmeter.

**Figure 12.** Cold traps for off-gas management

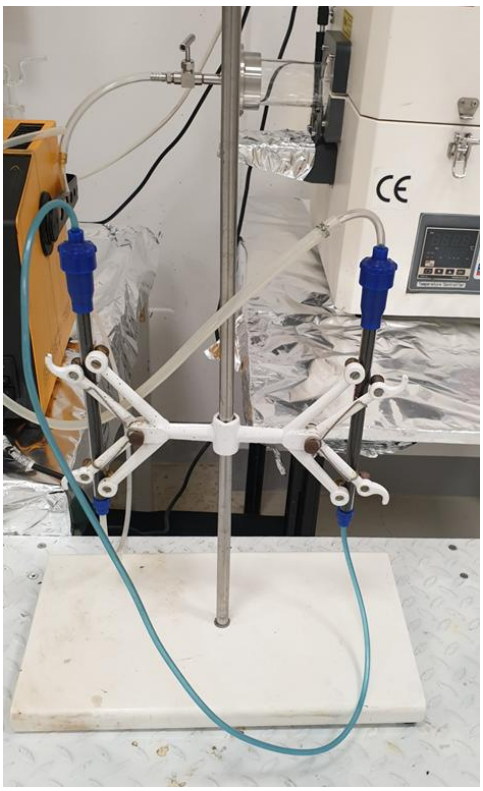

**Figure 13.** Packed columns with adsorbent material

The flow diagram of the treatment system, from the transport carrier to the off-gas measurement and control system is shown in Figure 14.

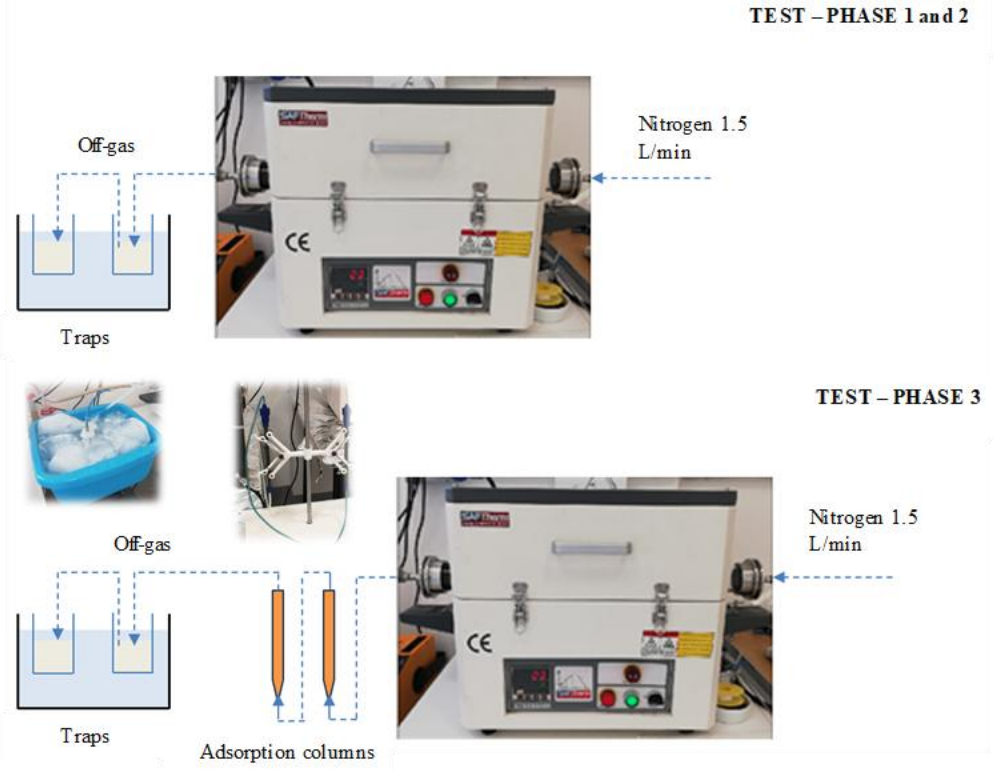


**Figure 14.** Representative diagram of the lab-scale plant, connected downstream with the off-gas management system.

Each TD test was performed by setting specific heating ramps, i.e. individual segments or work steps of the tubular furnace obtained by setting heating times and temperatures. In general, the work steps considered were the following:

- heating from room temperature (around 20°C) to 105°C for the removal of residual humidity;
- constant maintenance of the drying temperature at 105°C for 20 minutes;
- heating up to the maximum temperature expected for each test, to be reached in 5 minutes;
- maintenance of the maximum design temperature for the pre-established desorption time;
- interruption of heating once the design desorption time at the maximum temperature has elapsed (furnace shutdown and end of test).

The heating ramps for the PHASE 1, 2 and 3 tests are shown in Figure 15.

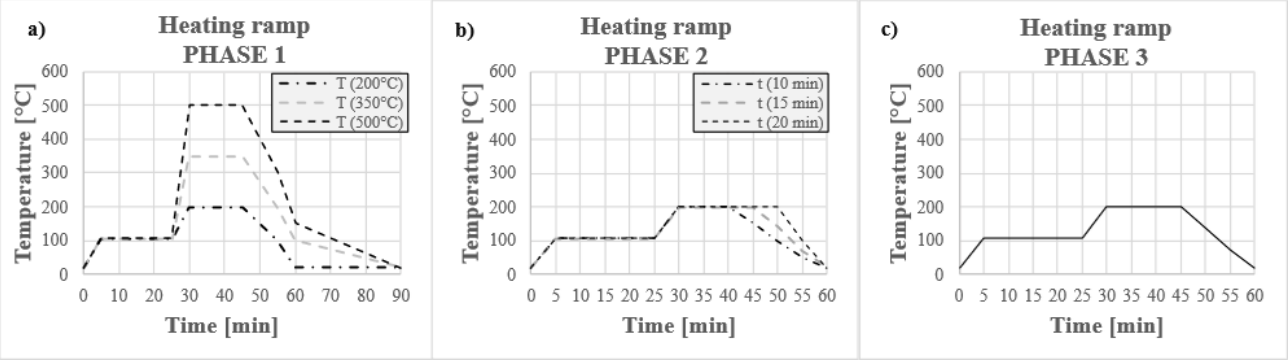


**Figure 15.** a) heating ramps as the temperature varies (PHASE 1); b) heating ramps as the contact times vary (PHASE 2) c) heating ramp for adsorbent material tests (PHASE 3).

## *4.1.5 Characteristics of adsorbent materials*

Adsorbent materials used to fill the adsorption columns in PHASE 3 are shown in Figure 16. The biochars used as innovative solution for the off-gases adsorption were provided by the University of Palermo. The two types of BIOCHAR, called B440 and B880, were obtained from the pyrolysis of tree species such as pine and eucalyptus. They had different characteristics, such as their granulometry size. B440 was characterized by particles with smaller dimensions than B880, which was made up of particles with a more rounded and coarse shape (>2mm). Further information on their characteristics is given in Table 3. Adsorbent columns were filled with GAC and with BIOCHAR B440 and B880 respectively. The columns were completely packed to fill the entire available volume (with variable masses of the adsorbent, depending on the individual specific density). Considering the different dimensional characteristics of the tested adsorption materials, the columns filled with activated carbons contained (both) approximately 6,0 g, while during the tests conducted with BIOCHAR the columns contained 4,5 g of B440 and approximately 2,0 g for B880.

At the end of each test, the adsorption capacity of biochars and GAC was assessed through the measurement of TPHs adsorbed directly in the studied matrices using the EPA 3545A method (pressurized fluid extraction) and subsequent analysis with GC/FID. To determine the effectiveness of thermal desorption experiments and the surface functionalities for B440 and B880, FTIR analysis was carried out using a Shimadzu IR Tracer spectrometer in mid-IR mode, equipped with a Universal ATR sampling device containing diamond/ZnSe crystal. The spectra were recorded in the range from 600 to 4000 1/cm, with a resolution of 4 1/cm, by averaging 64 scans, the spectra were baseline corrected and normalized.

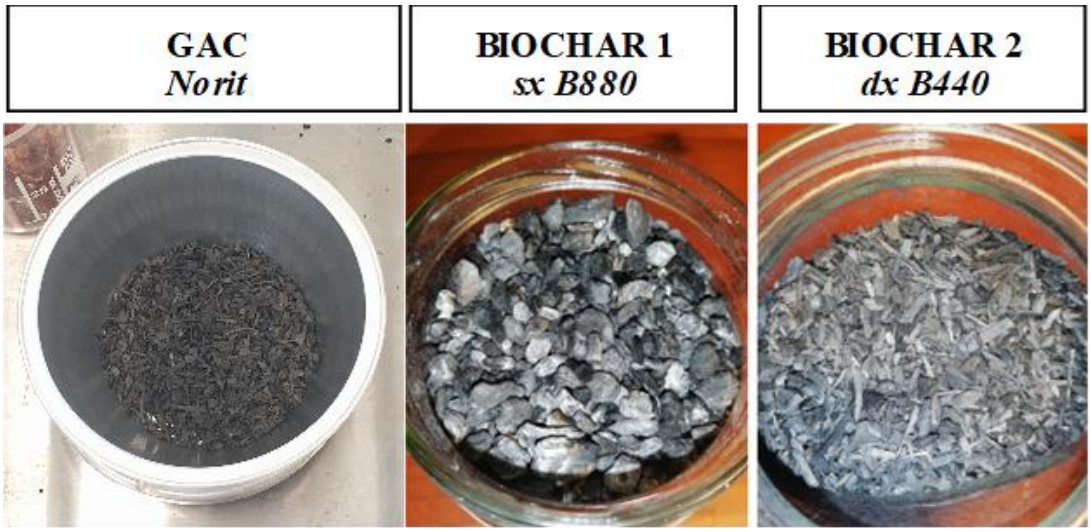


**Figure 16.** Adsorbent material used in PHASE 3.

**Table 3.** Characteristics of the tested biochars and GAC.

| Parameters | U.M. | GAC (Norit) | B880 | B440 |
|---|---|---|---|---|
| pH | - | 8 | 10 | 9 |
| moisture | % | 3,9 | 6,7 | 3,1 |
| bulk density | g/L | 176 | 63 | 125 |
| Total pore volume | $cm^3/g$ | 95 | 51 | 38 |
| Surface area | $m^2/g$ | 279 | 227 | 164 |
| Electric conductibility | dS/m | / | 2.0 | 1,3 |
| Ashes at 550°C | % | 8 | 6,4 | 3,4 |
| Total carbon (TC) | % | / | 72 | 65 |
| Total nitrogen (TN) | % | / | 0,3 | 0,3 |

# 4.2 Modelling and Simulation approach

The second part of the experimental activities of the thesis work concerned the implementation of a solar concentration system suitable for a thermal desorption process. Since experiments are very expensive, some researchers are more interested in theoretical studies (Agagna et al., 2018). For this reason, the development of the innovative and sustainable system was conducted through modelling and simulation activities, mainly based on heat transfer phenomena, therefore falling into the CFD branch. Initially focusing on the study of heat transfer phenomenon by the PTC (Parabolic Trough Collector) to HCE (Heat Collector Element) and then to TD system, design choices were then made referring to the characteristics of an existing thermal process and different design hypotheses. Being the scope of this thesis work on the power system using renewable sources, the vapor treatment system was not considered in this experimental phase. Following paragraphs provide a detailed description of these activities, also including geometric models that have not been tested mainly due to problems related to the limited version of the CFD software used, although hypotheses and simplifications have made it possible to overcome the problem.

# Materials and methods

## *4.2.1 Reference TD process*

A target parameter in the selection of the geometrical model is the energy requirement to be converted into heat transferred to the polluted soil. To fix some key parameters of TD process, the main reference for the development of this work was the Thermal Conductive Heating (TCH) technology patented by Haemers Technologies. It involves the use of metal heating tubes and vapour extraction tubes distributed throughout the treatment zone, which has to be appropriately insulated. Heating tubes can be placed either in a vertical or horizontal configuration. Vapour extraction tubes are connected with the Vapour Treatment Unit (VTU), whose treatment chain may vary depending on the application and target contaminants. Contaminants need to be exposed to target temperatures sufficiently long to guarantee their effective treatment. The equipment required for the successful implementation of TCH typically encompasses:

- heaters, generating the necessary heat for the process;
- temperature sensors and control panels for temperature monitoring and control;
- vacuum pumps and extraction wells for the extraction of contaminants;
- monitoring probes and data loggers to assess heat distribution/monitor;
- thermal blankets to trap heat and enhance the heating process efficiency;
- barrier systems around the treatment zone to contain and control the flow of vapour.

Referring to this TD process, it was considered a typical application case for a certain volume of soil contaminated by hydrocarbons, with implementation of the process as ISTD, i.e. assuming the vertical arrangement of the heating elements connected with the renewable energy supply system in the form of thermal energy (Falconi M. et al., 2024, 2025).

## *4.2.2 Heat transfer phenomena*

To assess the efficiency of a solar collector system and the effectiveness of soil remediation process, several physical phenomena have been studied, mainly based on heat transfer. Specifically, heat transfer phenomena were first referred to the optical and thermal efficiency, i.e. the amount of radiation absorbed by the receiver and the transfer efficiency of the incident radiation to the HCE (then to the HTF), and secondly to the heat transfer from the HCE to the heating tubes placed in the soil to allow the reaching of the target temperature. Since PTC technology is already quite consolidated in terms of optical efficiency range, i.e. thanks to the materials used and the biaxial solar ray tracking system which maximizes the rate of incident radiation in the receiver, the main dependence for radiation intensity can be referred to the geographical coordinates.

In general, the governing equations of fluid flow and heat transfer can be considered as mathematical formulations of the conservation laws of fluid mechanics: continuity equation (the principle of mass conservation), energy equation (considering incompressible Newtonian fluids) and Navier-Stokes or momentum equations (referring to conservation of momentum for viscous fluid). These equations are shown below in compact form.

Continuity equation:

$$\partial\rho/\partial t + \nabla \cdot (\rho\, u) = 0$$

- $\rho$: fluid density [kg/m$^3$];

- t: time [s];
- u: velocity vector of the fluid [m/s];
- $\nabla \cdot (\rho\, u)$ : divergence of the mass flux, representing the net outflow of mass per unit volume.

This equation states that the rate of change of mass in a control volume plus the net mass flux out of the volume is zero. It expresses the principle of conservation of mass. For incompressible fluids $\rho$ becomes constant and it reduces to:

$$\nabla \cdot u \;=\; 0$$

Energy equation:

$$\rho\, cp\, (\, \partial T/\partial t \;+\; u \cdot \nabla T\, ) \;=\; \nabla \cdot (k\, \nabla T) \;+\; \Phi \;+\; \dot{q}$$

- $\rho$: fluid density [kg/m$^3$];
- cp: specific heat at constant pressure [J/kg*K];
- T: temperature field [K];
- $\partial T/\partial t$: transient (local) temperature variation;
- $u \cdot \nabla T$: convective heat transport (temperature change due to fluid motion);
- $\nabla \cdot (k\, \nabla T)$: conductive heat transfer, with k the thermal conductivity [W/m*K];
- $\Phi$: viscous dissipation term;
- $\dot{q}$: volumetric heat generation term (e.g., due to radiation absorption, chemical reactions, or imposed heat sources).

This equation expresses the first law of thermodynamics for a moving fluid: the rate of change of thermal energy equals the sum of conduction, convection, viscous dissipation, and heat sources.

Navier–Stokes Equations (Momentum Conservation):

$$\rho\, (\, \partial u/\partial t \;+\; (u \cdot \nabla) u\, ) \;=\; -\nabla p \;+\; \mu\, \nabla^2 u \;+\; \rho\, g \;+\; F_{ext}$$

- $\rho$: fluid density [kg/m$^3$];
- u: velocity vector [m/s];
- $\partial u/\partial t$: local acceleration term (variation of velocity with time at a fixed point);
- $(u \cdot \nabla) u$: convective acceleration (variation of velocity due to motion in space);
- $-\nabla p$: pressure gradient force per unit volume [N/m$^3$];
- $\mu\, \nabla^2 u$: viscous diffusion term (momentum transport due to viscosity);
- $\rho\, g$: body force per unit volume due to gravity vector;
- $F_{ext}$: other possible external forces (e.g., electromagnetic, inertial).

It represents the mathematical form of Newton's second law applied to fluids: the rate of change of momentum of a fluid element equals the sum of the forces acting on it (pressure, viscous stresses, body forces).

To solve this system of equations, it is necessary to use numerical methods and discretization methods. By enforcing these conservation laws over discrete spatial volumes in a fluid domain, it is possible to achieve a systematic account of the changes in mass, momentum and energy as the flow crosses the volume boundaries. In other words, by dividing the computational domain into a collection of control volumes or cells, the partial derivative equations are integrated in each control volume, resulting in discrete equations that relate the average values of the flow variables (such as

velocity, pressure, and density) within each cell. This method is referred as Finite Volume Method (FVM) and resolution of these equations in each time-step or control volume is entrusted to iteration operations in CFD software, such as Ansys Fluent.

Moreover, when turbulent flows occur (depending on Reynolds number), it is necessary to relate continuity, energy and momentum equations to a turbulence numerical model: Direct Numerical Simulation (DNS), Large Eddy Simulation (LES) or Reynolds Averaged Navier-Stokes (RANS) model. The first two guarantee high accuracy on defining turbulence features, but they require excessive computations, while RANS model is the most used in industrial and environmental application, it requires stochastic model to generate instantaneous fluctuations and allows to evaluate averaged velocities and turbulent features in the referred control volume.

RANS equations:

$$\rho\,(\,\partial\bar{u}/\partial t\,+\,\bar{u}\,\cdot\,\nabla\bar{u}\,)\,=\,-\nabla\,\bar{p}\,+\,\mu\,\nabla^2\bar{u}\,+\,\nabla\,\cdot\,(-\rho\,\overline{u}'\,\overline{u}')\,+\,\rho\,g$$

- $\nabla\,\cdot\,(-\rho\,\overline{u}'\,\overline{u}')$: divergence of Reynolds stress (turbulent term), given by the correlation between velocity fluctuations;
- $\bar{u}$: Reynolds-averaged velocity vector;
- $\bar{p}$: Reynolds-averaged pressure;

Using Boussinesq closure for Reynolds stress:

$$-\rho\,\overline{u}'\,\overline{u}'\,=\,\mu\_t\,(\,\partial\bar{u}\_i/\partial x\_j\,+\,\partial\bar{u}\_j/\partial x\_i\,)\,-\,2/3\,\rho\,k\,\delta ij$$

- $\mu\_t$: turbulent (or eddy) viscosity;
- k: turbulent kinetic energy;
- $\delta ij$: Kronecker delta.

To calculate turbulent viscosity is required a turbulent model such as k–ε model (Menter, 1994), used when there are wall effects present within the model and which presents a set of transport equations for k, ε and $\mu_t$ evaluation:

Transport equation for k:

$$\partial(\rho\,k)/\partial t\,+\,\nabla\,\cdot\,(\rho\,\bar{u}\,k)\,=\,P\_k\,-\,\rho\,\varepsilon\,+\,\nabla\,\cdot\,[\,(\mu\,+\,\mu\_t/\sigma\_k)\,\nabla k\,]$$

- $P_k$: production of turbulent kinetic energy;
- $\sigma_k$: model constant = 1

transport equation for ε:

$$\partial(\rho\,\varepsilon)/\partial t\,+\,\nabla\,\cdot\,(\rho\,\bar{u}\,\varepsilon)\,=\,C\_\varepsilon 1\,(\varepsilon/k)\,P\_k\,-\,C\_\varepsilon 2\,\rho\,\varepsilon\text{^}2\,/\,k\,+\,\nabla\,\cdot\,[\,(\mu\,+\,\mu\_t/\sigma\_\varepsilon)\,\nabla\varepsilon\,]$$

- $C_{\varepsilon 1}$, $C_{\varepsilon 2}$, $\sigma_\varepsilon$: model constants respectively equal to 1.44, 1.92, 1.3.

$\mu_t$:

$$\mu\_t\,=\,C\_\mu\,k^2\,/\,\varepsilon$$

- ε: turbulent dissipation rate;
- $C_\mu$: standard constant = 0.09

Finite Volume Method (FVM) and the resolution of these equations in each time-step or control volume is entrusted to iteration operations in CFD software, such as Ansys Fluent. In particular, heat flux distribution and temperature evolution will be performed by solving continuity, energy and momentum equation in turbulent regime (requiring turbulence model, such as k-Ɛ model from RANS equations) involving several thermophysical fluids properties (such as water, HTF). Turbulent flow is assessed by Reynolds number; generally, it quantifies the ratio of inertial to viscous forces and determines the flow regime. For internal flows, Re > 4000 is commonly regarded as turbulent.

$$Re = \frac{\rho U D}{\mu}$$

- D: hydraulic diameter;
- U: velocity vector;
- μ: dynamic viscosity.

In this thesis work Ansys Fluent was used as CFD software. To account for turbulent flows in heat transfer process, turbulent models are implemented in software for simulations, as shown by the following figure.

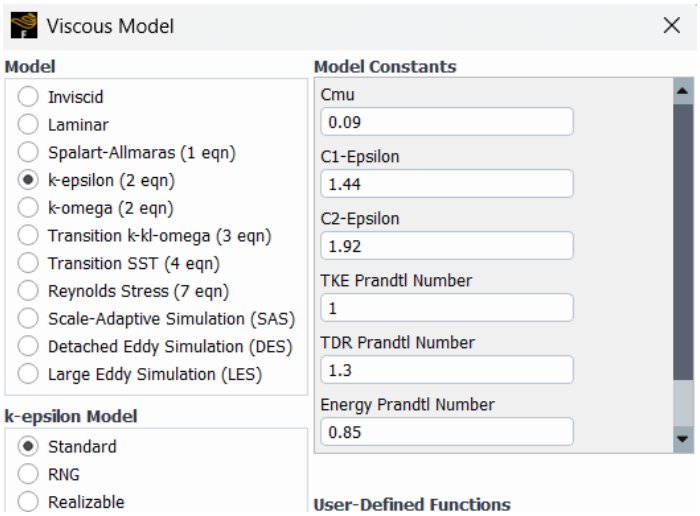


**Figure 17.** Selecting turbulent model window in Ansys Fluent,

The design parameter to be defined is mainly the PTC surface area necessary for each heating tube to satisfy the required energy amount to treat polluted soil. In the present work, Therminol-VP1 is adopted as the HTF due to its favourable thermophysical properties in the temperature range relevant to hydrocarbons thermal desorption applications. In PTC technology, parabolic mirrors/reflectors concentrate the direct normal irradiance onto an absorber tube consisting of outer glass shield tube and an inner copper or steel tube, where the HTF flows and is heated through the balance of absorbed radiation, convective heat transfer, and thermal losses. In this way, solar energy is transformed in thermal energy. The thermal energy carried by the HTF is subsequently transferred to heating tubes vertically placed in a contaminated soil domain, with the objective of raising soil temperature to the values that enhance contaminant volatilization and remediation processes. This governing thermal process can be described by the following energy balance equation, which in differential form is:

$$\dot{m}\, cp\, dT/dx \;=\; q''in\, \pi\, Di \;-\; q''out\, \pi\, Do$$

- $\dot{m}$: mass flow rate of the heat transfer fluid [kg/s];
- $c_p$: specific heat capacity of the fluid at constant pressure [J/(kg*K)];
- $dT/dx$: axial temperature gradient of the fluid along the tube [K/m];
- $q''in$: incoming heat flux per unit surface area [W/m²], can represent heat absorbed from the solar collector or heat transferred from the fluid to the heating tube in soil;
- $D_i$: inner tube diameter [m];
- $\pi D_i$: internal perimeter (surface available for heat transfer per unit tube length) [m];
- $q''out$: heat flux lost from the tube to the surroundings [W/m²], can represent heat lost from outer tube of the HCE to the environment or heat transferred from the heating tube to the soil;
- $D_o$: outer tube diameter [m];
- $\pi D_o$: external perimeter [m];

To maximize overall efficiencies, several assumptions have been made to overlook negative energy contributions (heat losses). These hypotheses will be discussed in the paragraph 4.2.5 '*Basic assumptions*'. Instead, the evaluation of heat absorbed from the solar collector is referred to Direct Normal Irradiance (DNI) expressed in W/m$^2$, the identification and processing of which is discussed in the next paragraph.

### *4.2.3 Geographical coordinates selection*

Evaluation of solar data is carried out using Solcast API tool (https://solcast.com). The possibility of free registration as a doctoral student was useful in order to have access to a DNI database referring to the desired geographical coordinates. This software allows to have a big database referred to several years of solar data with different time-step. Available data involve not only DNI but up to 20 different parameters (such as air temperature, GHI, wind speed, etc..). The geographical coordinates chosen were referred to the city of Gela. As is well known, in 2000, the Italian Ministry of the Environment designated 795 hectares in land and 4560 in sea within the territory of the municipality of Gela as SNI (Site of national interest). The subsequent characterization of the area pointed out a severe state of contamination, including hydrocarbons pollution (Re et al., 2019). In addition to its industrial history, Gela is characterized by high solar radiation intensity and duration. This substantial solar resource makes it an ideal candidate for solar energy applications, such as Concentrating Solar Power plants. In Solcast API tool, Gela coordinates were selected as coordinates (lat. 37,07; long. 14,24) and DNI and air temperature with a time granularity of 60 minutes, for a reference time of 10 years, from 1$^{st}$ January 2015 to 1$^{st}$ January 2025, in order to have a huge database of solar data. These steps are shown in Figure 18 and 19.

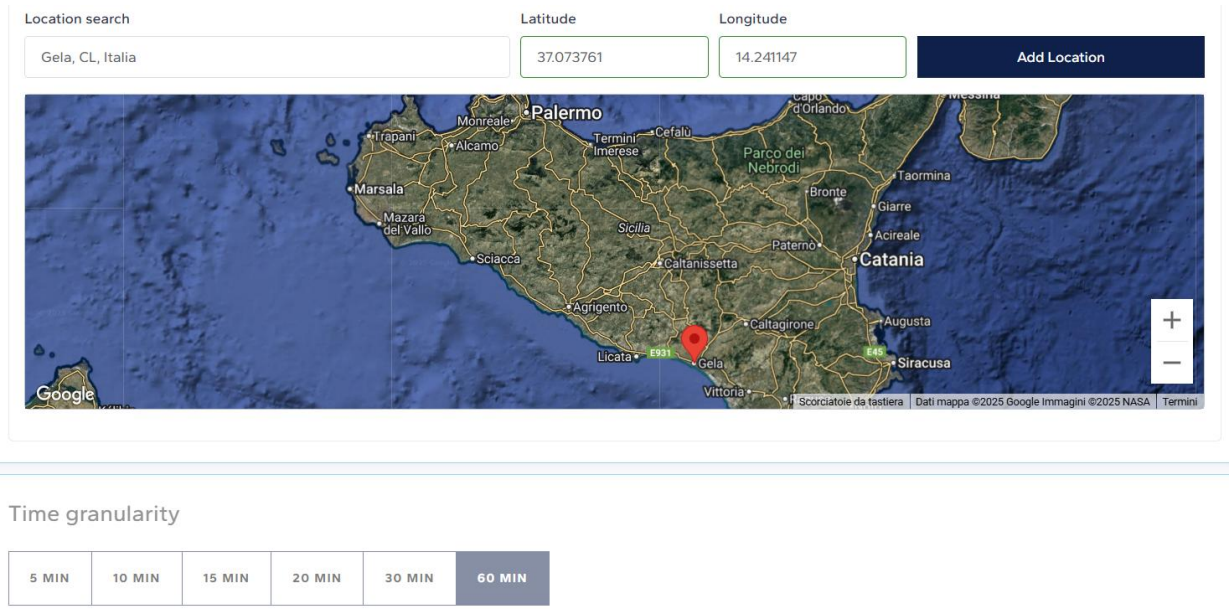


**Figure 18.** Coordinates selecting in Solcast API tool (https://toolkit.solcast.com /historical/timeseries/request).

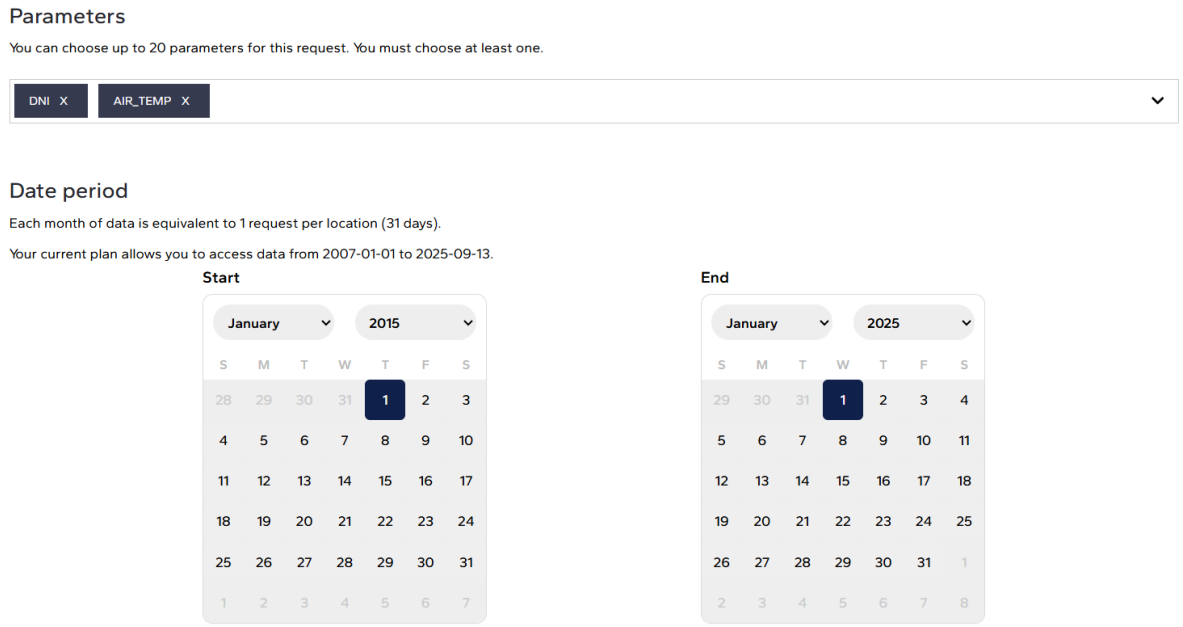


**Figure 19.** Parameters and reference period selecting in Solcast API tool.

Within the ten years of DNI data, only 6 months of hourly DNI data were selected for simulations. The following graphs show the daily DNI values for Gela coordinates referring to two different periods of the year randomly taken. The random variation in solar radiation, commonly detected via pyranometer or solarimeter, is strongly influenced by the presence of clouds and obstacles that lead to an intensity reduction at the pyranometer, as demonstrated by the graphs in the Figure 20.

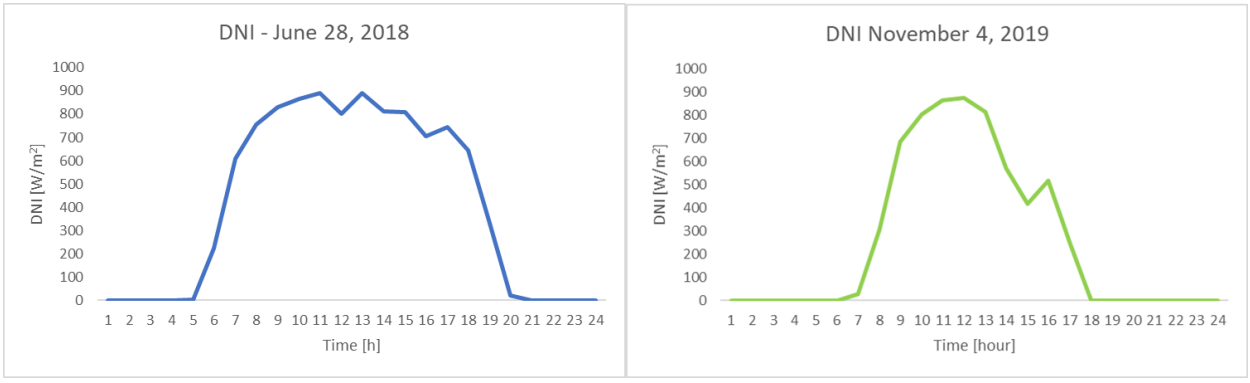


**Figure 20.** Daily pattern of DNI in Gela, example in summer and autumn season.

Even if Ansys Fluent provides the possibility of using solar radiation models, such as S2S (surface to surface) model or Montecarlo model, in this work solar radiation data were considered for simulations through a particular code implemented in C, a high-level programming language widely used for scientific and engineering applications (although now replaced by more recent programming languages). This code generated a specific User-Defined Function (UDF) to be used in ANSYS Fluent. A UDF is a custom function that allows the user to extend or modify the default capabilities of the solver. UDFs can be used to define custom boundary conditions, source terms, material properties, or complex user-specific models, enabling the simulation of physical phenomena that are not available through the standard Fluent models. More details about the UDFs used to customize the simulations can be found in paragraphs '*Basic assumptions*' and '*Numerical simulation*'.

### *4.2.4 Geometrical models*

Geometrical model for subsequent simulations was created and meshed using Gambit, a specific software and alternative solution to Ansys Workbench, in which geometry can be modelled using ANSYS Design Modeler or ANSYS SpaceClaim. Gambit's operating principle remains identical but less automated in the creation of geometric models to have control of every single node created in the geometric model. Initially, geometry was referred to a complete 3D model consisting of the solar concentration system, the PTC, and a soil volume in which the heating pipes are placed in a vertical configuration. Geometry was discretized with a structured multi-block mesh. After meshing, the subsequent step was to specify cell zone conditions (discretising solid and fluid). With reference to current applications of TCH process patented by Haemers Technologies, a plant configuration of the heating elements referring to previous real applications was used. Specifically, heating tubes with a length of 10 meters were modelled, with reference to the configuration in which the inter-distance between the heating elements is equal to 1,5 meters. In mostly Heamers Technologies applications this parameter varies between 1-3 meters. In addition, reference was made to a typical case of TD for the remediation of soils contaminated with hydrocarbons, in which the design temperature to be reached at specific points of monitoring (at the centre of the triangle formed by three heating tubes, called cold points) in the soil volume is typically 250°C (Falconi M. et al., 2025).

In this case, the heating tube isn't connected to the Smart Burners but it consists of a circular outer well and an inner tube in which flows the HTF. Inner tube was modelled with a geometrical configuration that is usually associated with geothermal systems, i.e. energy storage in the soil, and it's called Borehole Thermal Energy Storage (BTES). Several tube configurations are utilized in

BTES systems, including single U-shaped, bent U-shaped, parallel double U-shaped, series double U-shaped or multi-U-shaped. In this work, a multi-U-shaped tube (Figure 23) configuration was selected (Baser and McCartney, 2015; McCartney et al., 2017; Tinti et al., 2023; Anna Hammerstingl, 2024). The complete geometric model and its mesh are shown in the Figure 21 and Figure 22.

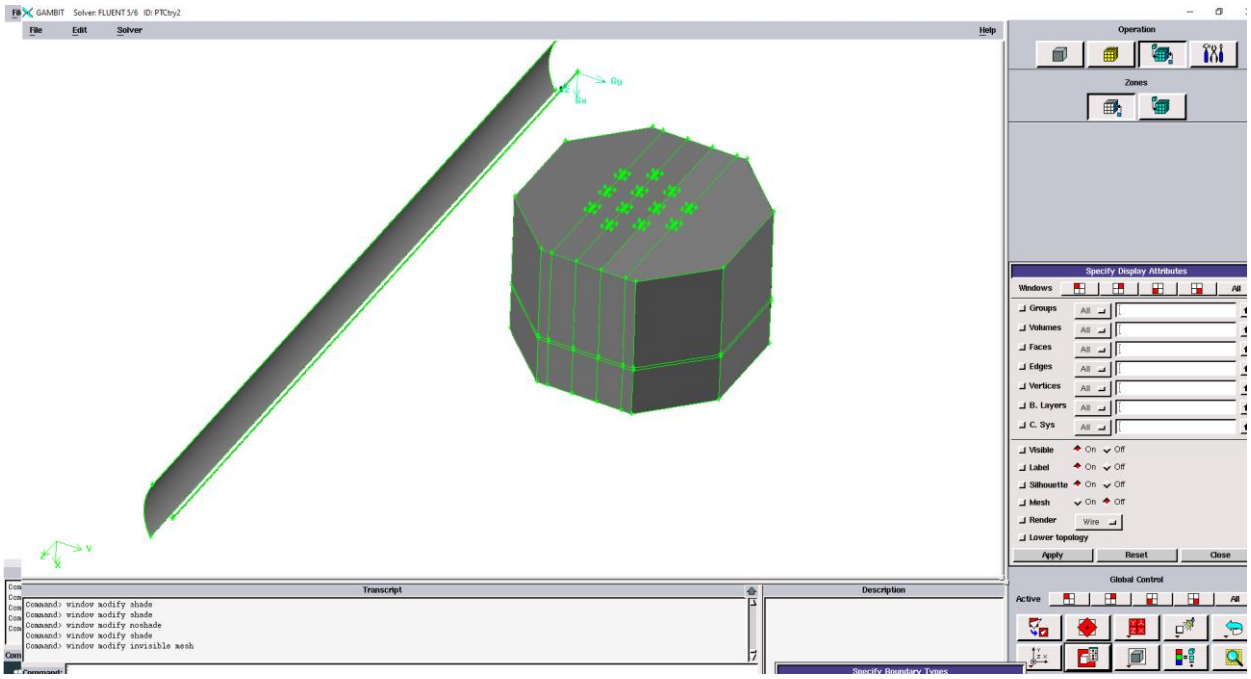


**Figure 21.** Geometrical model created in Gambit.

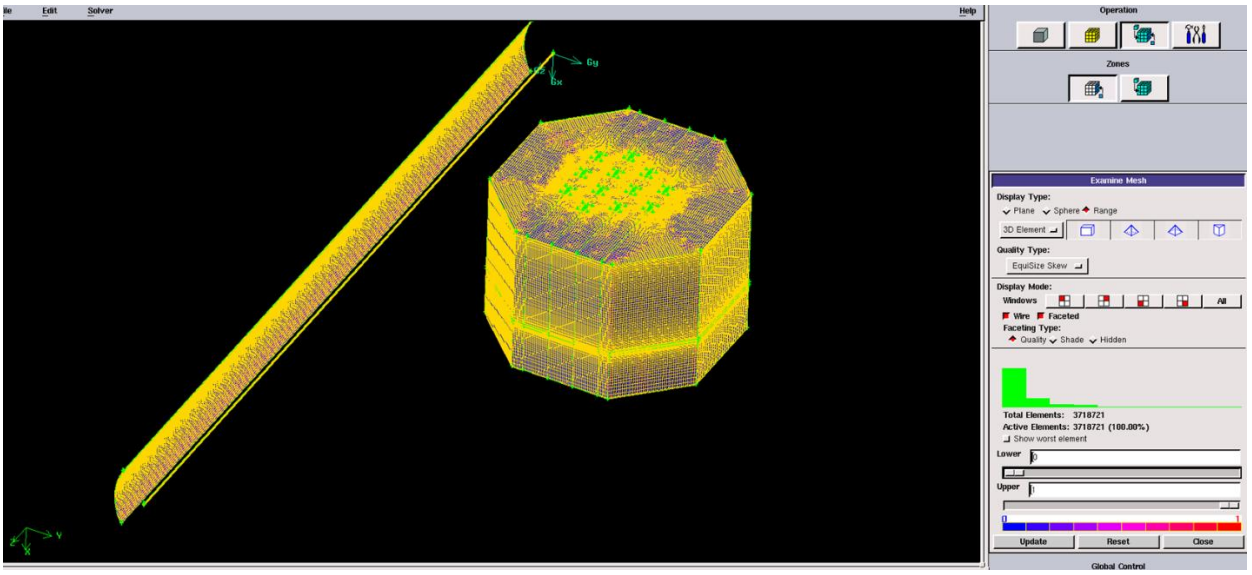


**Figure 22.** Mesh generated in Gambit, 3,7 million of elements.

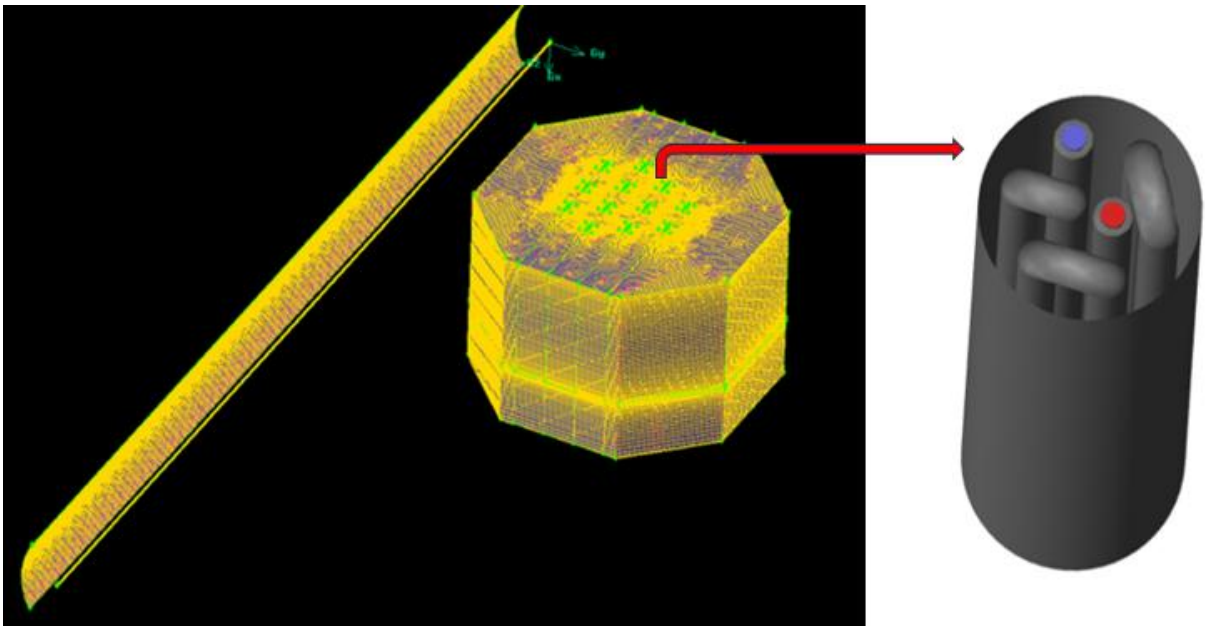

**Figure 23.** Complete model and heating U-tube configuration.

Geometrical characteristics of different elements showed in the above figures, are referred to the choice to implement numerical evaluation with the aim of extending it to a potential pilot plant. The pilot model was hypothesized with 12 heating elements in which the HTF from the HCE flows. Considering that in Haemers Technologies applications, the energy to be supplied to heating pipes is on average 0.8 kW/m, when considering the placement of tubes with 1.5 m of interdistance and the target temperature to reach is 250°C in soil monitoring points, these parameters were of fundamental importance as first assumption, as well as several research studies on parabolic trough collector design (S Mathew et al., 2010; Gujrathi et al., 2017; Bellos and Tzivanidis, 2018b; Munawwar Khalil, 2023; Singh and Chandra, 2023).

The different geometrical parameters of PTC were hypothesized starting from the analytical representation of a parabola equation having symmetry about the y axis, and f is the focal length of the parabola:

$$y = \frac{x^2}{4f}$$

By putting x = a/2, where a is the aperture of receiver, height (H) is obtained as:

$$H = \frac{a^2}{16f}$$

Although a numerical simulation with Ansys Fluent on the complete model was not carried out due to several factors, including the limitations of the student version, its geometric characteristics are shown in the tables below.

**Table 4.** Geometrical characteristics PTC.

| **Receiver** | | |
|---|---|---|
| Length of the receiver, L | 40 | m |
| aperture width, a | 3 | m |

| | | |
|---|---|---|
| focal length, f | 1,5 | m |
| Height, H | 0,38 | m |
| ratio, f/a | 0,5 | m |
| Aperture area, $A_{ap}$ | 120 | $m^2$ |
| **HCE** | | |
| Annular space (vacuum) | 0,024 | m |
| Outer tube - glass shield | | |
| Diameter, $d_o$ | 0,06 | m |
| Thickness | 0,0045 | m |
| Inner tube - steel | | |
| Diameter | 0,035 | m |
| Thickness | 0,001 | m |

**Table 5.** Geometrical characteristics of heating tubes and soil.

| **Heating tubes** | | |
|---|---|---|
| Number of heating tubes | 12 | - |
| outer tube diameter | 0,14 | m |
| U-tube size (internal diameter) | 15,6 | mm |
| Number of Folds in the U-Tube | 6 | - |
| U-tube length | 80 | m |
| Heating layer (depth) | 10 | m |
| inlet area U-tube | 0,000192 | $m^2$ |
| Spacing tubes | 1,5 | m |
| Soil volume | 212,1 | $m^3$ |

The qualitative evaluation of PTC geometric characteristics, referring to the focal distance i.e. the distance between the receiver and the HCE, was carried out using the Tonatiuh software. It's an open-source program that uses ray tracing and Monte Carlo methods to simulate the optical behaviour of solar concentrating systems. Considering 6 meters of receiver length with the geometric characteristics described in Table 4, and assuming that the PTC is equipped with a solar ray tracking system, it is legitimate to project the sun's rays perfectly perpendicular to the receiver, regardless of the position of the sun relative to the receiver. By adding optical and thermal properties of the elements (depending on the material), selecting geographical coordinates (referred to Gela, CL, Italy) with date and time, the result of ray tracing simulation is shown in the following figure.

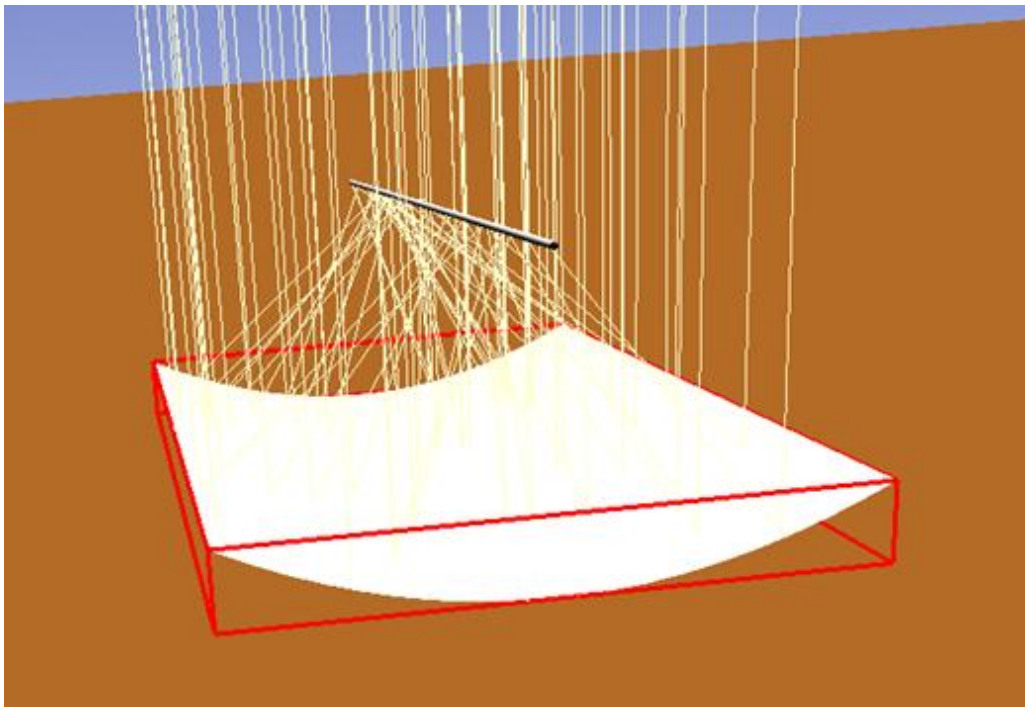

**Figure 24.** Solar rays' incidence in PTC (Tonatiuh software)

The student version of commercial software such as Ansys Fluent is limited by the possibility of simulating models that have a mesh with maximum number of cells of around 1 million (Figure 25). Also, given the complexity and size of the system (heterogeneous, 3D, includes fluid circulation and transient systems), which is very demanding in terms of computing time and resources, this approach was abandoned in favour of simulation based on local solar irradiation data and several assumptions. This alternative greatly simplifies the system without moving far away from reality, provided that thermal efficiencies (losses and efficiency of the semi-cylindrical system) are carefully selected. Due to these problems and to the elements number of the complete model (3,7 million elements, Figure 21), simulations were applied to a model consisting of one heating tube and a soil volume of $212,1/12 \approx 17,7$ m$^3$, referring to the design and dimensional characteristics above discussed and reported in Table 5, Figure 26, 27 and 28. The PTC model was therefore used exclusively for the evaluation of ray tracing through Tonatiuh software, while its energy contribution and the required surface area in Fluent simulations were considered using specific codes better explained in the next paragraphs.

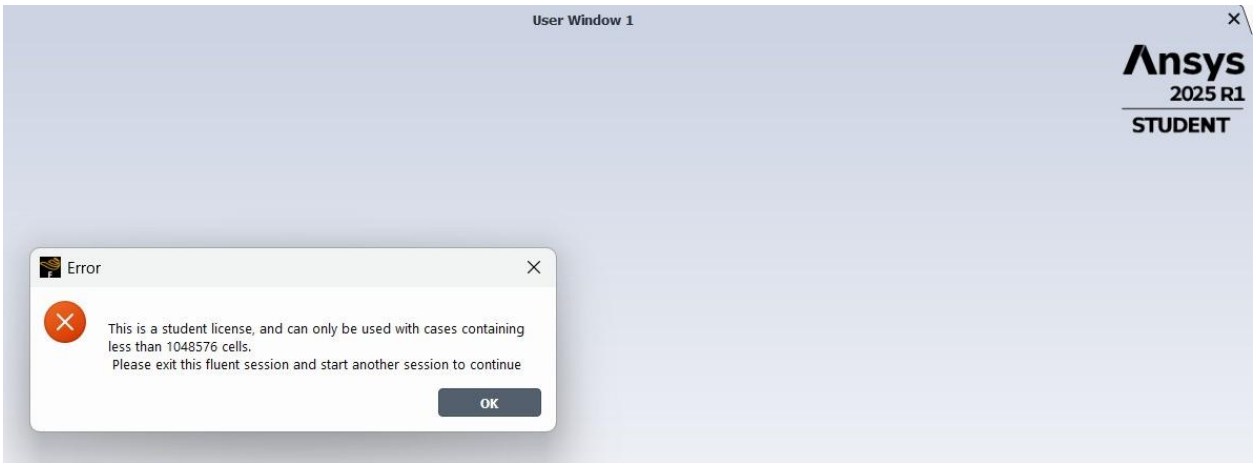


**Figure 25.** Student license limitations in Ansys Fluent CFD software**.**

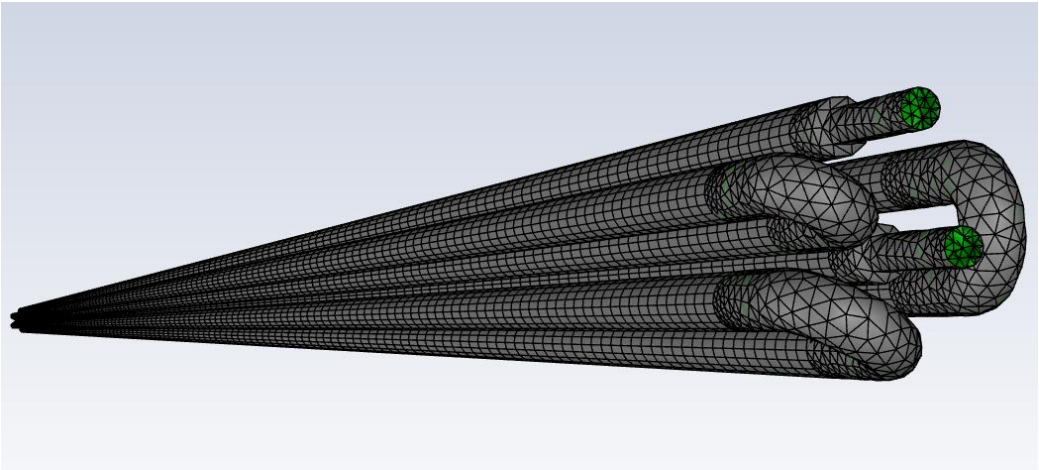

**Figure 26.** multi-U-shaped inner tube

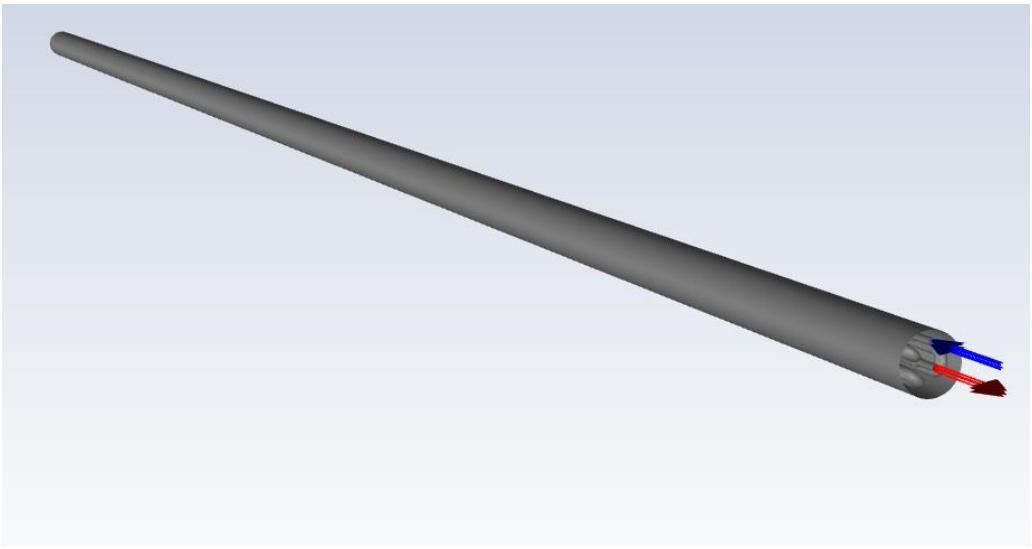

**Figure 27.** Heating inner and outer tube, indication of the inlet (blue arrow) and outlet (red arrow) surface in the U-tube

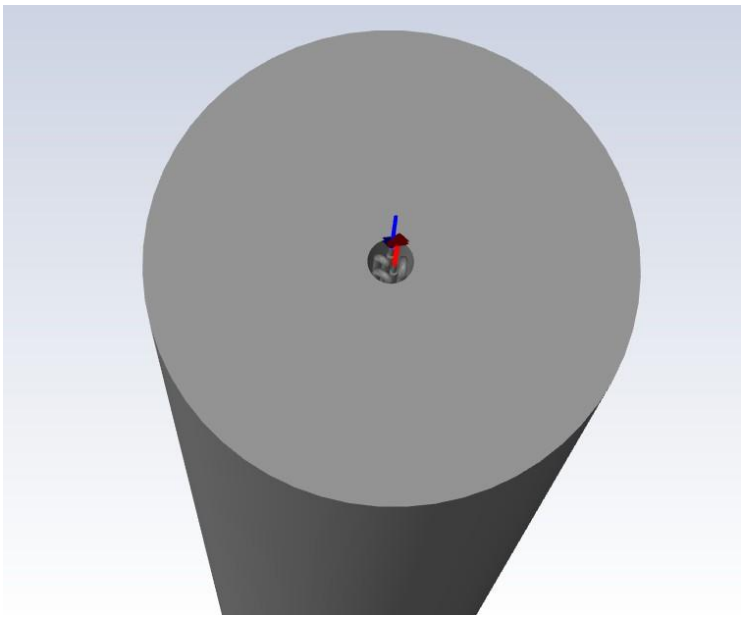

**Figure 28.** Heating (inner and outer) tube placed in soil volume.

### *4.2.5 Basic assumptions*

Main target of simulation is to evaluate the size of the PTC system, i.e. the size of reflector, in order to reach target temperature in the monitoring point of the soil (in the vadose zone) through the heating tube showed in Figure 26 and 27. The basic idea of the process implemented through simulation is a close loop process and it involved the following steps:

- DNI is transferred to HCE in which HTF flows, taking into account transfer efficiency;
- HTF is transferred from the outlet section of HCE to the inlet section of multi shaped U-tube, even in this case considering transfer efficiency;
- HTF flows from inlet section to outlet section of multi shaped U-tube and it's recirculated back to the inlet section of HCE.

Different assumptions have been made: first of all, the HTF selected is TherminolVP1 (Biphenyl/diphenyl oxide (DPO) eutectic mixture), which could allow to reach high temperature inside the receiver. This fluid has a maximum bulk temperature of 400°C and crystallizing point at 12°C. Its thermal properties, depending on temperature, are similar to the water, even if its heat capacity is the half compared with water. Several applications were found in literature about the use of Therminol-VP1 as heat transfer fluid in PTC system (S Mathew et al., 2010; Abed et al., 2020; Kannaiyan and Bokde, 2022) and, considering the target temperature required for TCH, it represents a suitable fluid. Therminol-VP1 properties are shown in Figure 29, while properties variation with temperature is shown in Figure 30.

## Typical Properties

| Property | Test Method | Typical Value, Units |
|---|---|---|
| **General** | | |
| Appearance | | Clear, water white liquid |
| Composition | | Biphenyl/diphenyl oxide (DPO) eutectic mixture |
| Maximum bulk temperature | | 400 °C (750 °F) |
| Maximum film temperature | | 430 °C (800 °F) |
| Normal Boiling Point | | 257 °C (495 °F) |
| Crystallization Point | | 12 °C (54 °F) |
| Flash Point | | |
| COC | ASTM D92 | 124 °C (255 °F) |
| PMCC | ASTM D93 | 110 °C (230 °F) |
| Autoignition Temperature | ASTM E659 | 601 °C (1114 °F) |
| | DIN 51794 | 621 °C (1150 °F) |
| Coefficient of thermal expansion | | |
| @ 200°C | | 0.000979 /°C (0.000544 /°F) |
| Heat of Vaporization[a] | | 206 kJ/kg (88.7 Btu/lb) |
| Viscosity, Kinematic | | |
| @ 100°C | ASTM D 445 | 0.99 cSt, $mm^2/s$ |
| @ 40°C | ASTM D 445 | 2.48 cSt, $mm^2/s$ |
| Liquid Density | | |
| @ 15°C | ASTM D 4052 | 1068 $kg/m^3$ (8.91 lb/gal) |
| @ 25°C | ASTM D 4052 | 1060 $kg/m^3$ (8.85 lb/gal) |
| Acidity | ASTM D 664 | <0.2 mg KOH/g |
| Molecular Weight (Average) | | 166 |
| Pseudocritical temperature | | 499 °C (930 °F) |
| Pseudocritical pressure | | 33.1 bar (480 psia) |
| Pseudocritical density | | 327 $kg/m^3$ (20.4 $lb/ft^3$) |
| Sulfur Content | ASTM D-7691 | <10 ppm |
| Copper Corrosion | ASTM D 130 | <<1a |
| Moisture Content, maximum | ASTM E-203 | 300 ppm |

**Figure 29.** Therminol VP1 typical properties (source: https://www.eastman.com/en/products).

| Temperature | | Liquid density | Liquid heat capacity | Heat of vaporization | Liquid enthalpy[b] | Liquid thermal conductivity | Liquid viscosity[c] | | Vapor pressure[d] |
|---|---|---|---|---|---|---|---|---|---|
| °C | °F | kg/m³ | kJ/(kg-K) | kJ/kg | kJ/kg | W/(m-K) | cP (mPa-s) | cSt (mm²/s) | kPa |
| 12 | 54 | 1070 | 1.523 | 419.0 | 0.0 | 0.1370 | 5.48 | 5.12 | — |
| 20 | 68 | 1064 | 1.546 | 414.7 | 12.3 | 0.1363 | 4.29 | 4.03 | 0.001 |
| 30 | 86 | 1056 | 1.575 | 409.3 | 27.9 | 0.1353 | 3.28 | 3.11 | 0.004 |
| 40 | 104 | 1048 | 1.604 | 403.9 | 43.8 | 0.1344 | 2.60 | 2.48 | 0.009 |
| 50 | 122 | 1040 | 1.633 | 398.6 | 60.0 | 0.1333 | 2.12 | 2.03 | 0.019 |
| 60 | 140 | 1032 | 1.662 | 393.3 | 76.4 | 0.1323 | 1.76 | 1.71 | 0.041 |
| 70 | 158 | 1024 | 1.690 | 388.1 | 93.2 | 0.1312 | 1.49 | 1.46 | 0.081 |
| 80 | 176 | 1015 | 1.719 | 382.9 | 110.2 | 0.1300 | 1.28 | 1.26 | 0.153 |
| 90 | 194 | 1007 | 1.747 | 377.8 | 127.6 | 0.1289 | 1.12 | 1.11 | 0.276 |
| 100 | 212 | 999 | 1.775 | 372.7 | 145.2 | 0.1277 | 0.985 | 0.986 | 0.477 |
| 110 | 230 | 991 | 1.803 | 367.6 | 163.1 | 0.1264 | 0.875 | 0.884 | 0.795 |
| 120 | 248 | 982 | 1.831 | 362.6 | 181.2 | 0.1252 | 0.784 | 0.798 | 1.28 |
| 130 | 266 | 974 | 1.858 | 357.5 | 199.7 | 0.1239 | 0.707 | 0.726 | 2.00 |
| 140 | 284 | 965 | 1.886 | 352.6 | 218.4 | 0.1225 | 0.642 | 0.665 | 3.05 |
| 150 | 302 | 957 | 1.913 | 347.6 | 237.4 | 0.1212 | 0.585 | 0.612 | 4.52 |
| 160 | 320 | 948 | 1.941 | 342.7 | 256.7 | 0.1197 | 0.537 | 0.566 | 6.56 |
| 170 | 338 | 940 | 1.968 | 337.7 | 276.2 | 0.1183 | 0.494 | 0.526 | 9.31 |
| 180 | 356 | 931 | 1.995 | 332.8 | 296.0 | 0.1168 | 0.457 | 0.491 | 13.0 |
| 190 | 374 | 922 | 2.021 | 327.9 | 316.1 | 0.1153 | 0.424 | 0.460 | 17.8 |
| 200 | 392 | 913 | 2.048 | 323.0 | 336.5 | 0.1138 | 0.395 | 0.432 | 23.9 |
| 210 | 410 | 904 | 2.075 | 318.0 | 357.1 | 0.1122 | 0.368 | 0.407 | 31.7 |
| 220 | 428 | 895 | 2.101 | 313.0 | 378.0 | 0.1106 | 0.345 | 0.385 | 41.5 |
| 230 | 446 | 886 | 2.128 | 308.0 | 399.1 | 0.1089 | 0.324 | 0.366 | 53.6 |
| 240 | 464 | 877 | 2.154 | 303.0 | 420.5 | 0.1072 | 0.305 | 0.348 | 68.4 |
| 250 | 482 | 867 | 2.181 | 297.9 | 442.2 | 0.1055 | 0.288 | 0.332 | 86.3 |
| 260 | 500 | 857 | 2.207 | 292.7 | 464.1 | 0.1038 | 0.272 | 0.317 | 108 |
| 270 | 518 | 848 | 2.234 | 287.5 | 486.3 | 0.1020 | 0.258 | 0.304 | 133 |
| 280 | 536 | 838 | 2.260 | 282.2 | 508.8 | 0.1002 | 0.244 | 0.292 | 163 |
| 290 | 554 | 827 | 2.287 | 276.8 | 531.6 | 0.0983 | 0.232 | 0.281 | 198 |
| 300 | 572 | 817 | 2.314 | 271.2 | 554.6 | 0.0964 | 0.221 | 0.271 | 239 |
| 310 | 590 | 806 | 2.341 | 265.6 | 577.8 | 0.0945 | 0.211 | 0.262 | 286 |
| 320 | 608 | 796 | 2.369 | 259.7 | 601.4 | 0.0925 | 0.202 | 0.254 | 340 |
| 330 | 626 | 784 | 2.397 | 253.8 | 625.2 | 0.0905 | 0.193 | 0.246 | 401 |
| 340 | 644 | 773 | 2.425 | 247.6 | 649.3 | 0.0885 | 0.185 | 0.239 | 470 |
| 350 | 662 | 761 | 2.454 | 241.3 | 673.7 | 0.0864 | 0.177 | 0.233 | 548 |
| 360 | 680 | 749 | 2.485 | 234.7 | 698.4 | 0.0843 | 0.170 | 0.227 | 635 |
| 370 | 698 | 736 | 2.517 | 227.8 | 723.4 | 0.0822 | 0.164 | 0.222 | 732 |
| 380 | 716 | 723 | 2.551 | 220.7 | 748.7 | 0.0800 | 0.158 | 0.218 | 840 |
| 390 | 734 | 709 | 2.588 | 213.2 | 774.4 | 0.0778 | 0.152 | 0.214 | 959 |
| 400 | 752 | 694 | 2.628 | 205.3 | 800.5 | 0.0756 | 0.146 | 0.211 | 1090 |
| 410 | 770 | 679 | 2.674 | 197.0 | 827.0 | 0.0733 | 0.141 | 0.208 | 1230 |
| 420 | 788 | 662 | 2.729 | 188.0 | 854.0 | 0.0710 | 0.137 | 0.206 | 1390 |

**Figure 30.** Therminol VP1 thermal properties varying with temperature.

To enhance overall efficiencies and avoid or limit heat loss phenomena, the following assumptions were considered for simulations:

- incident angle of DNI in the receiver is 0 due to the hypothesized ray tracking system that allow to maintain optical alignment with the sun;
- reflector surface is cleaned and made of high-reflectivity materials (e.g. aluminium sheets) to optimize solar flux concentration;
- HCE is modelled as an outer glass tube and an inner steel tube, with vacuum between them to significantly reduce convection heat loss;
- mass flow of HTF is considered constant within the absorber, thus influencing continuity equation;
- the top soil surface into which the heating tube is placed is thermally insulated (with appropriate insulating material and concrete layer) and heat losses are considered through external emissivity and a convective heat transfer coefficient;
- to maximize heat transfer process, dry sand is inserted between inner U-tube and outer tube;
- the pipeline system from the PTC to the heating tube is made of material with high thermal insulation;

From those assumptions and referring to other scientific studies, thermal efficiency of PTC system was fixed to 75%, while thermal efficiency of heating tube was fixed to 90% (Kutscher et al., 2012; Gujrathi et al., 2017; Bellos and Tzivanidis, 2018a; Munawwar Khalil, 2023).

Further simplification of the model has been directed to the mass of contaminants. In contaminated soils, the thermal energy required for volatilization processes is predominantly influenced by the water content rather than by the mass of hydrocarbon contaminants. There is no doubt that a soil containing an hydrocarbons concentration of 10 g/kg results as highly contaminated soil. Moreover, TD applications usually involve a soil moisture of 10-20% (Zhang et al., 2022; Xu et al., 2024; Falconi M. et al., 2025). Considering a representative example of soil containing 15% water by mass and 10 g/kg of hydrocarbon contaminants, a quantitative analysis demonstrates this disparity. For 1 kg of soil, the water content corresponds to 0,15 kg, while the hydrocarbon mass is only 0,01 kg. The latent heat of vaporization of water is approximately 2,26 x $10^6$ J/kg, whereas for a heavy hydrocarbon such as eicosane, it is around 2 x $10^5$ J/kg (Yaws C.L., 2008). Consequently, the energy required to evaporate the water fraction is:

$$Qw = 0{,}15 \times 2{,}26 \times 10^6 = 339000\,J$$

while the energy required to volatilize the hydrocarbons is:

$$Qh = 0{,}01 \times 2 \times 10^5 = 2000\,J$$

This calculation indicates that the energy demand for water evaporation is roughly 170 times greater than that for hydrocarbon volatilization, highlighting that the water fraction overwhelmingly controls the energy consumption of TD treatment. For this reason, the model simulated didn't account for the mass of contaminants in the soil, but rather for the presence of water by implementing its thermal properties.

As already mentioned in the previous paragraphs, codes were implemented in C to generate UDFs useful to define custom boundary conditions, source terms and user-specific models to account for solar data. Two different codes were implemented/compiled, one to consider soil moisture (and water evaporation) and one to exploit conductive heat transfer phenomena in combination with solar data and system efficiencies. The heat transfer-UDF consisted of some input parameters defined to account the properties of the heat transfer fluid, the geometric properties of the U-tube, 6 months of solar data (defined in the code through a file containing the data) and a DNI threshold value for which Therminol-VP1 flows inside the tube, mainly referring to the conduction heat transfer equation, also inserted in the code, which allows to implement the close loop. In particular, the defined input parameters are as follow:

- Max-hours of simulation: 4392 (183 days);
- Heat threshold: 150 W/$m^2$;
- Therminol-VP1 Cp: average value 1700 J/kg*K;
- Therminol-VP1 density: average value 1000 kg/$m^3$;
- U-tube inlet/outlet area: 0,000192 $m^2$;
- Fluid velocity when DNI $\geq$ 150 W/$m^2$: 0,15 m/s (corresponding to a mass flow of 103,68 kg/h and to a fluid crossing time in the heating tube of 533 s or 8,8 minutes);
- Fluid velocity when DNI < 150 W/$m^2$: 0 m/s;

The water evaporation-UDF, however, has been implemented in order to consider thermal properties of the fluid as a function of temperature (density, thermal conductivity, specific heat) and to update the energy contribution sequestered by the evaporation of water in the form of latent heat of vaporization, which does not allow to exceed the temperature of 100°C in the soil volume until all the water content has evaporated.

### *4.2.6 Numerical simulation*

The required PTC area has been iteratively assessed through simulations and depending on the achievement of treatment objectives. Simulations were carried out using Ansys Fluent 2025 R1 student license in double precision setting to gain more accuracy, even if it uses more memory. User-Defined Functions are added by compiling them from the appropriate section. General setup, models, materials, cell zone definitions, and boundary conditions need to be set from the case view window (Figure 31).

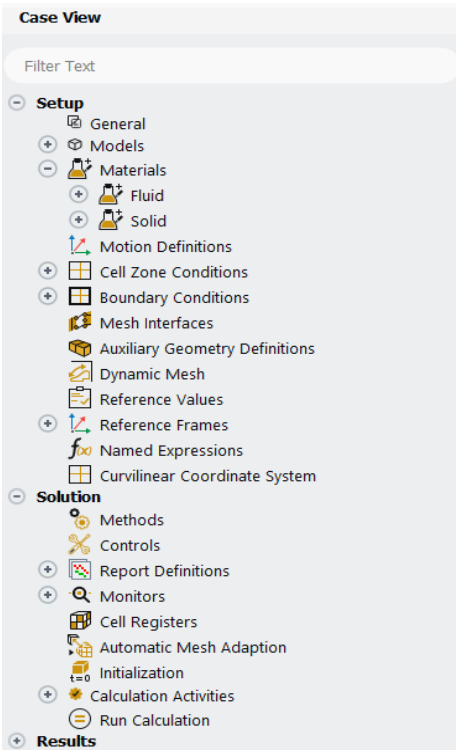


**Figure 31.** Setup menu in Ansys Fluent.

In General setup, solver was set as pressure-based in transient mode. Pressure-based solver is widely used in heat transfer, natural/forced convection, evaporation at low velocities, internal flows (pipes, exchangers), and it's the standard choice for incompressible or mildly compressible flows. Simulation was run in transient mode because the physics of the problem are time-dependent or unsteady (heating of a solid/fluid, evaporation processes). In models, energy equation was activated and k-ε was selected as turbulent model, while radiation was not activated as it was entered as input data (source term) into the UDF. In the database of materials already existing on Fluent there is no Therminol-VP1 as fluid, which was therefore created by assigning its thermal properties (density, specific heat, thermal conductivity). As solid, steel was selected in the materials database, while two types of sandy soil were created: dry-sand as medium between inner and outer heating tube (Figure 32) and sand whose thermal properties varied as the water content varied (Figure 33) and this

dependency is taken into account in the UDF, except for the specific heat, which has been considered through a piecewise-polynomial function that describes its trend.

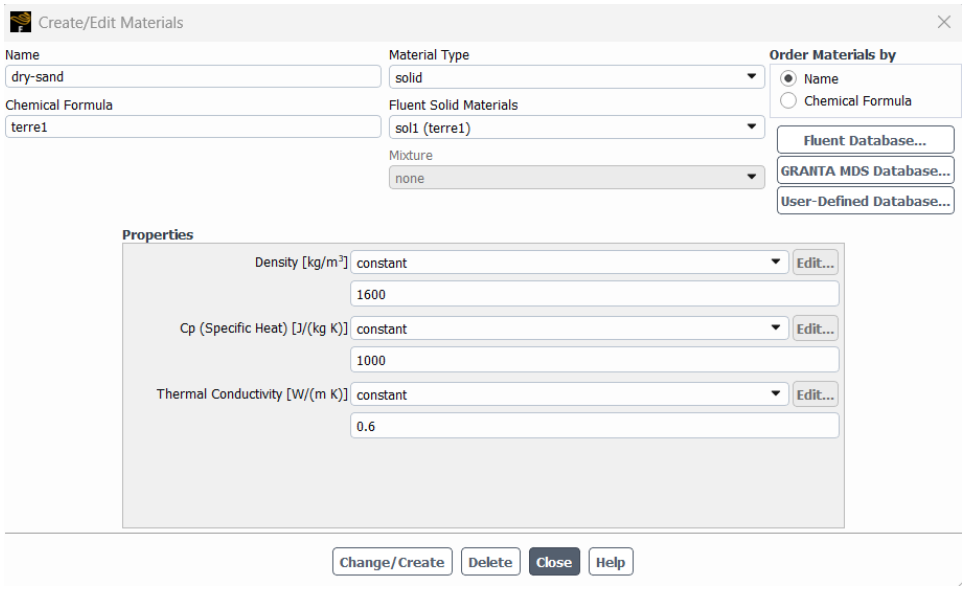


**Figure 32.** Dry-sand properties.

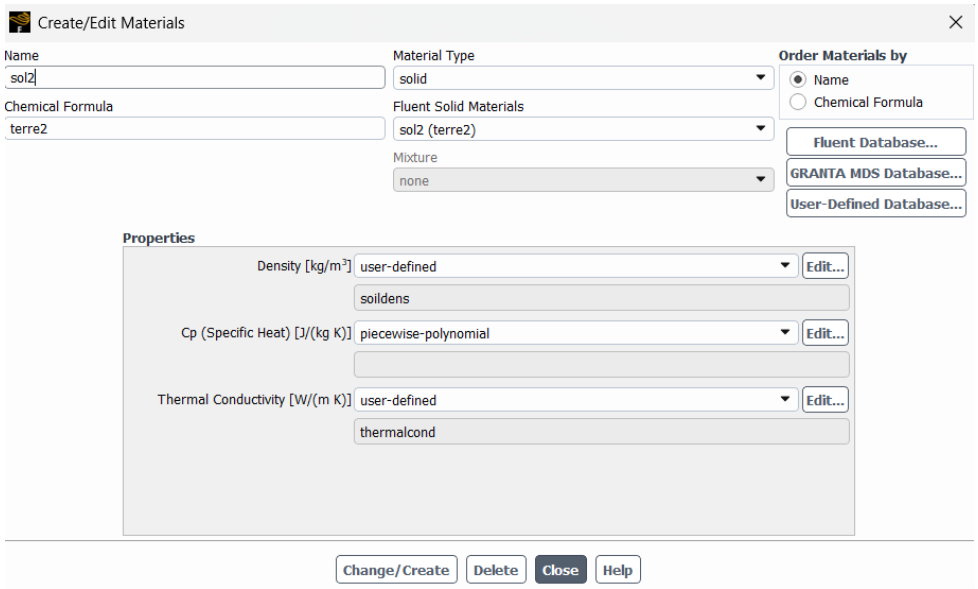


**Figure 33.** Soil properties, UDF depending.

In cell zone conditions, Therminol-VP1 is assigned to the inlet and outlet surface area of the U-tube, as those elements had been modelled as a fluid in Gambit. A source term is added to soil, specifying in this way that the amount of water to be evaporated is contained in soil.

Different boundary conditions were set: at inlet and outlet section of U-tube, UDF was assigned as velocity and temperature profile (which means their values are depending on DNI and on close loop simulation process); all other model elements have been set as walls.

As mentioned in the previous paragraphs, a specific monitoring point in soil volume was considered to evaluate the achievement of the target temperature. This choice is also considered in Haemers Technologies' TCH applications, where the placement of smart burners and heating pipes with a triangular configuration involve monitoring the so-called cold or coldest point (Figure 34). In the simulated model, monitoring point (Figure 35) was placed at 5 m depth and at the edge of the soil's lateral surface (at a distance of 0,75 m from the center of the tube). Monitoring has also been extended to the inlet and outlet sections of the U-tube to evaluate the temperature.

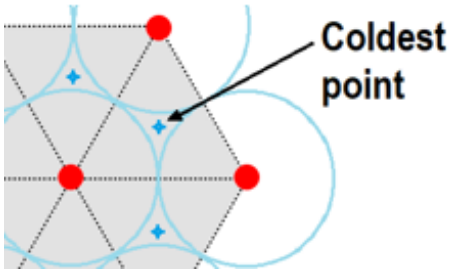


**Figure 34.** Heamers Tehnologies monitoring point (cold or coldest point).

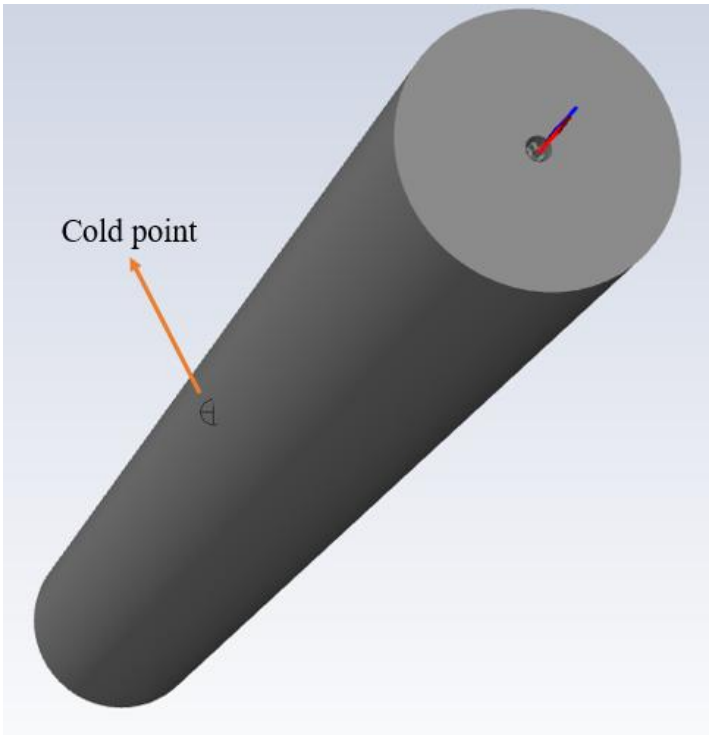


**Figure 35.** Indication of the monitoring point.

Each simulation was run with a time-step of 1 h, for a total of 4392 hours, including 10 iterations per each time-step to increase the accuracy of simulation result (Figure 36).

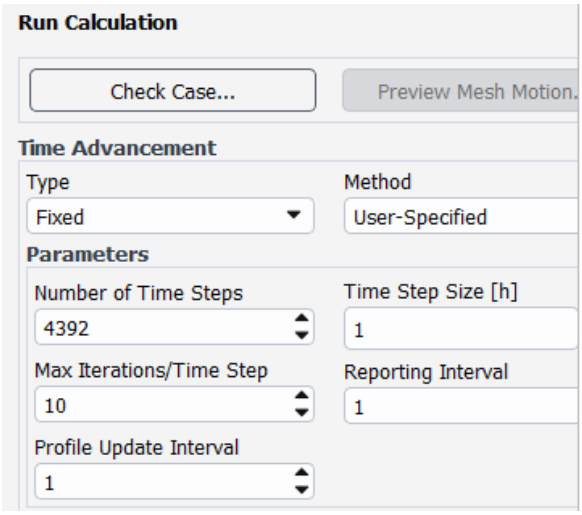


**Figure 36.** Simulation parameters: time-step and iterations.

Based on the considerations explained in paragraph 4.2.5, the evaluation of the energy contribution associated with the target temperature was referred to a sandy soil, varying its water content in the ranges usually frequent for the application of thermal desorption, neglecting the concentration of contaminants as they have little energy impact for reaching the target temperature. For this reason, simulations were started for different cases of water content in soil: dry-soil (Case 1) and soil with 15% (Case 2) and 20% (Case 3) of water content. Before running simulations, in UDFs were selected input parameters from the choice of humidity (whose code string is shown in figure 37) and assuming the specific receiver surface (size of PTC) for the heating tube in the conduction equation (Figure 38).

```
#include "udf.h"

DEFINE_INIT(initialisation_evapwater1, domain)
{
  cell_t c;
  Thread *t;
  real xt;
  real humidite_0;
  int last_ts;
  int tlast_ts;
  int slast_ts;
  int clast_ts;
  humidite_0 = 15; /*Cp (0%) = 920; Cp (5%) = 1100; Cp (10%) = 1250; Cp (15%) = 1415;Cp (20%) = 1560;Cp (25%) = 1747;Cp (30%) = 2060*/

  thread_loop_c (t,domain)
    {
          begin_c_loop(c,t)
           {
```

**Figure 37.** Selection of water content in the UDF.

```
    if (heat_source >= HEAT_THRESHOLD)
    {
        new_temperature_in = temperature_out + ( PTCsurface * 0.75 * 0.9 * heat_source ) / (VELOCITY_ACTIVE * CROSS_SECTION_AREA *
FLUID_DENSITY * Cp_fluide);
    }
    else
    {
        new_temperature_in = temperature_out;
    }

    begin_f_loop(f, thread)
    {
        F_PROFILE(f, thread, position) = new_temperature_in;
    }
    end_f_loop(f, thread)
}
```

**Figure 38.** Selection of PTC surface in the UDF.

Further simulations were addressed to the potential evaluation of a particular alternative reuse of the remediated site. Using same geometrical model, the U-tube as Borehole Thermal Energy Storage system, the aim was referred to the evaluation of energy amount potentially stored in the soil volume. Geothermal systems involve different management stages of the energy: charging, storing, and discharging. Specifically, solar energy is a suitable source to be stored in soil in the form of thermal energy through the HTF, and in the same way it flows within the heating tube to remediate soil, it can also be simply stored and then retrieved when it's needed. Simulations for geothermal purposes didn't need water evaporation-UDF, but rather the use of heat transfer-UDF in which input data has been changed.

Specifically, the adopted approach considered simulations in which thermal energy (as source term) was supplied to the heating tube at a constant rate for 8 hours per day, followed by 16 hours without fluid circulation. This configuration alternated between phases of energy storage, where the soil acted as a thermal reservoir, and phases of energy release, during which the stored heat was progressively dissipated, thereby simulating an external energy supply. The transition between heating and cooling cycle was governed by the temperature at the cold point: once the soil approached 100 °C, the heating phase was interrupted and replaced by a cooling phase, which continued until the cold point temperature decreased to approximately 30 °C.

A second simulation approach was also implemented, based on real solar radiation data for Gela over an entire year (from 1$^{st}$ May 2022 to 30 April 2023). In this case, two threshold values were introduced: the DNI (set at 150 W/m$^2$), and the ambient air temperature (threshold set at 13 °C). Accordingly, the developed UDF was structured around conditional '*if*' cycles that alternated among three possible operating modes: energy supply to the heating tube and soil, energy withdrawal from the soil (representing its utilization for external purposes such as meeting energy demands), or complete absence of fluid circulation. The primary objective was to evaluate the energy storage capacity in those geographical coordinates and in those operating conditions, thereby linking thermal desorption to broader concepts of energy management and sustainable resource utilization.

# Chapter 5 - Results

## 5.1 Laboratory activities

Results of the contamination (Table 1) showed significant pollution of all samples, exceeding the CSC foreseen by Legislative Decree n. 152/2006 (part IV, Table 1, column B, Annex 5- Italian law) valid for TPHs and equal to 750 mg/kg$_{DM}$ for "sites for commercial and industrial use". As pointed out in Chapter 4, the experimental investigation was developed in three different phases:

- PHASE 1 and PHASE 2 respectively aimed at evaluating the optimal TD process temperature and contact time to remediate hydrocarbons polluted sediments;
- PHASE 3 aimed at preliminary evaluating TPHs adsorption capacities of two type of biochar, to be considered as an alternative to the activated carbons commonly used in contaminant management systems in real TD applications.

### 5.1.1 PHASE 1: process temperature

Considering sediment samples resulting from first and second contamination, three TD tests were conducted for each polluted sediment sample by varying the maximum temperature reached during the treatment. Following an initial drying step at 105°C in an inert atmosphere (flowing nitrogen), the heating ramp included the reaching of the maximum treatment temperature, respectively set to 200, 350 and 500°C for a contact time of 15 minutes.

Results obtained from the analysis of the residual concentration of TPH in the sediments treated in PHASE 1 (Figure 39), highlighted very high effectiveness of TD treatment, also for the test conducted at a maximum temperature of 200°C (in LTTD range). The treatment of sediment sample with 1335 mg/kg$_{DM}$ (first contamination) resulted in TPH residual concentration of 16,2 mg/kg$_{DM}$(RE equals to 98,8 %), 0,65 mg/kg$_{DM}$ (RE equals to 99,95%) and 0 mg/kg$_{DM}$ (RE equals to 100%), respectively for test at 200, 350 and 500°C, guaranteeing compliance with regulatory limit (CSC) of 50 mg/kg$_{DM}$ for "sites with a residential, public, or green use". Tests repeated for sediment sample with 35011 mg/kg$_{DM}$ (second contamination), also resulted in high removal efficiencies: 99,8% was achieved after test conducted at 200°C with residual concentration of 57 mg/kg$_{DM}$, strictly close to CSC value for "sites with a residential, public, or green use"; tests conducted at 350 and 500°C allowed to obtain RE respectively equals to 99,97 and 99,99%.

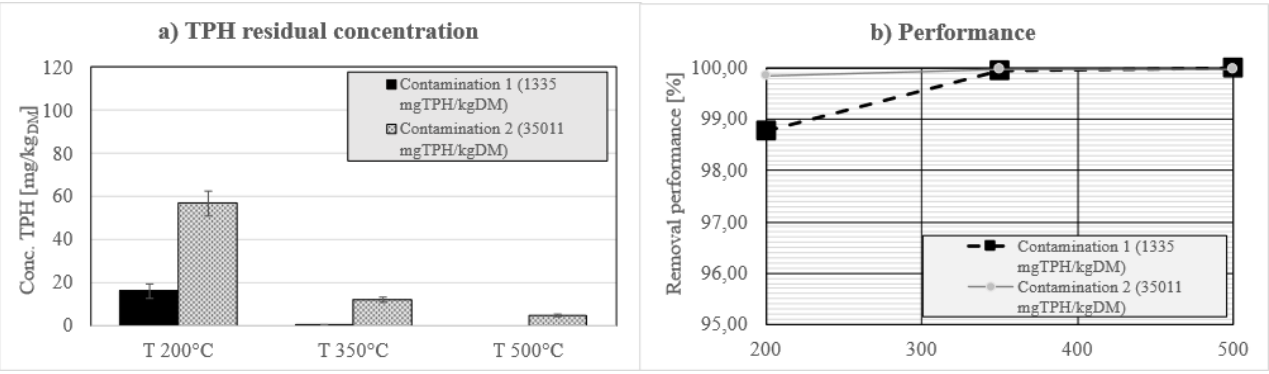


**Figure 39.** TPHs residual concentration (a) and removal efficiencies (b) varying TD maximum temperature for first and second contamination

## 5.1.2 PHASE 2: contact time

In PHASE 2 the experimental campaign was set up in the same way as in PHASE 1, but in this case the matrix/heat source contact time was varied during the experimental tests. Following an initial drying step at 105°C in an inert atmosphere, TD tests were carried out setting contact times of 10, 15 and 20 minutes at a maximum process temperature of 200°C.

Analysis of TPHs residual concentration in the treated sediments (Figure 40), highlighted the compliance with the limits set by the current legislation relating to COLUMN B of Italian Legislative Decree 152/2006, part IV, Table 1, Annex 5, for all conditions and both samples of contaminated sediment. Referring to the limit (CSC) of COLUMN A (50 mg/kg$_{DM}$) and to the treatment of highly contaminated samples (second contamination), the results didn't ensure compliance for the test conducted with a contact time of 10 minutes (91 mg/kg$_{DM}$). For this sediments sample, TPH residual concentration was 50,9 mg/kg$_{DM}$ and 37 mg/kg$_{DM}$ after tests varying contact time respectively of 15 and 20 minutes. TD tests on sediments from first contamination resulted in TPHs residual concentration of 32 mg/kg$_{DM}$ (10 mins), 19,5 mg/kg$_{DM}$ (15 mins) and 15,8 mg/kg$_{DM}$ (20 mins), corresponding to removal efficiencies between 97,6 and 98,8%.

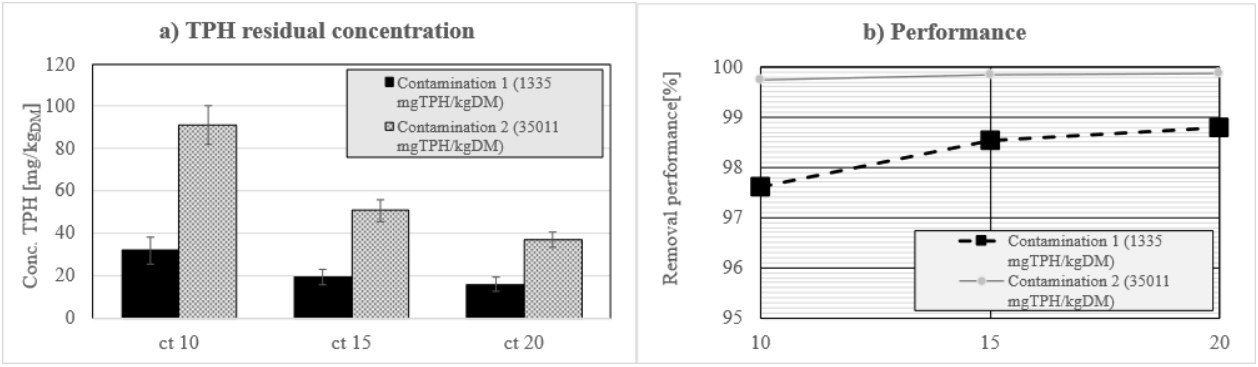


**Figure 40.** TPHs residual concentration (a) and removal efficiencies (b) varying TD contact time for first and second contamination

To sum up, removal efficiencies obtained in PHASES 1 and 2 were consistently high, despite the difference in TPHs initial concentration in the treated sediments. Referring also to Regulation limits, the best working scenario is characterized by a maximum process temperature of 200°C and a contact time of 15 minutes. Results show the convenience of LTTD despite the high levels of TPHs contamination in sediments. In literature, several other authors have obtained high efficiencies in the low temperature range when solid matrix presented high level of hydrocarbons contamination. Zivdar et al., 2019, applying TD through an electric furnace, showed the convenience of LTTD for diesel polluted soil (20000 mg/kgDM) in a range between 180°C and 340°C, and a contact time between 5-20 minutes, achieving a maximum RE of 97,5% (Zivdar et al., 2019). Falciglia et al., 2011, using a tubular electric furnace eliminated diesel with an initial concentration of 700 ppm from five types of soil, including coarse sand, medium sand, fine sand, loam and clay at 250 °C in 30 min. The maximum removal efficiency of the diesel fuel was about 95%, which was reported for sandy soils (Falciglia et al., 2011). Liu et al., 2019, through a bench-scale apparatus, demonstrated the convenience of low temperatures (≤ 300°C) to remove high concentrations (up to 60000 ppm) of TPH in a silty-sand soil, achieving RE = 99,92% after 30 minutes of treatment at 300°C (Liu et al., 2019). Finally, to corroborate the convenience of LTTD, Sang et al., 2021, by applying TD in the temperature range below 350°C demonstrates that considering low temperature heating parameters, lead to better soil

physicochemical properties and to the rapid recolonization capacity of microbial communities (Sang et al., 2021).

## 5.1.3 PHASE 3: adsorbent materials

To prevent uncontrolled atmosphere emissions of desorbed VOCs, during PHASE 1 and PHASE 2, a condensing off-gas management system was set up through condensing traps. However, the characterization of the trapped/condensed off gases has highlighted the need to integrate an additional unit for the management of contaminants. Referring to the test in PHASE 2, and in particular the one conducted with T=200°C and ct=15 minutes for sediment sample with higher contamination, the chromatograms of analysed traps are showed in Figure 41. This analysis highlighted the recovery of VOCs in both traps (placed in series): in greater quantities for the first trap, smaller but not zero for the second. The presence of closely eluting peaks in the two chromatograms as a function of acquisition time (between 10 and 12 min) can potentially be associated with key VOCs such as alkanes and heavy aromatics. Nevertheless, a quantitative assessment was not possible due to instrumental limitations. From the qualitative analysis, the lack of almost zero peaks in the second trap showed the need to integrate the off-gas management system. As previously introduced, two different off-gas treatment systems were tested: an activated carbon adsorption system, and biochar adsorption system using residual material from pyrolytic process of tree species, pine and eucalyptus.

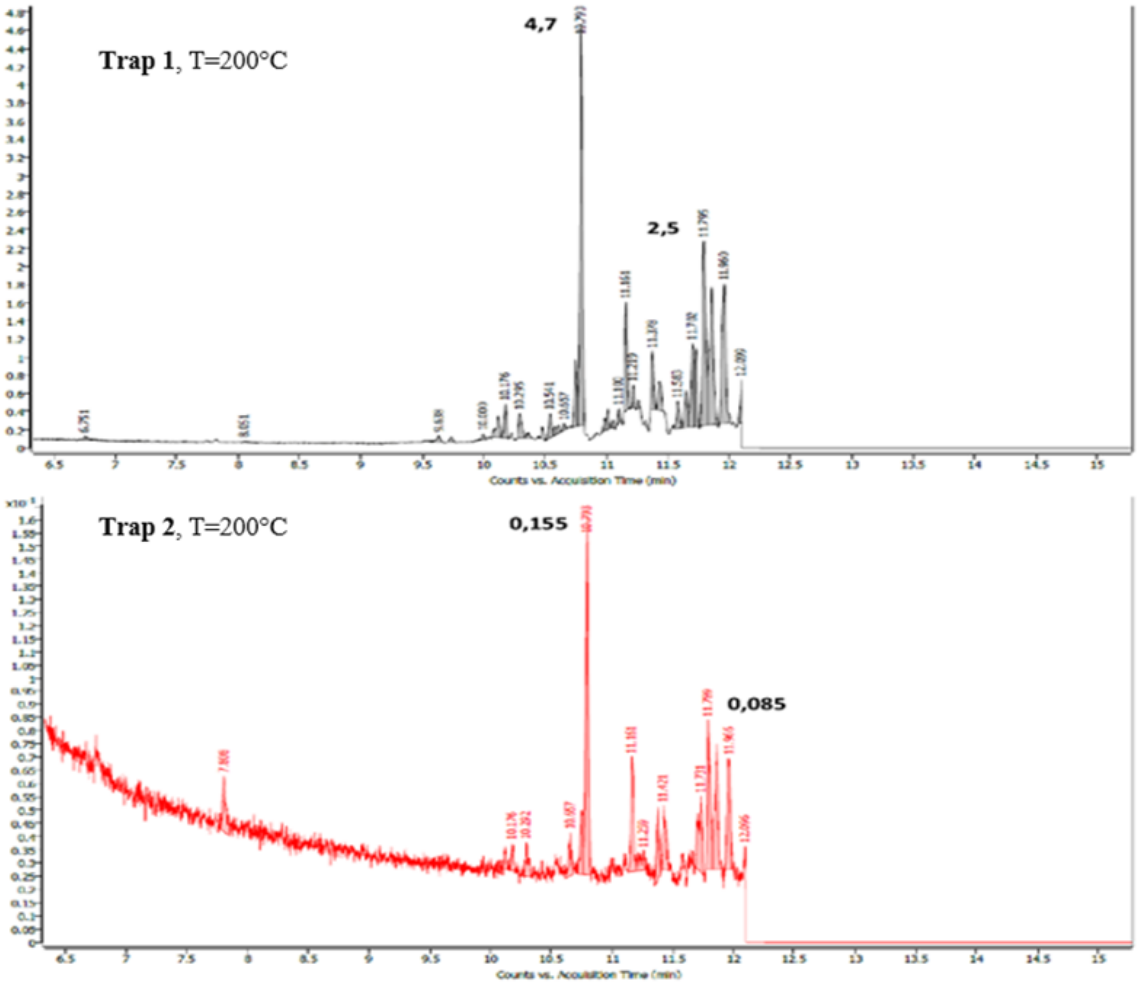


**Figure 41.** Chromatograms of the chemical compounds recovered in the two traps, referring to test at T=200 °C and ct=15 min.

In PHASE 3, all the tests conducted at working temperature at 200°C and with a contact time of 15 minutes, confirmed the results and the repeatability of the test previously observed in PHASE 1 and 2:

- residual concentration of TPHs in sediments was 17±2 mg/kgDM;
- average removal efficiency equals to 99.8%.

Therefore, it is fair to state that TD tests have always guaranteed high hydrocarbon removal efficiencies, even in the LTTD range. As regards pollutants management system, the preliminary analysis was based on the measurement of TPHs adsorbed in the studied matrices (Norit, B880 and B440) and condensed in the final traps. Results have shown the efficacy of the system consisting of adsorption columns and cold traps, especially when B880 is used as adsorbent material. In fact, from the evaluation of TPHs concentration, carried out for the two columns of each adsorbent material tested, the high adsorption efficiency of BIOCHAR B880 emerged. Its adsorption performance was equal to an average of 78% of the pollutants desorbed from the sediments, a value close to the 83% observed using commercial activated carbons. BIOCHAR B440 performed the worst, with an average adsorption capacity of about 67%. Adsorbed TPHs were distributed homogeneously between the first and second columns, with a slight prevalence for the second column for NORIT and B440, and in the

first column in the case of B880. The differences are generally considered to be the effect of the type of experimental setup (bench-scale) rather than the effects of packing, due to differences in density or intrinsic characteristics. Figure 42 highlights that the specific adsorption efficiency of B880 is higher than that of B440 which in turn is higher than the commercial NORIT activated carbon, with values of 43, 18 and 16 $mg_{TPH}/mg_{adsorbent}$ respectively. On the contrary, in terms of TPHs adsorbed per adsorbent volume the values are very similar (2±0.1 $mg_{TPH}/cm^3$): this condition is undoubtedly due to the different density of the adsorbent materials which, at least in terms of volume of adsorbent, mitigates the differences in volumetric adsorption.

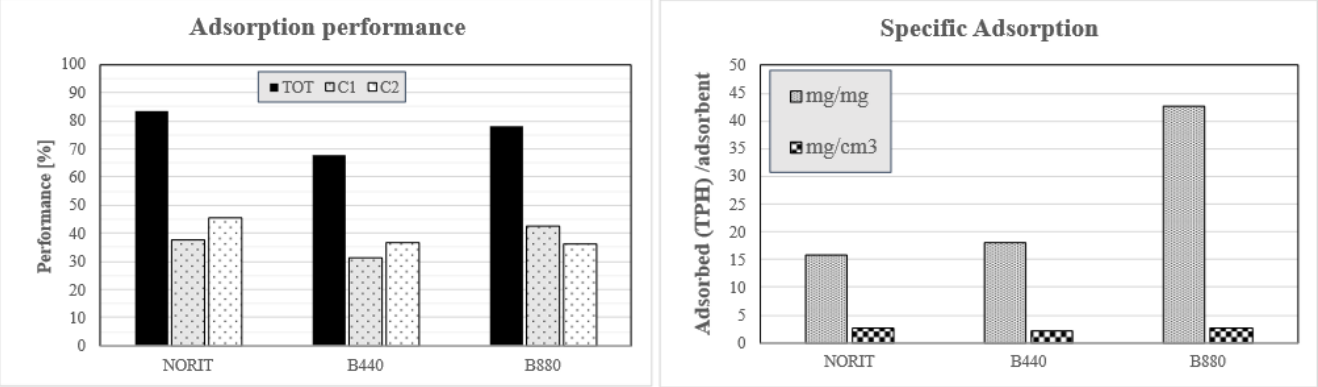


**Figure 42.** Adsorption performance (a) and specific adsorption per unit mass and volume (b) of the adsorbent materials.

Despite the interesting results, considering the important contamination level of the solid matrix, the adsorption system was not effective enough to recover all the TPHs desorbed during heating treatment. In fact, a significant percentage (which varies between around 20% for NORIT and 30% for B440) was recovered inside the condensing trap.

Using a Shimadzu IR Tracer spectrometer in mid-IR mode, equipped with a Universal ATR sampling device containing diamond/ZnSe crystal, the surface chemistry characterization of sediment, diesel and the two types of biochar was carried out. FTIR spectra (wavelength on the abscissa and percentage of infrared transmission on the ordinate) highlighted bands in the comparison between pure diesel and contaminated sediment (Figure 43). For diesel, FTIR spectra shows the typical bands in the range between 2900 and 2800 $cm^{-1}$ attributed to the stretching of the aliphatic C-H bonds (CH2 and CH3), and the sharp bands between 1450 and 1300 $cm^{-1}$ attributable to the stretching of the C-C bond always of the linear paraffins. It can be observed how the bands around 2900-2800 are perfectly visible also in the contaminated sediment while the paraffin bands between 1450 and 1300 $cm^{-1}$ are covered by the very intense band attributable to the C-O stretching of the carbonate ion (calcium carbonate present in the original sediment). Sediment also shows a very intense band around 100/200 $cm^{-1}$, attributable to the silicates originally present in the sediment too. The comparison between Biochar B880 before and after thermal desorption (Figure 44), clearly shows how biochar adsorbed the contaminant volatilized from the sediment during desorption (typical aliphatic C-H stretches around 2900-2800 $cm^{-1}$, visible in the spectrum of Biochar 880 after the desorption experiment). Even for Biochar B440 (Figure 45) was observed the adsorption capacity of the contaminant as it can be seen from the C-H IR stretching around 2900-2800 $cm^{-1}$ for the red line (after thermal desorption test). These results support the hypothesis of using these recycled materials as an alternative to activated carbon, above all considering the greater value they can have from a sustainability point of view.

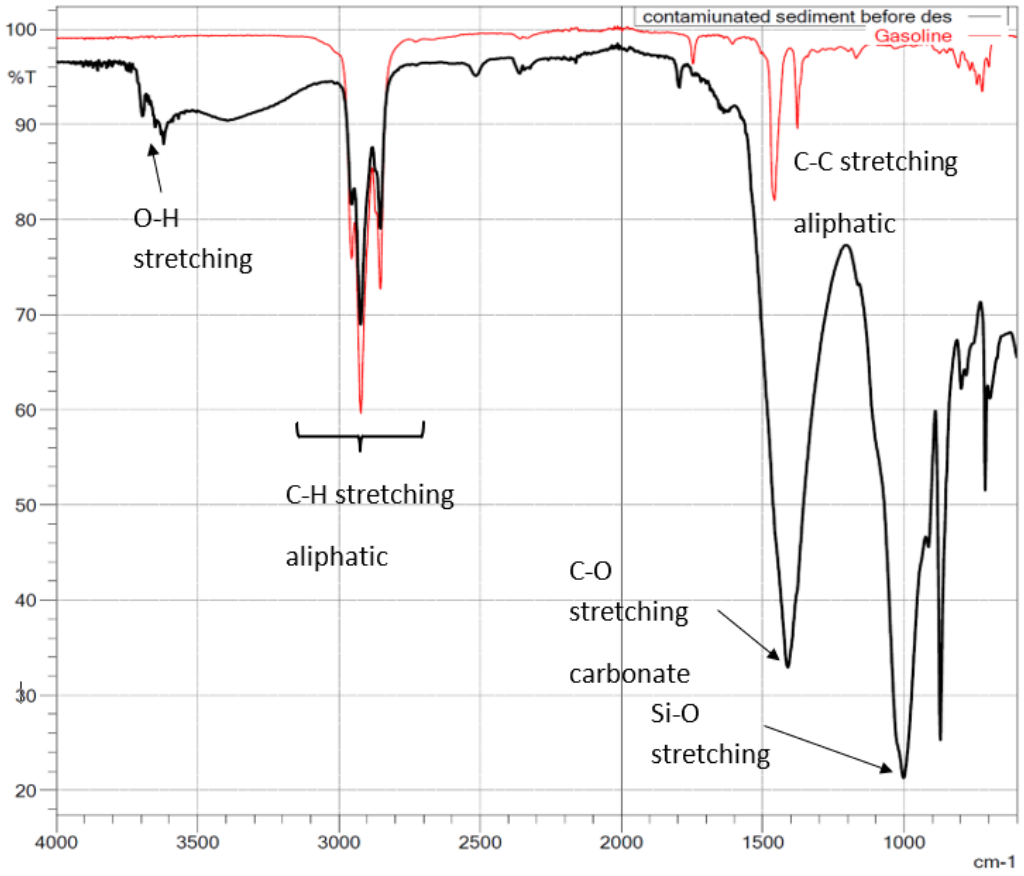


**Figure 43.** FTIR spectra comparison between diesel and diesel contaminated sediment.

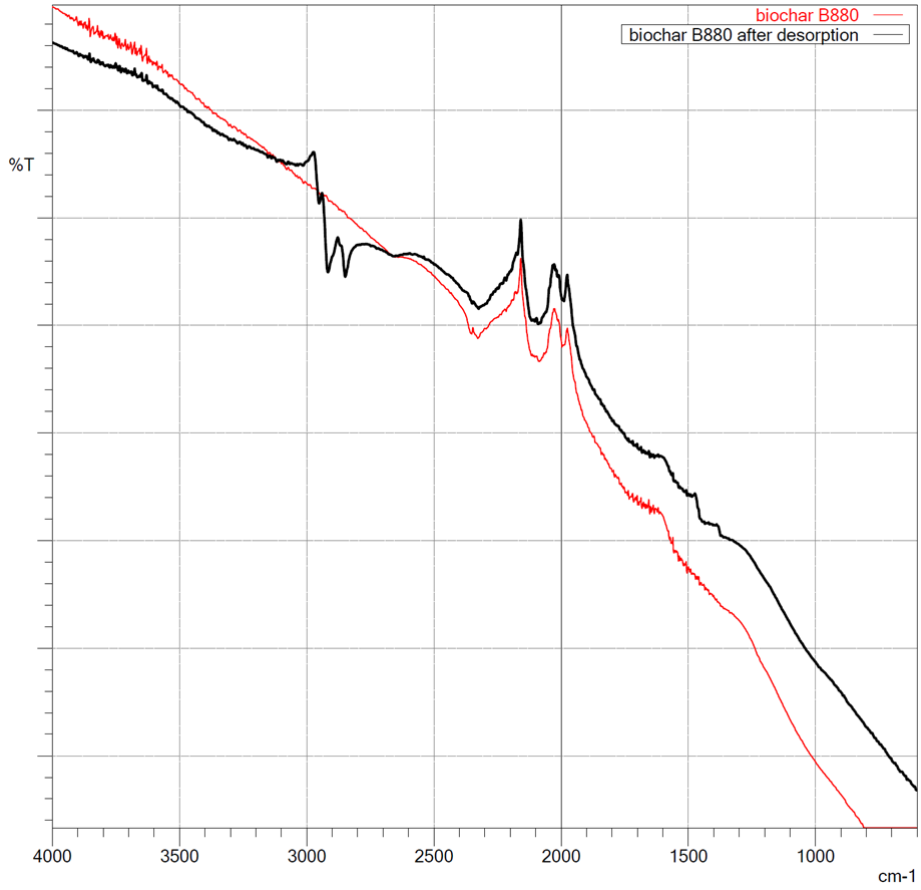


**Figure 44.** FTIR spectra comparison for Biochar B880 before and after the desorption experiment.

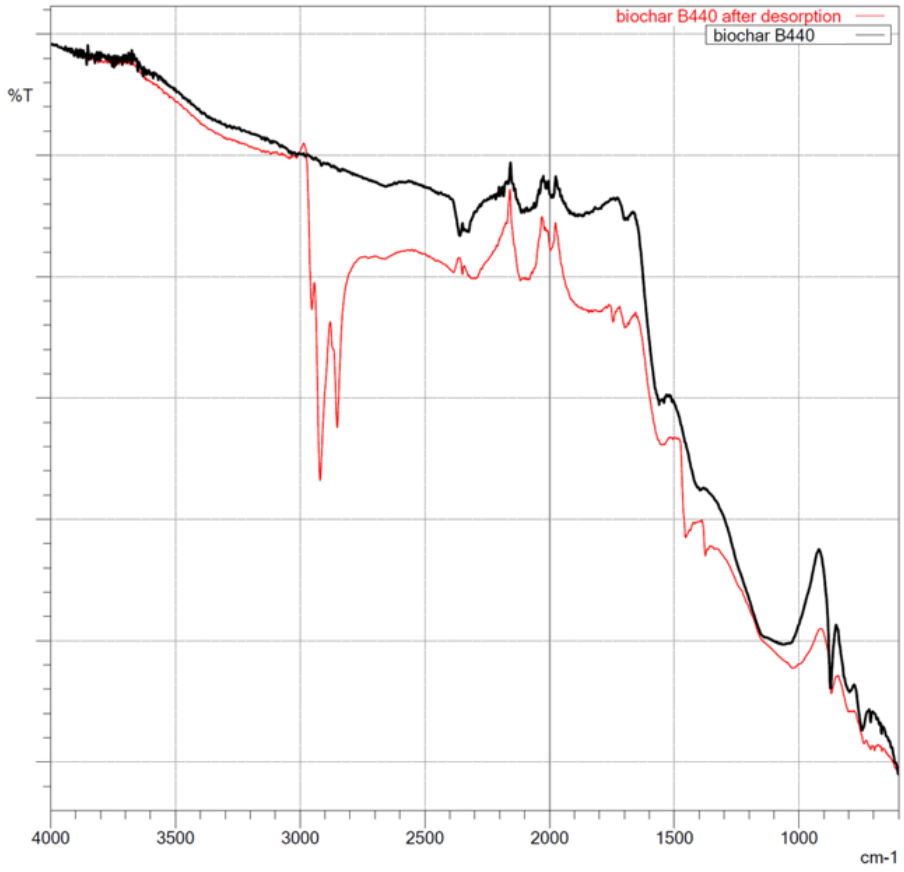


**Figure 45.** FTIR spectra comparison for Biochar B440 before and after the desorption experiment.

## 5.1.4 Energy consumption

Although the experimental study was conducted at a laboratory scale, the analysis of the energy consumption of the plant was undoubtedly particularly useful, as it can provide quantitative information regarding energy savings in LTTD range and about costs. For the evaluation of energy consumption a digital wattmeter was used, allowing to obtain an approximate value of the electrical energy consumed through its transfer to the furnace resistance. As can be seen from the comparison reported in Table 6a, energy consumption was equal to 3,75 kWh/kg$_{SEDIMENT}$ when thermal desorption was applied at the maximum process temperature of 500°C and 20 minutes of contact time. At lower working temperatures (350°C) and equal treatment times, consumption was reduced by about a third (2,67 kWh/kg$_{SEDIMENT}$) and by almost 60% at 200 °C (1,59 kWh/kg$_{SEDIMENT}$). Varying contact time and considering the maximum process temperature of 200°C, further reductions can be obtained as can be seen in Table 6b. Further saving of 14,2% was referred to a contact time of 15 minutes (1,37 kWh/kg) and a further 27,1% at contact time of 10 minutes (1,16 kWh/kg).

**Table 6.** Energy consumption: a) by varying the process temperature; b) by varying the contact time at 200 °C

| **a) Consumption reduction varying T [%], ct=20 mins** | | | **b) Consumption reduction varying ct [%], T=200 °C** | | |
|---|---|---|---|---|---|
| Tmax [°C] | Ce [kWh/kg] | ΔCe [%] | ct [min] | Ce [kWh/kg] | ΔCe [%] |

| | | | | | |
|---|---|---|---|---|---|
| 500 | 3,75 | - | 20 | 1,59 | - |
| 350 | 2,67 | 28,75 | 15 | 1,37 | 14,20 |
| 200 | 1,59 | 57,46 | 10 | 1,16 | 27,14 |

This analysis confirmed the convenience of applying thermal desorption in low temperatures range, obtaining satisfactory yields for hydrocarbons removal, slightly lower than those obtained at high temperatures (350 and 500°C), and guaranteed a reduction in energy consumption equal to 40-70% compared to applications at medium-high temperatures. In particular, if the average cost of energy (for industrial applications) at the time of the investigation was 0,23 €/kWh + VAT, the treatment of contaminated sediments with LTTD at 200°C varies between 325 and 383 €/t with a process conducted respectively with a contact time of 10 or 15, compared to over 1000 €/t for the treatment conducted at 500°C and 20 minutes of contact time.

# 5.2 Numerical modelling

## 5.2.1 Solar driven-TD

In the second part of chapter 4, details of the simulations using Ansys Fluent were explained, whose aim was to evaluate the achievement of certain conditions, such as the target temperature at the monitoring point in the soil. The close loop simulations had a maximum duration of 183 days, in which the heat transfer to the soil was simulated via HTF (which represented the carrier of solar energy converted into thermal energy) flowing within the heating tube. The simulations were carried out using solar radiation data from May 1$^{st}$ to October 31$^{st}$, 2018, since this period represents the most favourable climatic conditions in Gela (Italy). These months are characterized by high solar irradiance and prolonged daily sunshine duration, which allow to define them as “solar months”. Such conditions enhance the thermal input available for the system, making the application of solar driven-thermal desorption process more efficient and cost-effective during this timeframe.

The complexity of the model, the use of multiple UDFs and the number of time-steps set, took a very long time to complete each simulation. In Ansys Fluent 2025 R1 student version and using a computer with 16 GB RAM (not really a High-Performance computer), each iteration lasted about 5 seconds; a time step (set at one hour) consisted of 10 iterations that required approximately 50 seconds to be completed, so 183 days of simulation took approximately 60 hours, which corresponds to two and a half days.

Three cases have been hypothesized: dry soil (Case 1), soil with 15% (Case 2) and 20% (Case 3) of water content, thus adding for cases 2 and 3 a given mass of water to be evaporated and equals to 4824 kg and 6432 kg respectively. These amount of water represented a lost energy contribution, which makes it impossible to reach temperatures above 100°C until the water content has been vaporized. This dynamic was also considered in the heating ramps set in the laboratory system to simulate thermal desorption (Figure 15), as moisture and subsequent water evaporation are key factors strongly affecting the efficiency of heat transfer. Simulations input parameters are showed in Table 7, and include the reflector surface area (PTC) hypothesized in each simulation and equal to 6 m$^2$. Temperature variation in the geometric model at the end of the simulations is shown in Figure 46.

This temperature distribution model was obtained in all the cases studied, with the difference mainly referring to the maximum temperature reached in the different cases. Undoubtedly, the highest temperature in soil occurred in the points closest to the heating pipe.

**Table 7.** Simulations input conditions.

| **Heating tube** | | |
|---|---|---|
| Number of heating tubes | 1 | - |
| outer tube diameter | 0,14 | m |
| U-tube size (internal diameter) | 15,6 | mm |
| Number of Folds in the U-Tube | 6 | - |
| U-tube length | 80 | m |
| Heating layer (depth) | 10 | m |
| inlet area U-tube | 0,000192 | $m^2$ |
| Spacing tubes | 1,5 | m |
| Soil volume | 17,7 | $m^3$ |
| Soil density | 1820 | $kg/m^3$ |
| moisture | 0, 15, 20 | % |
| Fluid density | 1000 | $kg/m^3$ |
| Cp fluid | 1700 | J/kg*K |
| Fluid velocity (if DNI>150) | 0,15 | m/s |
| Fluid mass flow | 103,68 | kg/h |
| Initial temperature | 15 | °C |
| Target temperature | 250 | °C |
| Hypothesized PTC surface | 6 | $m^2$ |

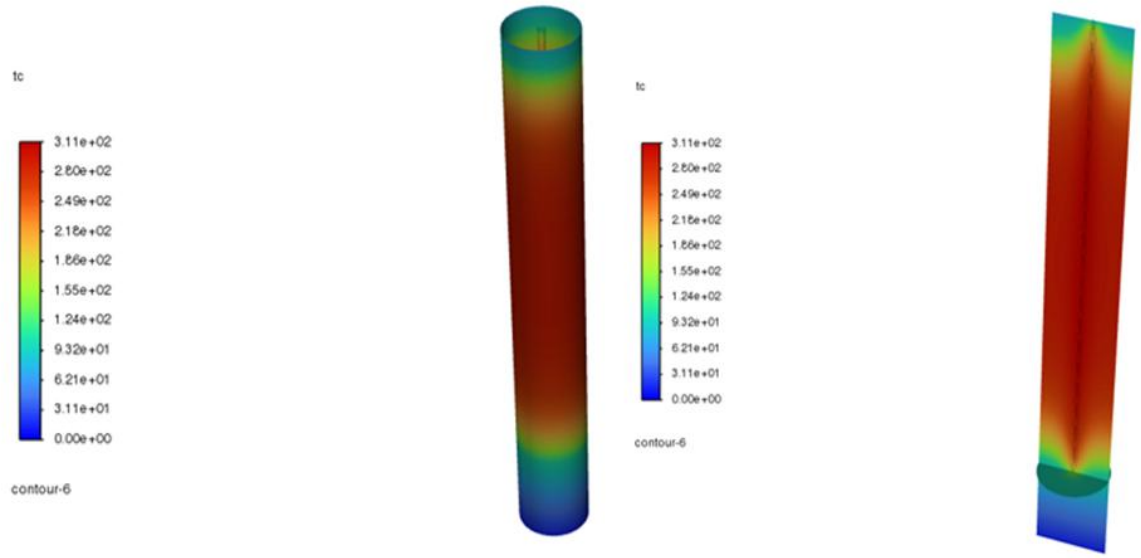


**Figure 46.** Temperature distribution in U-tube and soil.

The results reported below refer to the temperature trend in the fluid inlet and outlet section in the U-tube, and at the soil monitoring point (cold point). Table 8 summarizes the results of case 1

simulation, while in Figure 47, 48 and 49 temperature trends of monitoring points are showed. Dry soil represents the ideal case as energy is totally supplied to the soil, thus excluding heat losses due to the evaporation of water. In this context, the results obtained guarantee the achievement of the target temperature (250°C) in 100 days.

**Table 8.** Results of Case 1 simulation.

| **Case 1 - dry soil** | | |
|---|---|---|
| Soil volume | 17,7 | $m^3$ |
| Soil density | 1820 | $kg/m^3$ |
| Soil mass | 32162 | kg |
| Water mass | 0 | kg water |
| PTC surface | 6 | $m^2$/tube |
| Min DNI | 0 | $W/m^2$ |
| Max DNI | 933 | $W/m^2$ |
| Max power transfer (in 1 h) | 3778,65 | W |
| simulation duration | 150 | days |
| | 3600 | hours |
| Final temperature | 284 | °C |
| Time to reach 100°C (cold point) | 30 | days |
| Time to evaporate water mass | 0 | days |
| Water evaporation phase | 0 | days |
| Time to reach target temperature | 100 | days |

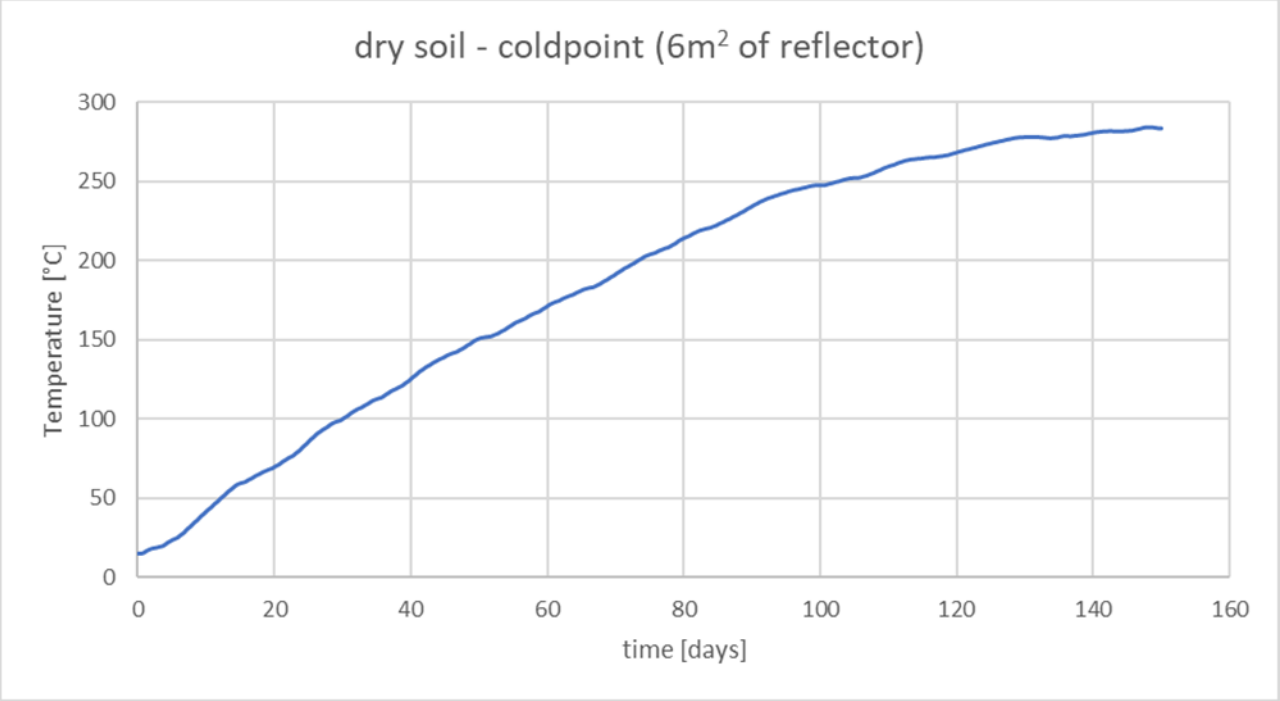


**Figure 47.** Case 1 - Cold point temperature, max T=284°C.

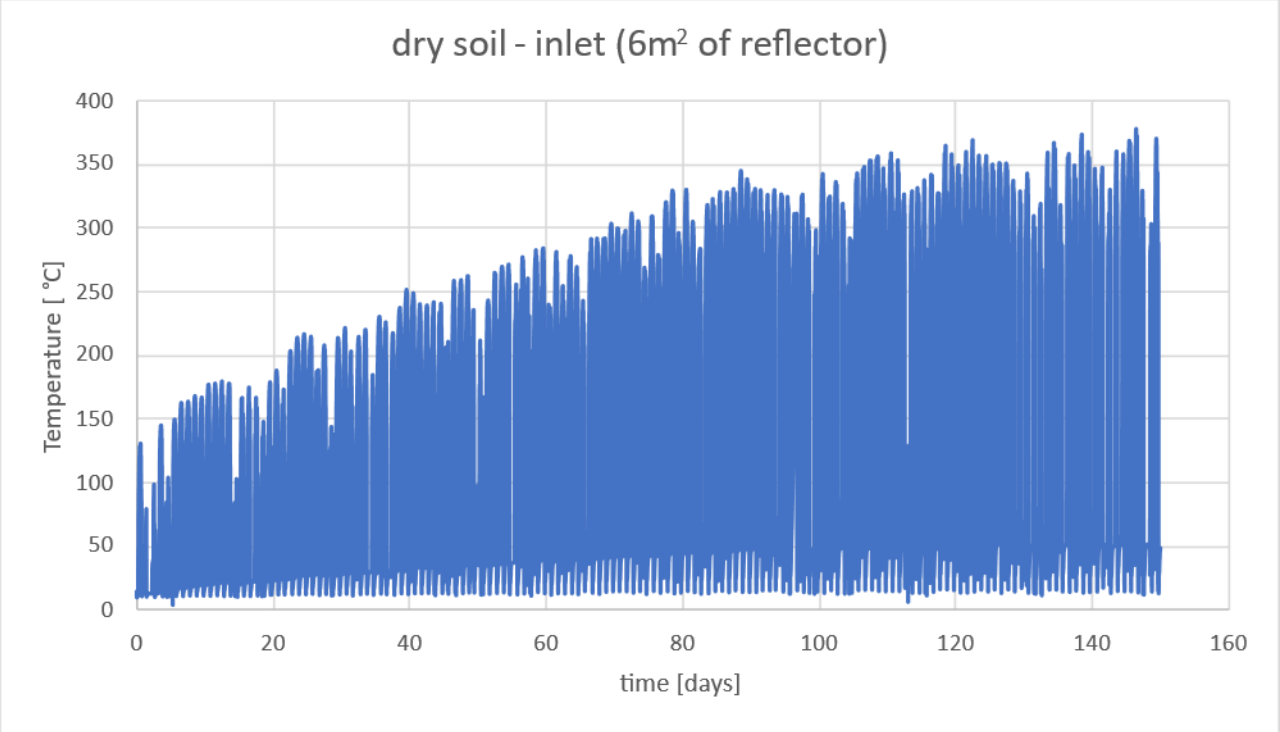


**Figure 48.** Case 1 – Fluid temperature in the U-tube Inlet section, max T=378,2°C.

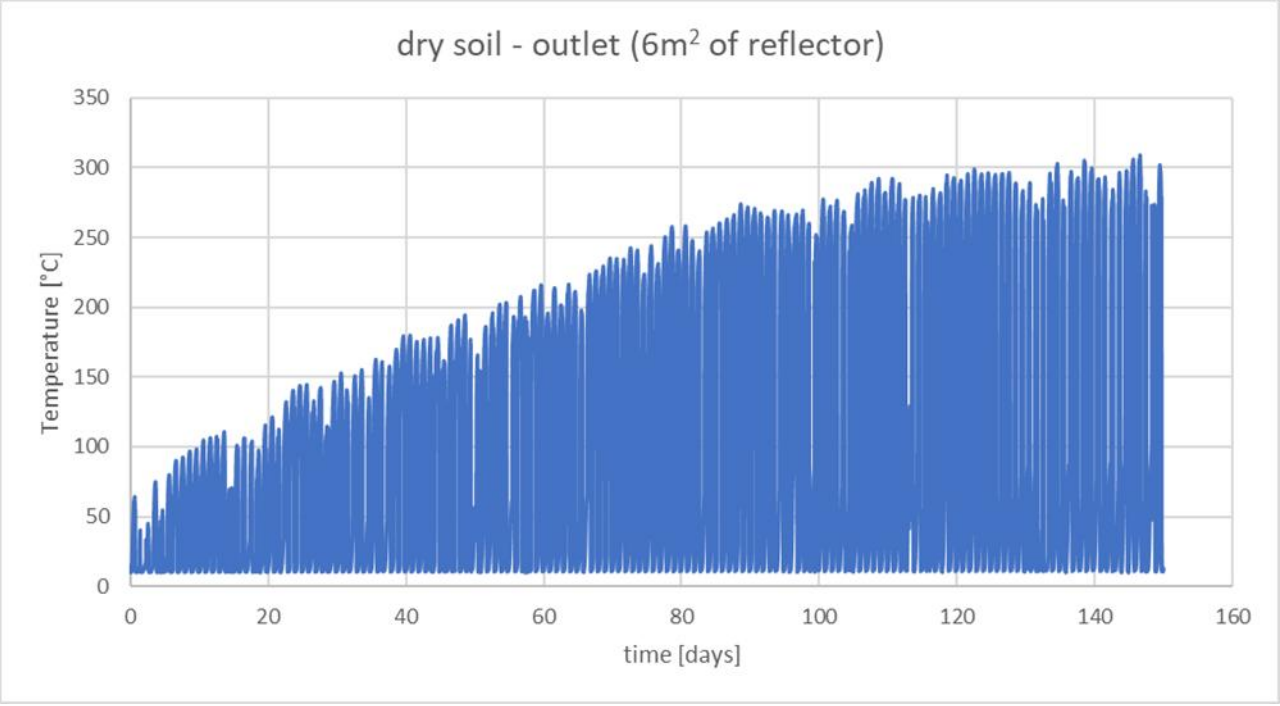


**Figure 49.** Case 1 – Fluid temperature in the U-tube Outlet section, max T=309°C.

In case 2, simulation was carried out also accounting a certain quantity of water in the soil to be evaporated. The results are summarized in the Table 9. In Figure 50, 51 and 52 temperature trends of monitoring points are showed. As it can see, including volatilization of water contained in the soil affects the temperature increase and the required time to let evaporate the amount of water. Soil with 15% of water content needed 50 days to reach 100°C in cold point and about 20 days to volatilize all

the amount of water, then 70 days more to reach the target temperature. In the temperature profile of the cold point (Figure 50), noticeable fluctuations occur around 100 °C. This behaviour is primarily associated with the presence of water within the soil matrix. As the soil temperature approaches the boiling point of water, continuous evaporation takes place, which absorbs a significant portion of the supplied thermal energy in the form of latent heat. This phase-change process reduces the effective temperature of the soil and results in a cooling effect that counteracts the heat transferred from the heating tube. Consequently, the energy consumed by water evaporation represents a negative contribution subtracted from the total heat input, thus influencing the overall thermal balance of the system. Despite this, the results obtained in Case 2 are more than satisfactory, as unlike Case 1, referred to dry soil conditions, a water content of 15% depicts a design condition closer to the real applications of thermal desorption.

**Table 9.** Results of Case 2 simulation.

| **Case 2 - water content 15%** | | |
|---|---|---|
| Soil volume | 17,7 | $m^3$ |
| Soil density | 1820 | $kg/m^3$ |
| Soil mass | 32162 | kg |
| Water mass | 4824 | kg water |
| PTC surface | 6 | $m^2$/tube |
| Min DNI | 0 | $W/m^2$ |
| Max DNI | 933 | $W/m^2$ |
| Max power transfer (in 1 h) | 3778,65 | W |
| simulation duration | 183 | days |
| | 4392 | hours |
| Final temperature | 287,9 | °C |
| Time to reach 100°C (cold point) | 50 | days |
| Time to evaporate water mass | 69 | days |
| Water evaporation phase | 19 | days |
| Time to reach target temperature | 142 | days |

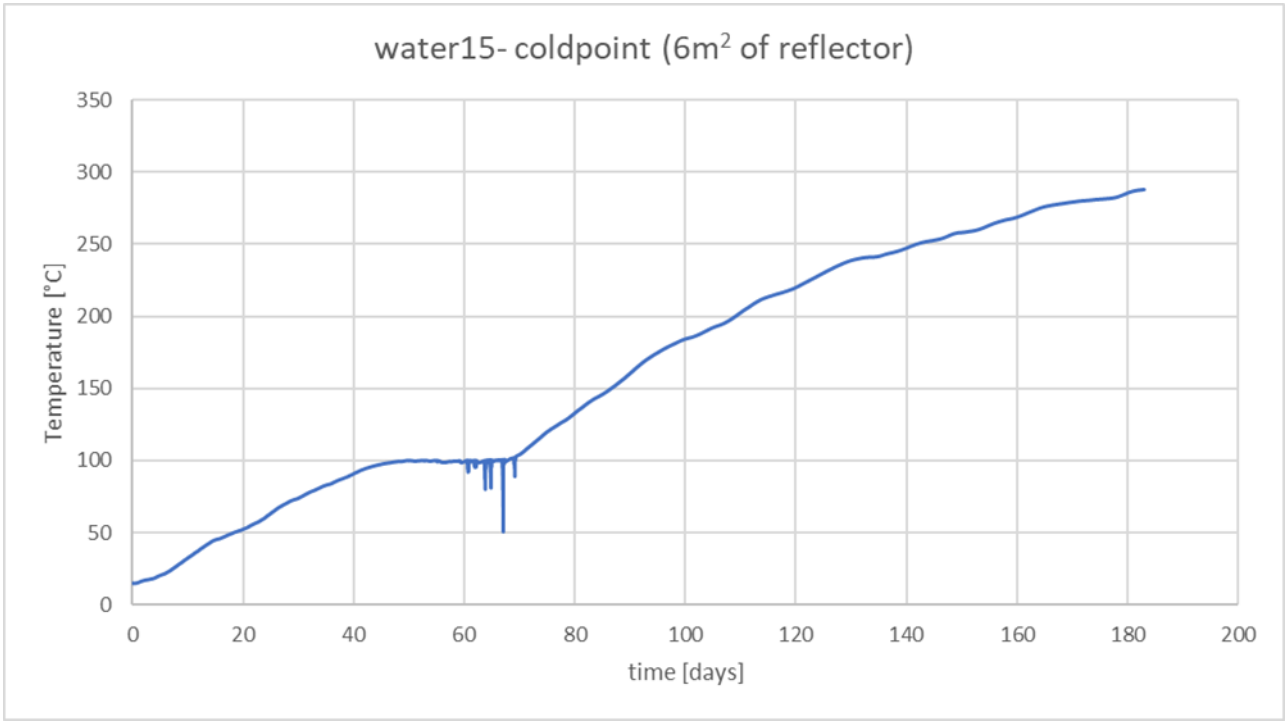


**Figure 50.** Case 2 - Cold point temperature, max T=287,9°C

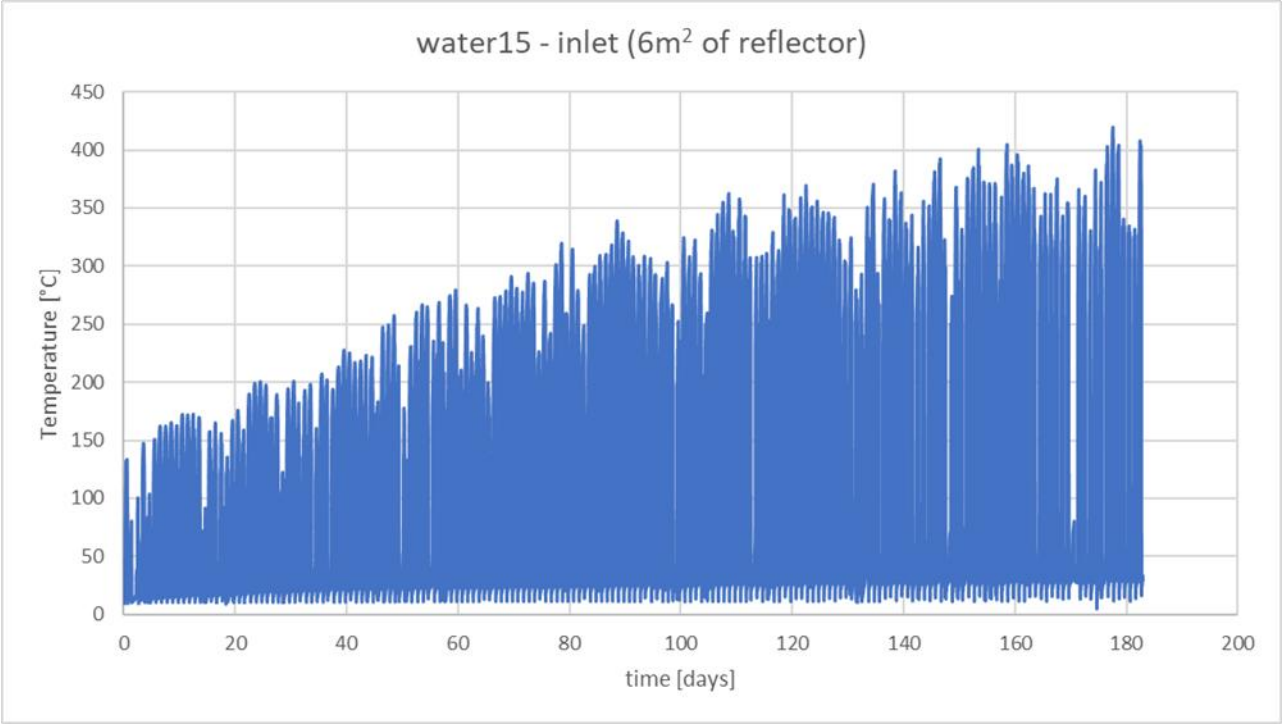


**Figure 51.** Case 2 – Fluid temperature in the U-tube Inlet section, max T=419°C.

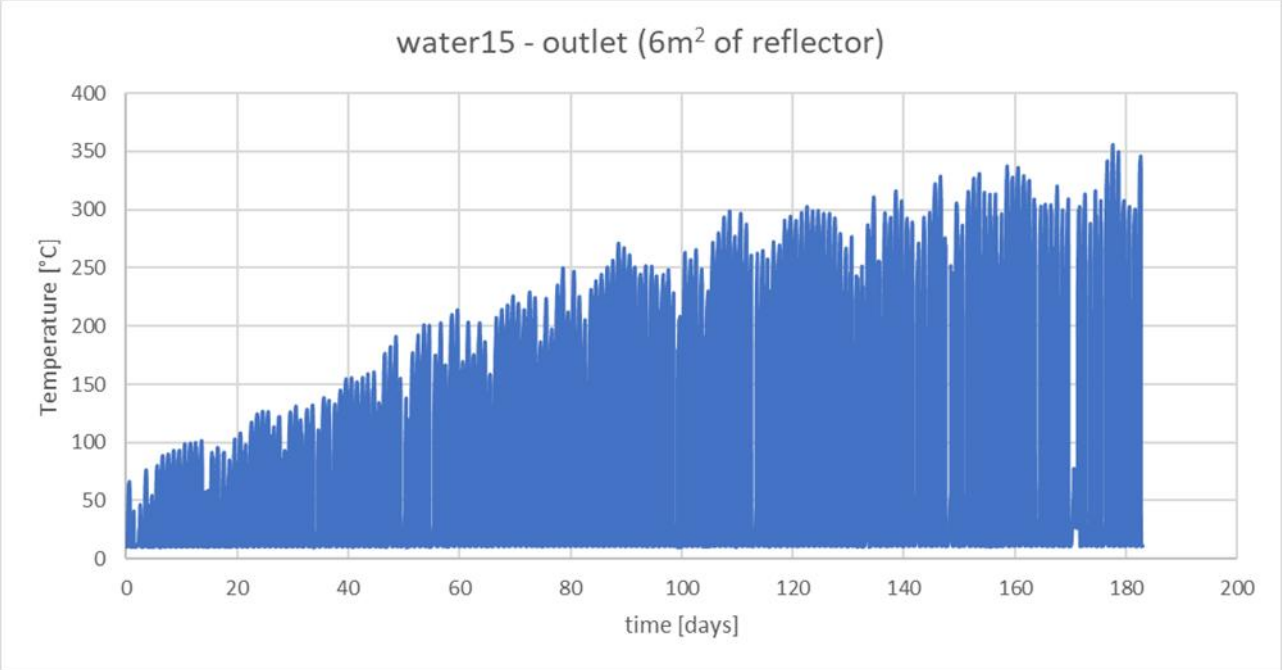


**Figure 52.** Case 2 – Fluid temperature in the U-tube Outlet section, max T=356°C.

Results of case 3 simulation are summarized in Table 10 and temperature trend in monitoring points is showed in Figure 53, 54 and 55. Increasing water content to 20% resulted in a lower maximum temperature in cold point after 183 days of simulation. After 58 days cold point reached 100°C, keeping this temperature for more than 35 days and then reaching at the end of simulation a maximum temperature of 230°C. Comparing Case 2 and Case 3, when soil water content is increased from 15% to 20%, the time required to reach 100 °C at the cold point remains comparable (50 days with 15% and 58 days with 20%). This similarity is due to the fact that the initial heating stage is mainly governed by the sensible heat needed to raise the soil–water system to the boiling point of water. However, at higher water content, a larger amount of latent heat is continuously consumed by evaporation, which reduces the net thermal energy available for soil heating. As a result, although the onset of boiling is achieved within a similar timeframe, the final temperature after 183 days is significantly lower. This does not imply that the innovative system would not be extendable to soils with 20% humidity, but rather requires longer remediation times, or a greater surface area of PTC per heating tube, or different boundary conditions, although the first alternative has to be favoured.

**Table 10.** Results of Case 3 simulation.

| **Case 3 - water content 20%** | | |
|---|---|---|
| Soil volume | 17,7 | $m^3$ |
| Soil density | 1820 | $kg/m^3$ |
| Soil mass | 32162 | kg |
| Water mass | 6432 | kg water |
| PTC surface | 6 | $m^2$/tube |
| Min DNI | 0 | $W/m^2$ |
| Max DNI | 933 | $W/m^2$ |
| Max power transfer (in 1 h) | 3778,65 | W |
| simulation duration | 183 | days |

| | | |
|---|---|---|
| | 4392 | hours |
| Final temperature | 229,4 | °C |
| Time to reach 100°C (cold point) | 58 | days |
| Time to evaporate water mass | 95 | days |
| Water evaporation phase | 37 | days |
| Time to reach target temperature | - | days |

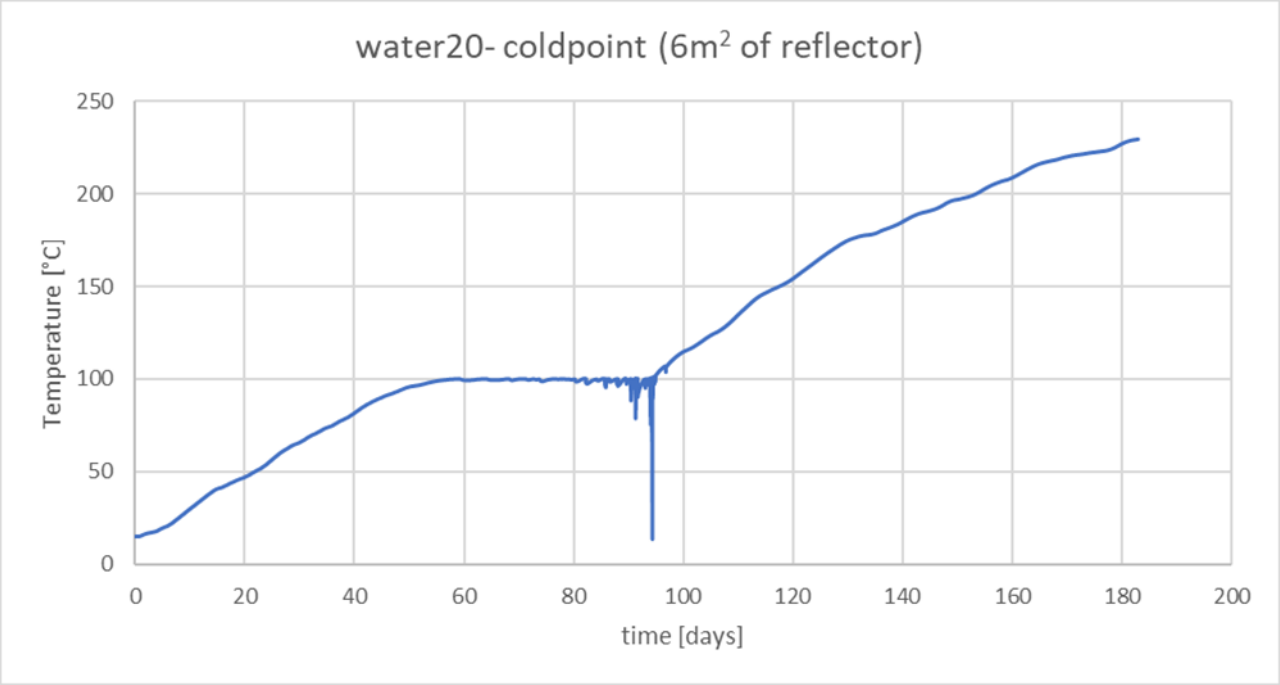


**Figure 53.** Case 3 - Cold point temperature, max T=229,4°C

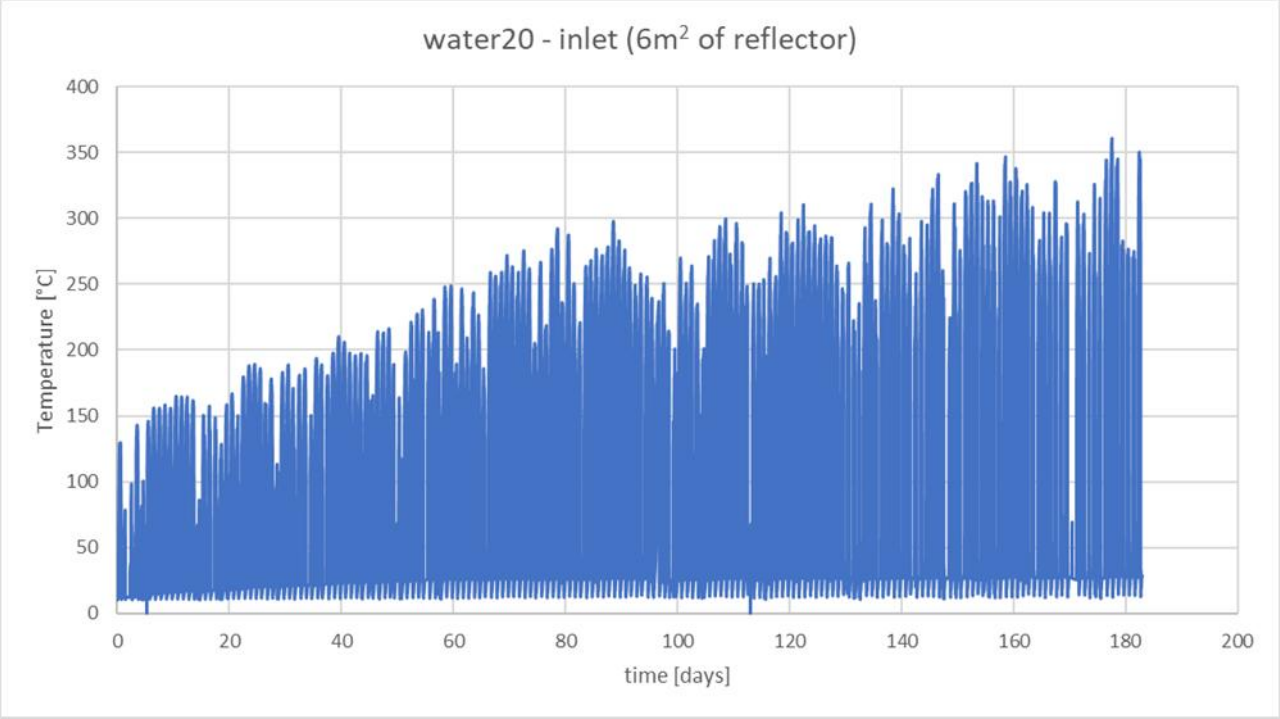


**Figure 54.** Case 3 – Fluid temperature in the U-tube Inlet section, max T=360,7°C.

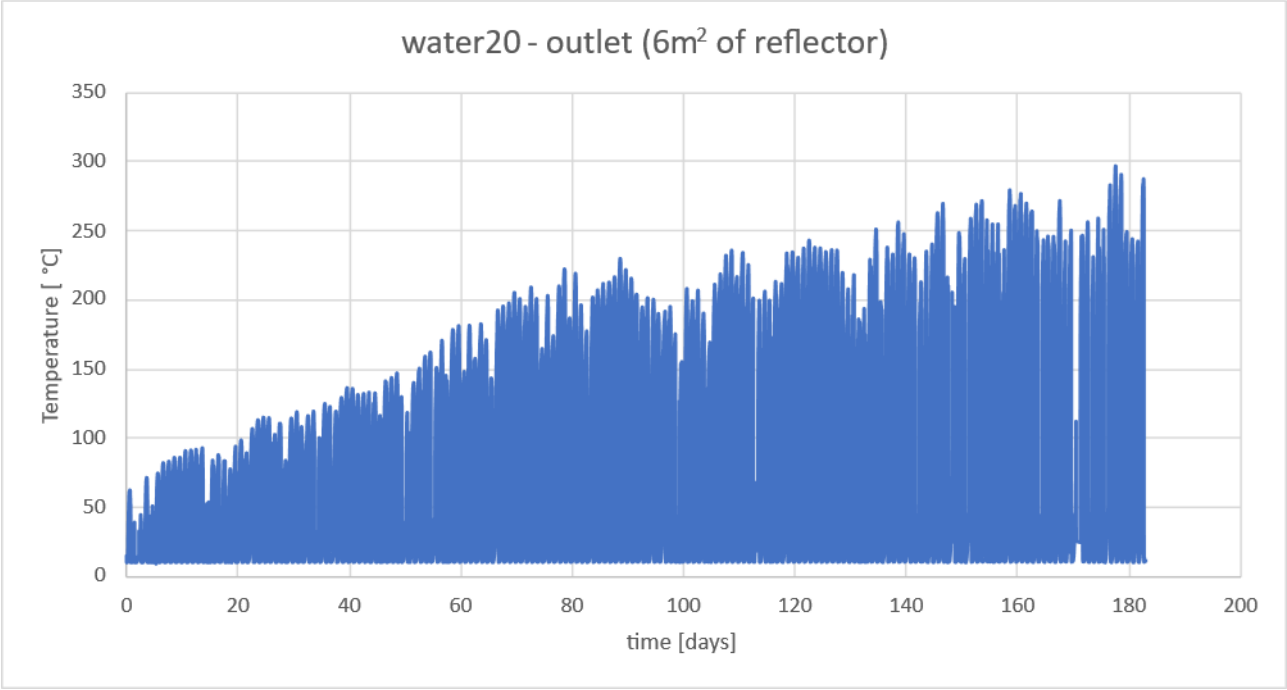


**Figure 55.** Case 3 – Fluid temperature in the U-tube Outlet section, max T=296,9°C.

With the aim of conducting a preliminary economic assessment for a system configuration representative of a pilot-scale plant, the results obtained were extended to the model consisting of 12 heating tubes and considering each heating tube requires 6 $m^2$ of PTC in the simulated conditions, at least 72 $m^2$ of PTC surface area is required. Taking account also the HTF flow rates, the closed-loop system considered 104 kg/h of Therminol-VP1; assuming a maximum daily operation of 12 h, it

corresponds to a total daily circulated mass of 14,976 kg (≈ 15 $m^3$). As the configuration is based on a closed-loop circulation, this volume represents the one-time fluid charge required to daily operate the system rather than a recurring daily consumption. Assuming the conservative hypothesis of an adding 20% spare volume/headspace of a necessary fluid storage tank, it implies a required 18 $m^3$ of thermally insulated storage tank, made at least of stainless steel and with cost range depending on the performance required, both for thermal insulation and for any necessary certifications. Both for PTC systems and Therminol-VP1, techno-economic analysis requires a detailed evaluation of current international market prices. Chinese manufacturers currently dominate the international market for trough modules due to their economies of scale, Therminol-VP1 (produced by Eastman) is supplied on the European and international markets through global distributors. In general, market prices vary widely by order quantity and sourcing country, thus an evaluation of different scenarios is crucial. Therminol-VP1 price ranges between 4,5-15 €/kg, while PTC system, when considering installing costs and key equipment (such as the tracking system), varies between 280-750 €/$m^2$. These identified ranges vary depending on the scale (or size) of the systems. The lower limit refers to larger plants; on the contrary the upper limit refers to small plants. However, market uncertainty does not allow a fixed price to be uniquely identified. For this reason, cost analysis is associated with three evaluated scenarios: optimistic (low), intermediate (medium), prudential (high). In summary, including a PTC surface area of 72 $m^2$ (referring to an existing solution in the market, https://gaiasolar.en.made-in-china.com/product/JSemqLoPXjkg/China-Parabolic-Solar-Concentrator-Fresnel-Lens-Solar-Concentrator.html), 12 heating tubes (outer tube 14 cm diameter, 10 m long; inner U-tube 15,6 mm diameter, 80 m long) assumed in stainless steel (density of 8000 kg/$m^3$) that imply a total mass of 2300 kg (6-15 €/kg range), a storage tank for Therminol-VP1 and a fluid circulating pump. To have a preliminary estimate of the characteristics required for the fluid circulation pump, reference can be made to the volumetric flow rate: 12 heating tubes have a Therminol-VP1 flow rate of 1248 kg/h, corresponding to 0,35 kg/s and 1,25 $m^3$/h. This volumetric flow may be met by i.e. industrial centrifugal circulation pumps and costs can range between 500-2500 € (Glatzmaier, 2011; Petrollese et al., 2019; Soomro et al., 2019; Elhashmi et al., 2020; Kurup, 2020; Cascetta et al., 2021; Roumpedakis et al., 2021; Zhou et al., 2021; Akar and Kurup, 2024; Giampietro et al., 2024; Sadeghi et al., 2024; Sarshar et al., 2024; Lüchinger et al., 2025). The assessment of investment costs associated with the three scenarios is shown in the table below. The highly variable market prices have led to the identification of cost ranges associated with the basic design ideal. Within this range, various combinations are potentially possible but they must also take into account additional equipment that must be provided in real application (also via pilot plant): i.e., safety or branch valves, nozzles, instruments for monitoring various parameters such as temperature and pressure, etc... are essential.

**Table 11.** Cost range of the main components of PTC-TD system for three different scenarios.

| Key equipment | **Scenarios** | | |
|---|---|---|---|
| | Low [€] | Medium [€] | High [€] |
| PTC (and installing) | 20160 | 36000 | 54000 |
| Therminol-VP1 | 67392 | 149760 | 224640 |
| Storage tank | 54000 | 135000 | 216000 |
| Heating tube | 13800 | 23000 | 34500 |
| Pump | 500 | 1500 | 2500 |
| **Total** | **155.852,00 €** | **345.260,00 €** | **531.640,00 €** |

## 5.2.2 Site reuse

The same geometrical model used for Solar driven-TD was considered for further simulations addressed to the evaluation of site reuse. Once the remediation treatment is completed, the underlying concept of the proposed two approaches was to explore the potential for geothermal applications, specifically for subsurface energy storage. In that way, the soil properly insulated as in the case of thermal desorption (TD) was considered not only as a remediation medium but also as a reservoir for storing thermal energy. The process relied on the circulation of Therminol-VP1 through the heating tubes, which, under this perspective, were reinterpreted as a Borehole Thermal Energy Storage (BTES) system. The geographic context was the same, but solar data were considered for a longer reference time: from 1st May 2022 to 30 April 2023.

First approach referred to heating-cooling cycles in which the well-insulated volume of soil (monitored at the cold point) was heated/cooled with the conditions shown in Table 12 and assessing the energy stored and the time required to reach temperatures just below 100°C in the heating phase (charging and storing), while in the cooling phase the evaluations were related to the energy dissipated (discharging), thereby simulating an external energy supply, and the time required to reach temperatures around 30°C. Both cycles were set up to provide or discharge a constant amount of energy for 8 h/day. These process conditions were included in two specific UDFs, through which the heat source (HS) was assigned to the boundary conditions, in particular to the inlet section of the U-tube in heating cycles and to the outlet section in cooling cycles.

**Table 12.** Heating-Cooling cycle input parameters.

| **Heating parameters** | | | **Cooling parameters** | | |
|---|---|---|---|---|---|
| HS | 900 | Wh | HS | -180 | Wh |
| t-active | 8 | h/day | t-active | 8 | h/day |
| t-inactive | 16 | h/day | t-inactive | 16 | h/day |
| v-active | 0,25 | m/s | v-active | 0,1 | m/s |
| Inlet area | 0,000192 | $m^2$ | Inlet area | 0,000192 | $m^2$ |
| density fluid | 1000 | $kg/m^3$ | density fluid | 1000 | $kg/m^3$ |
| Flow-mass | 172,8 | kg/h | Flow-mass | 69,12 | kg/h |

Results obtained are given in below tables. Figure 56, 57 and 58 show temperature trends for monitoring points. As can be noticed, the first cycle required longer time to reach acceptable temperatures than the other two cycles, as the starting temperature in soil was 15°C and due to an initial transient in which more energy was retained in the soil before the system approached a quasi-steady behaviour in subsequent cycles. To limit the maximum and minimum temperatures achievable during the various cycles, the 3 heating phases lasted 160, 132 and 130 days, while the cooling phases lasted 155, 150 and 140 days. The amount of energy stored or dischargeable per one heating tube is in the order of 2 million kJ in all simulated cycles.

**Table 13.** Cycle duration and respective temperature reached in soil cold point.

| **Max/Min Temperature and Duration cycles [days]** | | | | | |
|---|---|---|---|---|---|
| H1 | C1 | H2 | C2 | H3 | C3 |
| 160 | 155 | 132 | 150 | 130 | 140 |
| max T [°C] | min T [°C] | max T [°C] | min T [°C] | max T [°C] | min T [°C] |
| 98,7 | 31,72 | 96,61 | 32,23 | 96,20 | 34,85 |

**Table 14.** Stored/discharged energy in H-C cycle 1.

| **Heating cycle 1** - time | 160 | days |
|---|---|---|
| Initial soil temperature | 15 | °C |
| Final soil temperature | 98,66 | °C |
| Total useful energy after H cycle | 2690662 | kJ/tube |
| **Cooling cycle 1** - time | 155 | days |
| Initial soil temperature | 98,66 | °C |
| Final soil temperature | 31,72 | °C |
| Total used energy after C cycle | -2152842 | kJ/tube |

**Table 15.** Stored/discharged energy in H-C cycle 2.

| **Heating cycle 2** - time | 132 | days |
|---|---|---|
| Initial soil temperature | 31,72 | °C |
| Final soil temperature | 96,61 | °C |
| Total useful energy after H cycle | 2086906 | kJ/tube |
| **Cooling cycle 2** - time | 150 | days |
| Initial soil temperature | 96,61 | °C |
| Final soil temperature | 32,23 | °C |
| Total used energy after C cycle | -2070460 | kJ/tube |

**Table 16.** Stored/discharged energy in H-C cycle 3.

| **Heating cycle 3** - time | 130 | days |
|---|---|---|
| Initial soil temperature | 32,23 | °C |
| Final soil temperature | 96,20 | °C |
| Total useful energy after H cycle | 2057218 | kJ/tube |
| **Cooling cycle 3** - time | 140 | days |
| Initial soil temperature | 96,20 | °C |
| Final soil temperature | 34,85 | °C |
| Total used energy after C cycle | -1973098 | kJ/tube |

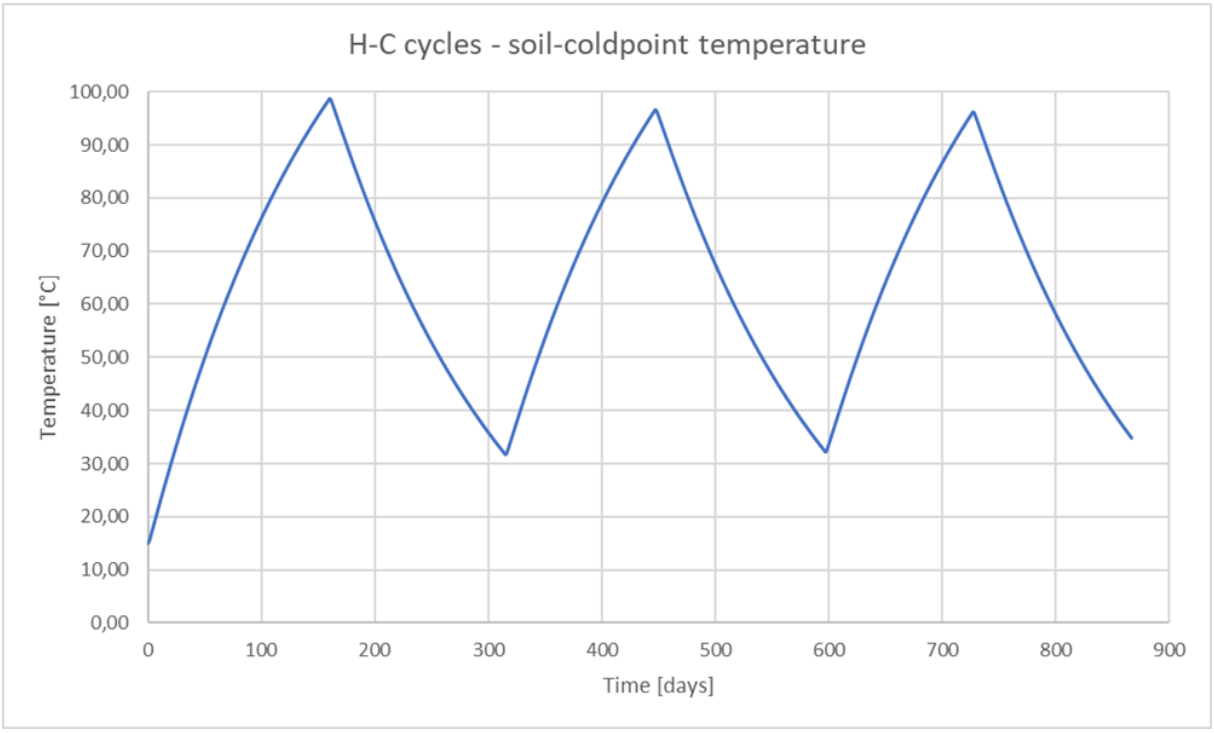


**Figure 56.** Cold point temperature trend during 3 H-C cycles, total simulation time= 867 days.

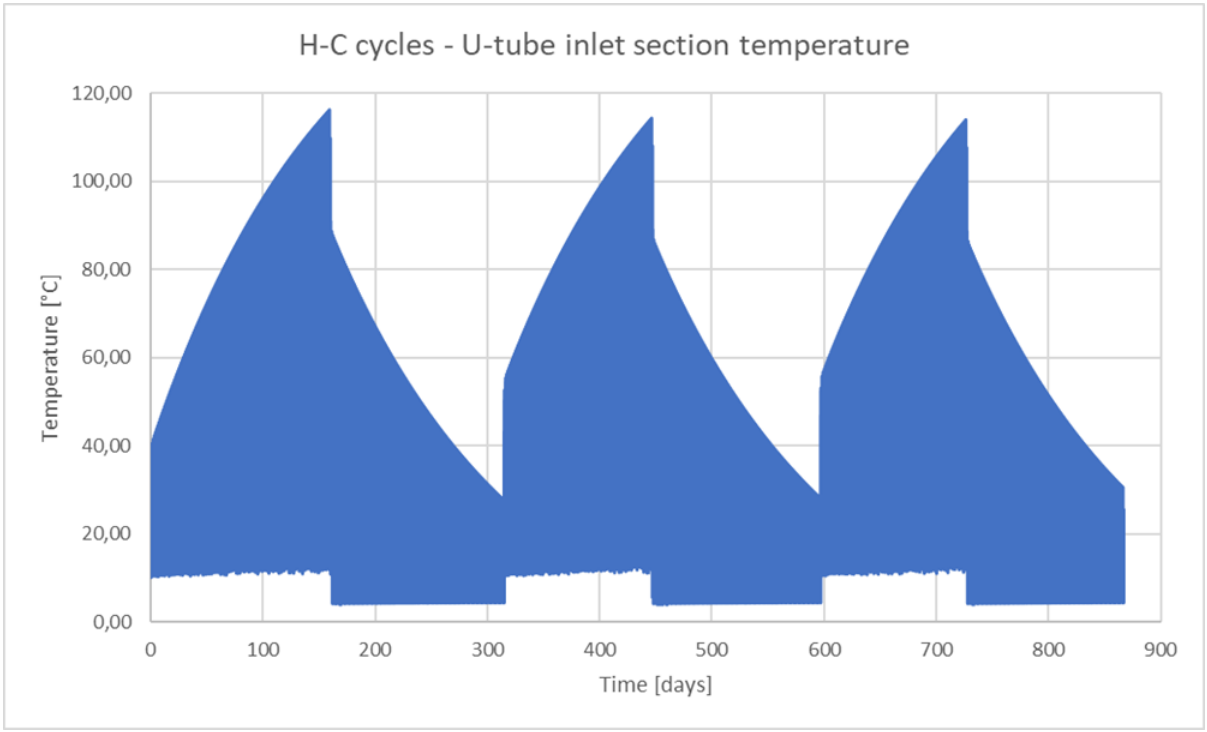


**Figure 57.** U-tube inlet section temperature trend during 3 H-C cycles.

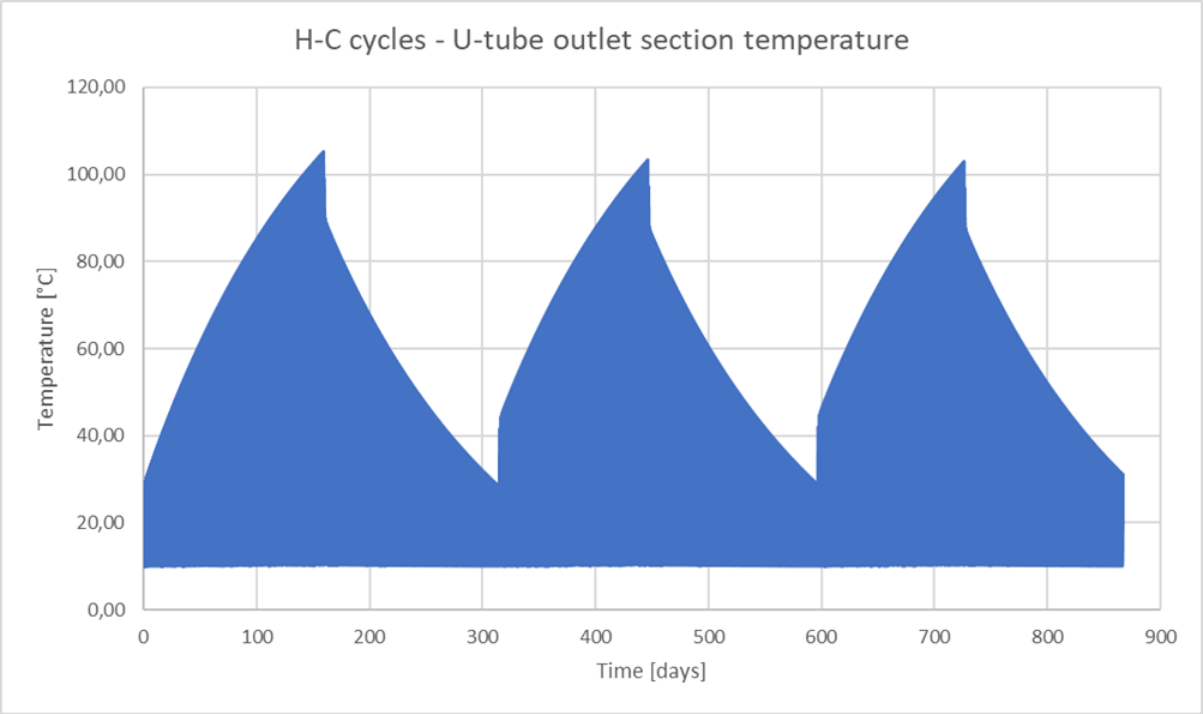


**Figure 58.** U-tube outlet section temperature trend during 3 H-C cycles.

The energy calculated as a function of the mass of soil (32162 kg) heated/cooled and the temperature variation by means of the specific heat, can be converted into kWh stored (from H cycles) or exploitable (from C cycles) considering the conversion factor:

$$1 \text{ kWh} = 3{,}6 \times 10^6 \text{ J}$$

Energy in kWh associated to each cycle is reported in Table 17. As BTES system, one heating tube in these simulation conditions can store a huge amount of energy in soil. To give an idea of the importance of the data, in Italy the average annual consumption per household is 2646 kWh per year of electric energy (Lage et al., 2024). This means that the amount of dischargeable energy is the 27% of the average electricity consumption in an Italian household. However, accounting for energy conversion yields this percentage is lower.

**Table 17.** Energy stored (H cycle)/discharged (C cycle)

| **1 tube** | time [days] | E [kJ] | E [kWh] |
|---|---|---|---|
| H1 | 160 | 2690662 | 747 |
| C1 | 155 | -2152842 | 598 |
| H2 | 132 | 2086906 | 578 |
| C2 | 150 | -2070460 | 575 |
| H3 | 130 | 2057218 | 571 |
| C3 | 140 | -1973098 | 548 |

**Table 18.** Total Energy stored and discharged normalized per year.

| time [days] | time [years] | $E_{stored}$ [kWh] | $E_{discharged}$ [kWh] |
|---|---|---|---|
| 867 | 2,38 | 1896 | 1721 |
| $E_{stored}$ [kWh/year] | | $E_{discharged}$ [kWh/year] | |
| 798,2 | | 724,5 | |

Nevertheless, the identification of the storable energy amount represents the fundamental parameter to potentially assess the size of PTC needed per one heating tube. For Gela coordinates, the average annual DNI is around 1900 kWh/m2, corresponding to an average daily value of 5,2 kWh/m2 (https://www.solaritaly.enea.it/index.php). The PTC overall efficiency in thermal energy transfer is between 0,6-0,75 (Kutscher et al., 2012; Gujrathi et al., 2017; Bellos and Tzivanidis, 2018a; Munawwar Khalil, 2023), thus corresponding to a more realistic average value of 3-3,7 kWh/$m^2$/day, which compared to a need of 2,2 kWh/day (798,2 kWh/year divided by 365 days/year) allows to obtain the PTC surface required per heating tube. The collector area needed for this type of site reuse is lower than 1 $m^2$, and in particular is between 0,6 and 0,73 $m^2$ per heating tube.

Second approach considered one year of data (Gela), from 1st May 2022 to 30th April 2023, and three different operating cases taking into account real variation of Direct Normal Irradiation and ambient temperature. This approach required a deep analysis and identification of threshold values, both for DNI and for ambient temperature, helpful to practically apply the theory behind geothermal systems:

1. charging and storing heat in the soil if DNI has acceptable values regardless of ambient temperature;
2. discharging heat from soil if DNI and temperature are less than threshold values;
3. stop the system if ambient temperature is higher than its threshold values and DNI is lower than the corresponding threshold value.

A summary of the input parameters of numerical simulation and the if-condition defined in the UDF is given in the following table. Discharged energy represents the heat lost from soil when the discharging conditions are satisfied (T<13°C and DNI<150 W/$m^2$), for which the flow-mass of Therminol-VP1 was set to 69 kg/h.

**Table 19.** Input parameters of 3-cases simulation.

| **3-cases conditions** | | |
|---|---|---|
| Number of time-step | 8760 | h |
| Initial temperature | 10 | °C |
| DNI threshold | 150 | W/$m^2$ |
| v-charging | 0,15 | m/s |
| Ambient Temp. threshold | 13 | °C |
| v-discharging | 0,1 | kg/$m^3$ |
| Flow-mass-charging | 103,68 | kg/h |
| Flow-mass-discharging | 69,12 | kg/h |
| Hypothesized PTC surface | 1 | $m^2$/tube |
| Discharged energy | -300 | Wh |

Results obtained, considering site-specific DNI and ambient temperature, inevitably tend to represent the typical climatic conditions of Gela, so a maximum temperature to be reached has not been set. Figure 59 illustrates the almost uniform distribution of heat in the soil volume at the end of simulation.

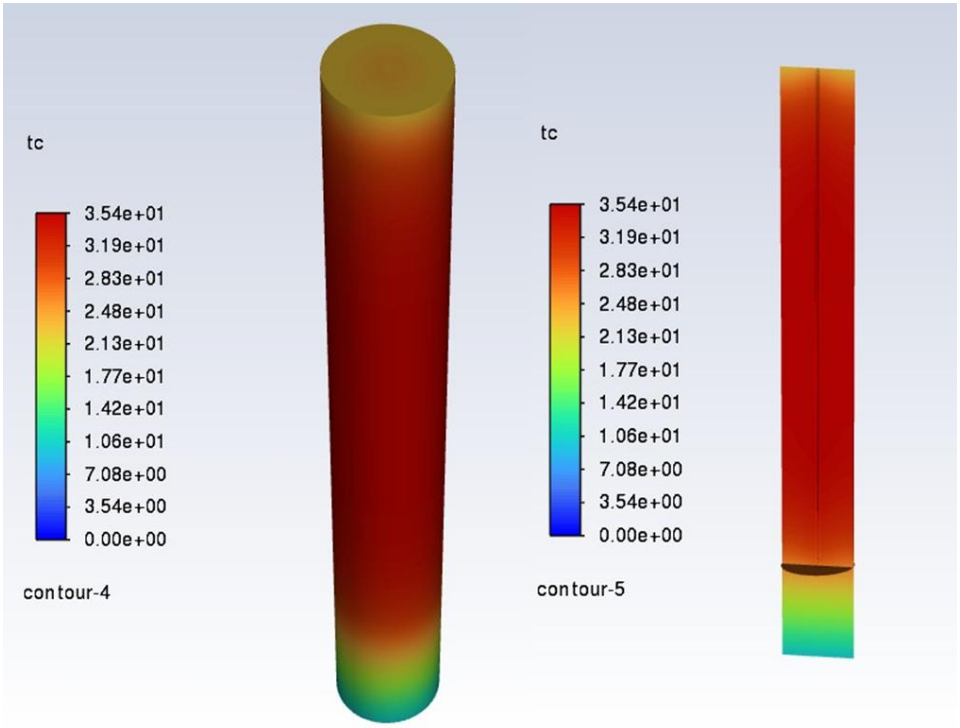


**Figure 59.** Temperature distribution in soil volume (after 365 days).

This approach resulted in a maximum temperature reached at the soil monitoring point of 66°C after 195 days (more than 6 months of continuous storage) and then discharging energy until reaching 29°C as minimum temperature after 117 days, as shown in Table 20 and Figure 60. The energy supplied or removed from the soil was evaluated as a function of the mass of soil (32162 kg) heated/cooled and the temperature variation by means of the specific heat. In this case, the energy stored in soil was found to be equal to 500kWh, while in the discharge period the energy "lost" from soil volume was equal to 330kWh. Even if this approach gave different results compared to the previous simulated case, it is certainly a more precise indication of the heat storage and discharge capacity as it refers to input data more consistent with the variation in solar radiation, specific to those geographical coordinates.

**Table 20.** Results of 3-cases simulation.

| **Final results** | | |
|---|---|---|
| Starting temperature | 10,0 | °C |
| Cold point-max temperature | 66 | °C |
| Time to reach max temperature | 195 | days |
| Cold point-min temperature | 29 | °C |
| Time to reach min temperature | 117 | days |
| Energy stored | 500,3 | kWh |
| Energy discharged | -330,6 | kWh |
| PTC surface | 1 | $m^2$ |

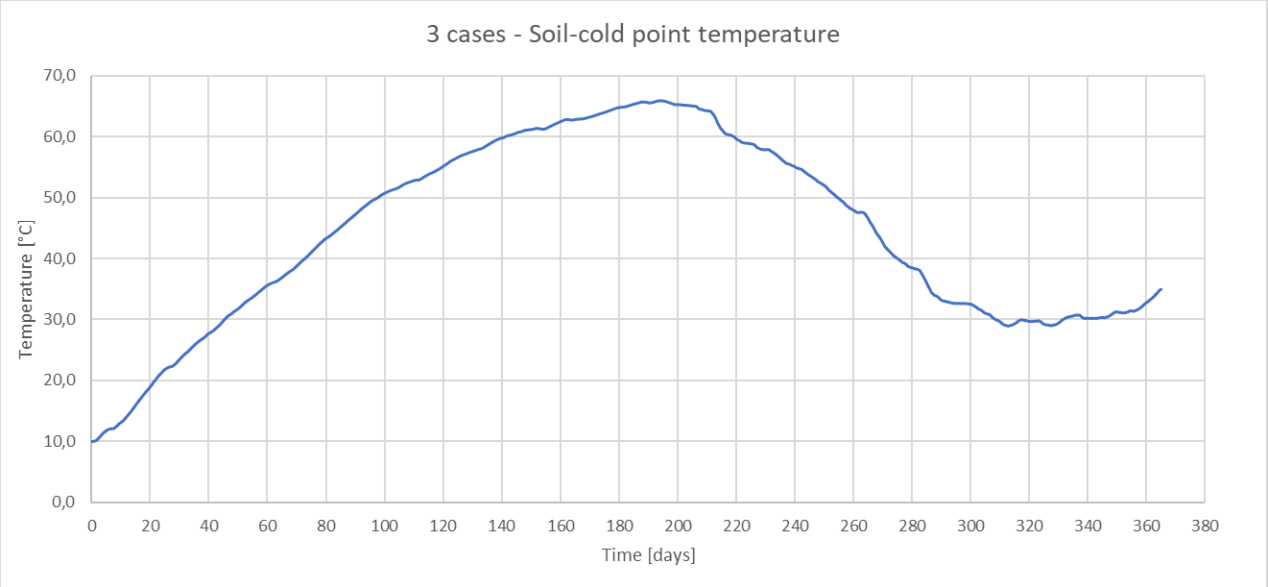


**Figure 60.** 3-cases simulation, cold point temperature trend, total simulation time= 365 days.

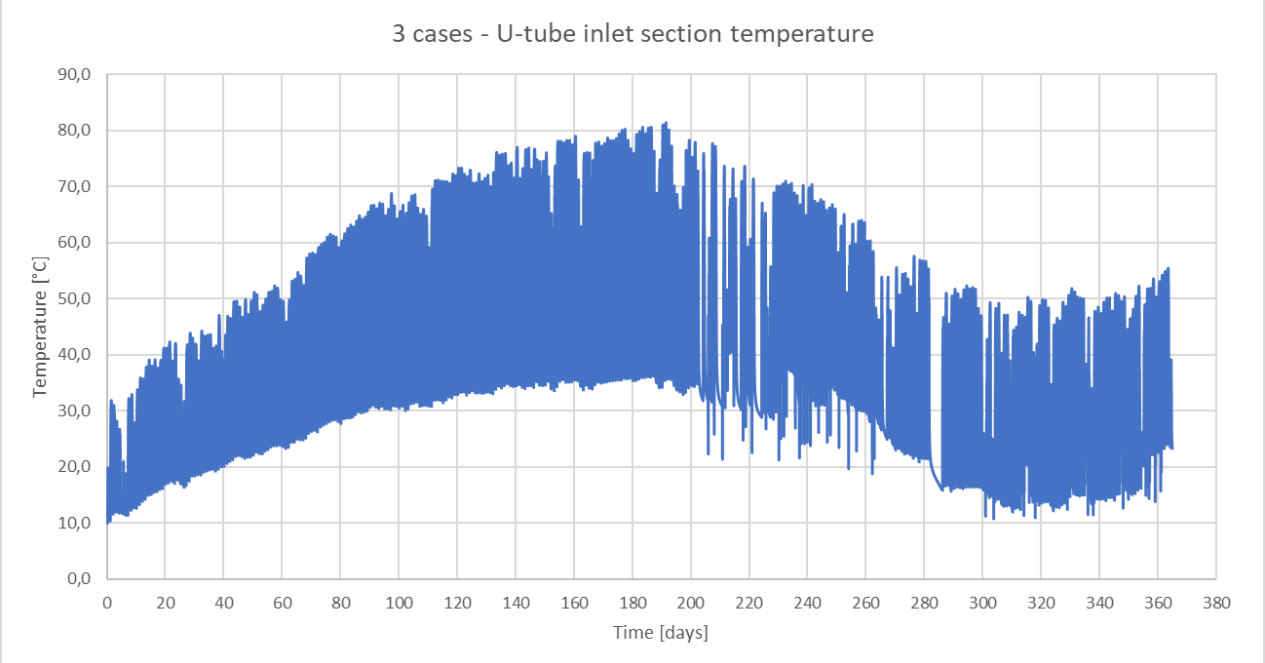


**Figure 61.** 3- cases, U-tube inlet section temperature trend, total simulation time= 365 days.

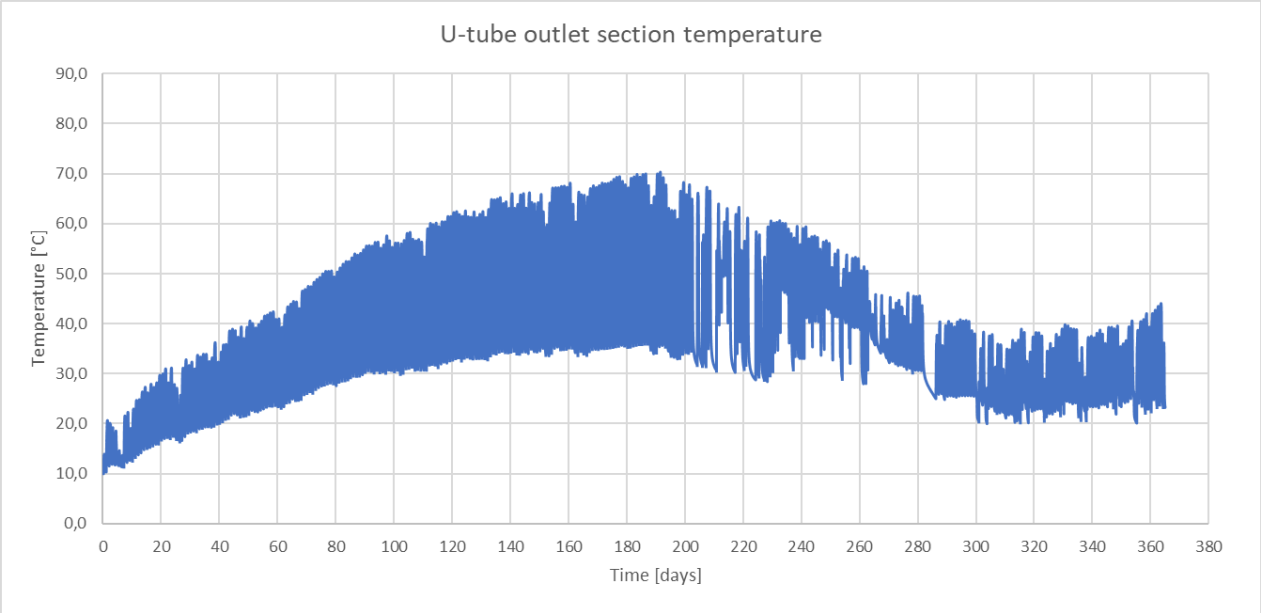


**Figure 62.** 3- cases, U-tube outlet section temperature trend, total simulation time= 365 days.

# Conclusion

This doctoral research was primarily oriented toward the comprehensive assessment of Thermal Desorption (TD), both through laboratory activities and through numerical modelling. The work was structured into two main components: experimental validation under controlled laboratory conditions and advanced modelling and simulation aimed at designing innovative renewable-driven configurations. Together, these complementary activities have provided a multi-scale perspective that contributes both to the fundamental understanding of TD as remediation treatment and to the practical assessment of its scalability and integration with solar thermal technologies. The laboratory work aimed to demonstrate that TD is a highly effective remediation treatment for soils and sediments contaminated with hydrocarbons, even at elevated pollution levels. In parallel, modelling and simulation activities were aimed to identify an energy supply strategy capable of replacing conventional fossil-fuel-based or electricity-derived heating with a renewable alternative. Given the well-established reliability of parabolic trough collectors (PTCs) in converting solar energy into thermal energy, the design evaluation was directed towards coupling PTC technology with conduction-based thermal desorption (referred as TCH technology). This approach was inspired by a process applied by Haemers Technologies (and in Italy by its partner company Icaro), through both in-situ (ISTD) and ex-situ (ESTD) configurations. Several simplifying assumptions were necessary due to the intrinsic complexity of the problem and the numerous variables requiring discretization under appropriate boundary conditions. The design scenario was hypothesized for the coordinates of Gela (CL, Italy), being an area both favourable for the exploitation of solar energy and also historically characterized by hydrocarbon contamination sites (in fact it falls within the Sites of National Interest). Since this design concept is fundamentally driven by heat transfer phenomena, computational fluid dynamics (CFD) simulations were employed using Ansys Fluent 2025 R1 (student license) to model the hypothesized scenarios. Simulations were customized using different User-Defined Functions (UDFs) to modify the default capabilities of the solver. UDFs were integrated to discretize the problem through boundary conditions and source terms suitable for numerical analysis, enabling the simulation of physical phenomena that were not available through the standard models. Furthermore, an alternative reuse pathway for the decontaminated soil was explored through simulation and UDFs, in which the same heating tube configuration used for TD was reinterpreted for Borehole Thermal Energy Storage (BTES), thus enabling the storage and reuse of energy in the soil under geothermal operation. All the UDFs implemented through C-coded routines and integrated into the simulations, proved to be fully operational and consistent with the intended modelling approach.

The experimental tests conducted with a tubular furnace confirmed the effectiveness of thermal desorption, especially in the low-temperature range (LTTD). Marine sediments with different contamination levels were successfully treated under all tested conditions, consistently achieving regulatory thresholds (CSC from Italian legislation) and high removal efficiencies (97,6-100%). Optimal operating conditions were identified as maximum treatment temperature at 200 °C with a contact time of 15 minutes, which proved effective in reaching the target remediation levels, and significantly moves away from thermal destruction temperatures, thus allowing to reduce energy costs and to prevent properties deterioration of solid matrix. To reinforce these claims, an appropriate evaluation could have been directed to ecotoxicological analyses. Additionally, in the off-gas management system or Vapour Treatment Unit (VTU) a specific adsorbent material, consisting of biochars derived from pine and eucalyptus pyrolysis, was evaluated as a potential alternative to

activated carbon, which is typically used for the management of contaminants downstream of TD. Although this was a preliminary assessment limited to adsorption capacity, biochar exhibited promising performance, comparable to activated carbon under identical laboratory testing conditions, while offering potential advantages in terms of cost and sustainability.

The modelling and simulation results, referred to the specific simulated configuration, highlighted that a minimum of 6 m² of PTC is required for each heating tube used for the remediation of hydrocarbon-contaminated soils. A preliminary investment cost evaluation was then carried out for a pilot-scale system consisting of 12 heating tubes and a collector field of approximately 72 m², with Therminol-VP1 employed as the heat transfer fluid, due to the required temperature to be achieved. Depending on the assumed cost scenarios and excluding some essential ancillary components (such as monitoring equipment and hydraulic fittings and tools), the estimated investment ranged between approximately 150.000 € and over 500.000 €. Within this range, further optimization is certainly possible, but would require more detailed design data and site-specific information. From a scientific standpoint, more detailed experimental studies are needed to validate the CFD assumptions, particularly in relation to soil heterogeneity (also accountable through modelling thanks to the versatility of the implemented UDFs, and by defining soil as multi-layer medium) or long-term thermal behaviour of the equipment. From a technological perspective, pilot-scale demonstrations are essential to assess the operational robustness of solar-driven TD systems under real field conditions, where variability in soil properties, contamination levels, and solar resource availability may strongly influence performance.

The evaluation of the site reuse for geothermal purposes highlighted the marked difference in PTC surface area required for this type of application compared to that necessary to apply PTC-TD. Among two geothermal approaches investigated, both cases resulted to a required PTC surface area of 1 $m^2$ for each heating tube, which in this case represented the key element of a BTES system.

Overall, this thesis should be regarded as a first step towards enabling the large-scale application of thermal desorption powered by renewable energy sources. By addressing the critical limitation of TD, such as its high energy demand and reliance on fossil-fuel-based energy carriers, this work paves the way for a more sustainable integration of solar thermal technologies into soil and sediment remediation practices.

# Bibliography

Abed, N., Afgan, I., 2020. An extensive review of various technologies for enhancing the thermal and optical performances of parabolic trough collectors. Int. J. Energy Res. 44, 5117–5164. https://doi.org/10.1002/er.5271

Abed, N., Afgan, I., Cioncolini, A., Iacovides, H., Nasser, A., 2020. Assessment and Evaluation of the Thermal Performance of Various Working Fluids in Parabolic Trough Collectors of Solar Thermal Power Plants under Non-Uniform Heat Flux Distribution Conditions. Energies 13, 3776. https://doi.org/10.3390/en13153776

Ahmad, A., Prakash, O., Kausher, R., Kumar, G., Pandey, S., Hasnain, S.M.M., 2024. Parabolic trough solar collectors: A sustainable and efficient energy source. Mater. Sci. Energy Technol. 7, 99–106. https://doi.org/10.1016/j.mset.2023.08.002

Akar, S., Kurup, P., 2024. Parabolic Trough Collector Cost Update for Industrial Process Heat in The United States, in: Proceedings of EuroSun 2024. Presented at the EuroSun 2024: 15th International Conference on Solar Energy for Buildings and Industry, International Solar Energy Society, Limassol, Cyprus, pp. 1–13. https://doi.org/10.18086/eurosun.2024.04.01

Akbarzadeh, S., Valipour, M.S., 2018. Heat transfer enhancement in parabolic trough collectors: A comprehensive review. Renew. Sustain. Energy Rev. 92, 198–218. https://doi.org/10.1016/j.rser.2018.04.093

Alaidaros, A.M., AlZahrani, A.A., 2024. Thermal performance of parabolic trough integrated with thermal energy storage using carbon dioxide, molten salt, and oil. J. Energy Storage 78, 110084. https://doi.org/10.1016/j.est.2023.110084

Alami, A.H., Olabi, A.G., Mdallal, A., Rezk, A., Radwan, A., Rahman, S.M.A., Shah, S.K., Abdelkareem, M.A., 2023. Concentrating solar power (CSP) technologies: Status and analysis. Int. J. Thermofluids 18, 100340. https://doi.org/10.1016/j.ijft.2023.100340

Anand, S., Kumar, S., 2024. Optimization of gaseous working fluid and internally finned absorber tube for enhancing the thermal performance of parabolic trough solar collector. Appl. Therm. Eng. 239, 122078. https://doi.org/10.1016/j.applthermaleng.2023.122078

Anna Hammerstingl, 2024. Techno-Economic Assessment and Optimization of Seasonal Borehole Thermal Energy Storage in District Heating Networks.

Anno, F.D., Rastelli, E., Sansone, C., Anno, A.D., Brunet, C., Ianora, A., 2021. Bacteria, fungi and microalgae for the bioremediation of marine sediments contaminated by petroleum hydrocarbons in the omics era. Microorganisms 9. https://doi.org/10.3390/microorganisms9081695

Avona, A., Capodici, M., Di Trapani, D., Giustra, M.G., Greco Lucchina, P., Lumia, L., Di Bella, G., Viviani, G., 2022. Preliminary insights about the treatment of contaminated marine sediments by means of bioslurry reactor: Process evaluation and microbiological characterization. Sci. Total Environ. 806, 150708. https://doi.org/10.1016/j.scitotenv.2021.150708

Backhaus, T., 2023. Commentary on the EU Commission's proposal for amending the Water Framework Directive, the Groundwater Directive, and the Directive on Environmental Quality Standards. Environ. Sci. Eur. 35, 22. https://doi.org/10.1186/s12302-023-00726-3

Baser, T., McCartney, J.S., 2015. Development of a Full-Scale Soil-Borehole Thermal Energy Storage System, in: IFCEE 2015. Presented at the IFCEE 2015, American Society of Civil Engineers, San Antonio, Texas, pp. 1608–1617. https://doi.org/10.1061/9780784479087.145

Bellos, E., Tzivanidis, C., 2018a. Analytical Expression of Parabolic Trough Solar Collector Performance. Designs 2, 9. https://doi.org/10.3390/designs2010009

Bellos, E., Tzivanidis, C., 2018b. Thermal analysis of parabolic trough collector operating with mono and hybrid nanofluids. Sustain. Energy Technol. Assess. 26, 105–115. https://doi.org/10.1016/j.seta.2017.10.005

Biache, C., Lorgeoux, C., Andriatsihoarana, S., Colombano, S., Faure, P., 2015. Effect of pre-heating on the chemical oxidation efficiency: Implications for the PAH availability measurement in contaminated soils. J. Hazard. Mater. 286, 55–63. https://doi.org/10.1016/j.jhazmat.2014.12.041

Bianco, F., Monteverde, G., Race, M., Papirio, S., Esposito, G., 2020. Comparing performances, costs and energy balance of ex situ remediation processes for PAH-contaminated marine sediments. Environ. Sci. Pollut. Res. 27, 19363–19374. https://doi.org/10.1007/s11356-020-08379-y

Biresselioglu, M.E., Limoncuoglu, S.A., Demir, M.H., Reichl, J., Burgstaller, K., Sciullo, A., Ferrero, E., 2021. Legal Provisions and Market Conditions for Energy Communities in Austria, Germany, Greece, Italy, Spain, and Turkey: A Comparative Assessment. Sustainability 13, 11212. https://doi.org/10.3390/su132011212

Brown, R.W., Mayser, J.P., Widdowson, C., Chadwick, D.R., Jones, D.L., 2021. Dependence of thermal desorption method for profiling volatile organic compound (VOC) emissions from soil. Soil Biol. Biochem. 160, 108313. https://doi.org/10.1016/j.soilbio.2021.108313

Bruce, P., Ohlsson, Y., 2020. Environmental Goals Addressed in Assessments of Contaminated Sediments. Integr. Environ. Assess. Manag. 16, 128–139. https://doi.org/10.1002/ieam.4223

Bu, X., Chen, W., Du, J., Wang, L., 2024. Performance analysis of high temperature thermal energy storage in shallow depth enhanced geothermal system. Front. Built Environ. 10, 1486884. https://doi.org/10.3389/fbuil.2024.1486884

Buscemi, A., Beccali, M., Guarino, S., Brano, V.L., 2023. Coupling a road solar thermal collector and borehole thermal energy storage for building heating: First experimental and numerical results. Energy Convers. Manag. 291. https://doi.org/10.1016/j.enconman.2023.117279

Bykova, M.V., Alekseenko, A.V., Pashkevich, M.A., Drebenstedt, C., 2021. Thermal desorption treatment of petroleum hydrocarbon-contaminated soils of tundra, taiga, and forest steppe landscapes. Environ. Geochem. Health 43, 2331–2346. https://doi.org/10.1007/s10653-020-00802-0

Calderón, A., Barreneche, C., Prieto, C., Segarra, M., Fernández, A.I., 2021. Concentrating Solar Power Technologies: A Bibliometric Study of Past, Present and Future Trends in Concentrating Solar Power Research. Front. Mech. Eng. 7, 682592. https://doi.org/10.3389/fmech.2021.682592

Cascetta, M., Petrollese, M., Oyekale, J., Cau, G., 2021. Thermocline vs. two-tank direct thermal storage system for concentrating solar power plants: A comparative techno-economic assessment. Int. J. Energy Res. 45, 17721–17737. https://doi.org/10.1002/er.7005

Chai, R., Wang, J., Zhan, M., Yuan, D., Chi, Z., Gu, H., Mao, J., 2022. Pre-Drying of Chlorine–Organic-Contaminated Soil in a Rotary Dryer for Energy Efficient Thermal Remediation. Int. J. Environ. Res. Public. Health 19, 16607. https://doi.org/10.3390/ijerph192416607

Chen, Zefeng, Chen, Zhiguo, Li, Y., Zhang, R., Liu, Y., Hui, A., Cao, W., Liu, J., Bai, H., Song, J., 2024. A review on remediation of chlorinated organic contaminants in soils by thermal desorption. J. Ind. Eng. Chem. 133, 112–121. https://doi.org/10.1016/j.jiec.2023.12.022

Cho, K., Kang, J., Kim, S., Purev, O., Myung, E., Kim, H., Choi, N., 2021. Effect of inorganic carbonate and organic matter in thermal treatment of mercury-contaminated soil. Environ. Sci. Pollut. Res. 28, 48184–48193. https://doi.org/10.1007/s11356-021-14024-z

Commission, H., 2022. HELCOM Guidelines for the disposal of dredged material at sea.

Copetti, D., Erba, S., 2024. A bibliometric review on the Water Framework Directive twenty years after its birth. Ambio 53, 95–108. https://doi.org/10.1007/s13280-023-01918-0

d'Errico, G., Nardi, A., Benedetti, M., Mezzelani, M., Fattorini, D., Di Carlo, M., Pittura, L., Giuliani, M.E., Macchia, S., Vitiello, V., Sartori, D., Scuderi, A., Morroni, L., Chiaretti, G., Gorbi, S., Pellegrini, D., Regoli, F., 2021. Application of a Multidisciplinary Weight of Evidence Approach as a Tool for Monitoring the Ecological Risk of Dredging Activities. Front. Mar. Sci. 8, 765256. https://doi.org/10.3389/fmars.2021.765256

D'Auria, M., Grena, R., Lanchi, M., Liberatore, R., 2024. Heat Supply to Industrial Processes via Molten Salt Solar Concentrators. Energies 17, 4541. https://doi.org/10.3390/en17184541

Decreto-legge del 24/02/2023 n. 13 - Disposizioni urgenti per l'attuazione del Piano nazionale di ripresa e resilienza (PNRR) e del Piano nazionale degli investimenti complementari al PNRR (PNC), nonche' per l'attuazione delle politiche di coesione e della politica agricola comune, 2023.

Ding, D., Song, X., Wei, C., LaChance, J., 2019. A review on the sustainability of thermal treatment for contaminated soils. Environ. Pollut. 253, 449–463. https://doi.org/10.1016/j.envpol.2019.06.118

Donga, R.K., Kumar, S., Velidi, G., 2025. Heat transfer enhancement in a parabolic trough collector using finned tubular absorber. Sci. Rep. 15, 24142. https://doi.org/10.1038/s41598-025-07825-6

Eggleton, J., Thomas, K.V., 2004. A review of factors affecting the release and bioavailability of contaminants during sediment disturbance events. Environ. Int. 30, 973–980. https://doi.org/10.1016/j.envint.2004.03.001

El Kouche, A., Ortegón Gallego, F., 2022. Modeling and numerical simulation of a parabolic trough collector using an HTF with temperature dependent physical properties. Math. Comput. Simul. 192, 430–451. https://doi.org/10.1016/j.matcom.2021.09.015

Elhashmi, R., Hallinan, K.P., Chiasson, A.D., 2020. Low-energy opportunity for multi-family residences: A review and simulation-based study of a solar borehole thermal energy storage system. Energy 204, 117870. https://doi.org/10.1016/j.energy.2020.117870

Environment, I.M. for the, 2016a. Ministerial Decree 172/2016. Regolamento recante criteri tecnici per la caratterizzazione dei sedimenti marini in siti di bonifica di interesse nazionale (SIN).

Environment, I.M. for the, 2016b. Ministerial Decree 173/2016. Regolamento recante modalità e criteri tecnici per l'autorizzazione all'immersione in mare dei materiali di escavo di fondali marini.

Esposito, L., Romagnoli, G., 2023. Overview of policy and market dynamics for the deployment of renewable energy sources in Italy: Current status and future prospects. Heliyon 9, e17406. https://doi.org/10.1016/j.heliyon.2023.e17406

European Parliament, C., 2018. Directive (EU) 2018/2001 on the promotion of the use of energy from renewable sources.

European Union, 2018. Directive (EU) 2018/851 of the European Parliament and of the Council amending Directive 2008/98/EC on waste.

European Union, 2008. Directive 2008/98/EC of the European Parliament and of the Council of 19 November 2008 on waste and repealing certain Directives.

Fadejev, J., Simson, R., Kurnitski, J., Haghighat, F., 2017. A review on energy piles design, sizing and modelling. Energy 122, 390–407. https://doi.org/10.1016/j.energy.2017.01.097

Falciglia, P.P., Giustra, M.G., Vagliasindi, F.G.A., 2011. Low-temperature thermal desorption of diesel polluted soil: Influence of temperature and soil texture on contaminant removal kinetics. J. Hazard. Mater. 185, 392–400. https://doi.org/10.1016/j.jhazmat.2010.09.046

Falciglia, P.P., Lumia, L., Giustra, M.G., Gagliano, E., Roccaro, P., Vagliasindi, F.G.A., Di Bella, G., 2020a. Remediation of petrol hydrocarbon-contaminated marine sediments by thermal desorption. Chemosphere 260, 127576. https://doi.org/10.1016/j.chemosphere.2020.127576

Falciglia, P.P., Malarbì, D., Roccaro, P., Vagliasindi, F.G.A., 2020b. Innovative thermal and physico-chemical treatments for the clean-up of marine sediments dredged from the Augusta Bay (Southern Italy). Reg. Stud. Mar. Sci. 39, 101426. https://doi.org/10.1016/j.rsma.2020.101426

Falconi M. et al., 2025. In-situ Thermal Desorption (ISTD) monograph (No. 2022/11 ISTD). IMPEL, COMMON FORUM, EIONET, NICOLE.

Falconi M. et al., 2024. Estrazione Multifase (MPE) Report (No. 2022/10 MPE IT).

Farmer, A.M., 2012. Manual of European Environmental Policy. IEEP.

Fernandes, M.R., Melo, E.S.D.P., Ancel, M.A.P., Guimarães, R.D.C.A., Hiane, P.A., Geilow, K.D.C.F., Bogo, D., Tschinkel, P.F.S., Rosa, A.C.G., Medeiros, C.S.D.A., Oliveira, R.J., Vilela, M.L.B., Garcia, D.A.Z., Nascimento, V.A.D., 2025. Assessment of the Risk to Human Health and Pollution Levels Due to the Presence of Metal(loid)s in Sediments, Water, and Fishes in Urban Rivers in the State of Mato Grosso do Sul, Brazil. Urban Sci. 9, 114. https://doi.org/10.3390/urbansci9040114

Ferrante, M., Copat, C., Mauceri, C., Grasso, A., Schilirò, T., Gilli, G., 2015. The importance of indicators in monitoring water quality according to European directives. Epidemiol Prev.

Ferruzzi, G., Delcea, C., Barberi, A., Di Dio, V., Di Somma, M., Catrini, P., Guarino, S., Rossi, F., Parisi, M.L., Sinicropi, A., Longo, S., 2023. Concentrating Solar Power: The State of the Art, Research Gaps and Future Perspectives. Energies 16, 8082. https://doi.org/10.3390/en16248082

Förstner, U., Salomons, W., 2010. Sediment research, management and policy: A decade of JSS. J. Soils Sediments 10, 1440–1452. https://doi.org/10.1007/s11368-010-0310-7

Giaconia, A., Tizzoni, A.C., Sau, S., Corsaro, N., Mansi, E., Spadoni, A., Delise, T., 2021. Assessment and Perspectives of Heat Transfer Fluids for CSP Applications. Energies 14, 7486. https://doi.org/10.3390/en14227486

Giampietro, D., Stefanizzi, M., Fornarelli, F., Dambrosio, L., Nicolini, D., Miliozzi, A., Camporeale, S.M., 2024. Energy and Cost Analysis of Concentrated Solar Thermal Plants Integrated With Latent Heat Thermal Energy Storage for the Decarbonization of Industrial Processes, in: GT2024. Volume 6: Education; Electric Power; Energy Storage; Fans and Blowers. https://doi.org/10.1115/GT2024-127835

Glatzmaier, G., 2011. Developing a Cost Model and Methodology to Estimate Capital Costs for Thermal Energy Storage (No. NREL/TP-5500-53066, 1031953). https://doi.org/10.2172/1031953

Government, I., 2017. Presidential Decree 120/2017. Regolamento recante la disciplina semplificata della gestione delle terre e rocce da scavo.

Government, I., 2006. Legislative Decree 152/2006. Norme in materia ambientale (Testo Unico Ambientale).

Gujrathi, A.S., Ingale, S.P., Patil, S.U., 2017. Analysis of Parabolic Trough Collector using Ansys Fluent Software 5.

Horst, J., Munholland, J., Hegele, P., Klemmer, M., Gattenby, J., 2021. In Situ Thermal Remediation for Source Areas: Technology Advances and a Review of the Market From 1988–2020. Groundw. Monit. Remediat. 41, 17–31. https://doi.org/10.1111/gwmr.12424

Huang, C.-C., Tien, C.-J., Sung, L.-K., Chen, C.S., 2025. Thermal Desorption Technologies for Remediating a Petroleum Hydrocarbon Contaminated Mega-Site. https://doi.org/10.2139/ssrn.5171117

Hullebusch, E.D.V., Lens, P.N.L., Tabak, H.H., 2005. Developments in bioremediation of soils and sediments polluted with metals and radionuclides. 3. Influence of chemical speciation and bioavailability on contaminants immobilization/mobilization bio-processes. Rev. Environ. Sci. Biotechnol. https://doi.org/10.1007/s11157-005-2948-y

Hylland, K., Assunção, M.G.L., 2022. OSPAR's Quality Status Report 2023 (No. 899/2022).
IEA, 2023. Italy 2023-Energy Policy Review. Paris.
ISPRA-SNPA, 2021. Lo stato delle bonifiche dei siti contaminati in Italia: i dati regionali.
Javidan, M., Gorji-Bandpy, M., Al-Araji, A., 2023. Investigation and simulation of parabolic trough collector with the presence of hybrid nanofluid in the finned receiver tube. Theor. Appl. Mech. Lett. 13, 100465. https://doi.org/10.1016/j.taml.2023.100465
Jebbar, Y., Fluiful, F., Khudhayer, W., 2024. Heat Transfer Enhancement of the Absorber Tube in a Parabolic Trough Solar Collector through the Insertion of Novel Cylindrical Turbulators. Fluid Dyn. Mater. Process. 20, 1279–1297. https://doi.org/10.32604/fdmp.2024.050753
Jordens, A., Makoudi, M., Saadaoui, H., Haemers, J., 2023. REMEDIATION OF DIOXIN-CONTAMINATED SOILS THROUGH THERMAL DESORPTION AND VAPOR MANAGEMENT VIA THERMAL OXIDIZER AT BIEN HOA AIRBASE, VIETNAM. Environ. Eng. Manag. J. 22, 1735–1744. https://doi.org/10.30638/eemj.2023.148
Kannaiyan, S., Bokde, N.D., 2022. Performance of Parabolic Trough Collector with Different Heat Transfer Fluids and Control Operation. Energies 15, 7572. https://doi.org/10.3390/en15207572
Kristanti, R.A., Khanitchaidecha, W., Taludar, G., Karácsony, P., Cao, L.T.T., Chen, T.-W., Darwish, N.M., AlMunqedhi, B.M., 2022. A Review on Thermal Desorption Treatment for Soil Contamination. Trop. Aquat. Soil Pollut. 2, 45–58. https://doi.org/10.53623/tasp.v2i1.68
Kurup, P., 2020. Hybrid Solar Heat Generation Modelling and Cases, in: Proceedings of the ISES EuroSun 2020 Conference – 13th International Conference on Solar Energy for Buildings and Industry. Presented at the EuroSun 2020, International Solar Energy Society, Online, pp. 1–14. https://doi.org/10.18086/eurosun.2020.03.05
Kutscher, C., Burkholder, F., Kathleen Stynes, J., 2012. Generation of a Parabolic Trough Collector Efficiency Curve From Separate Measurements of Outdoor Optical Efficiency and Indoor Receiver Heat Loss. J. Sol. Energy Eng. 134, 011012. https://doi.org/10.1115/1.4005247
Lage, M., Castro, R., Manzolini, G., Casalicchio, V., Sousa, T., 2024. Techno-economic analysis of self-consumption schemes and energy communities in Italy and Portugal. Sol. Energy 270, 112407. https://doi.org/10.1016/j.solener.2024.112407
Leite, E.C.P., Rodrigues, F.M., Horimouti, T.S.T., Shinzato, M.C., Nakayama, C.R., Freitas, J.G.D., 2021. Thermally-induced changes in tropical soils properties and potential implications to sequential nature-based solutions. J. Contam. Hydrol. 241, 103808. https://doi.org/10.1016/j.jconhyd.2021.103808
Li, F., Zhang, Y., Wang, S., Li, G., Yue, X., Zhong, D., Chen, C., Shen, K., 2020. Insight into ex-situ thermal desorption of soils contaminated with petroleum via carbon number-based fraction approach. Chem. Eng. J. 385, 123946. https://doi.org/10.1016/j.cej.2019.123946
Li, X., Xie, L., Zheng, X., 2012. The comparison between the Mie theory and the Rayleigh approximation to calculate the EM scattering by partially charged sand. J. Quant. Spectrosc. Radiat. Transf. 113, 251–258. https://doi.org/10.1016/j.jqsrt.2011.09.020
Li, Y., Wei, M., Yu, B., Liu, L., Xue, Q., 2022. Thermal desorption optimization for the remediation of hydrocarbon-contaminated soils by a self-built sustainability evaluation tool. J. Hazard. Mater. 436, 129156. https://doi.org/10.1016/j.jhazmat.2022.129156
Liao, J., Guo, H., Bordoloi, S., Li, D., Zhang, Y., Ni, J., Yuan, H., Zhao, X., 2025. Thermal desorption remediation effects on soil biogeochemical properties and plant performance: Global meta-analysis. Biogeotechnics 3, 100140. https://doi.org/10.1016/j.bgtech.2024.100140
Liu, C., Shi, H., Wang, C., Fei, Y., Han, Z., 2022. Thermal Remediation of Soil Contaminated with Polycyclic Aromatic Hydrocarbons: Pollutant Removal Process and Influence on Soil Functionality. Toxics 10, 474. https://doi.org/10.3390/toxics10080474

Liu, H., Li, J., Zhao, M., Li, Y., Chen, Y., 2019. Remediation of oil-based drill cuttings using low-temperature thermal desorption: Performance and kinetics modeling. Chemosphere 235, 1081–1088. https://doi.org/10.1016/j.chemosphere.2019.07.047

Lüchinger, R., Hendry, R., Walter, H., Worlitschek, J., Schuetz, P., 2025. Cost Analysis for Large Thermal Energy Storage Systems. ASME J. Eng. Sustain. Build. Cities 6, 021006. https://doi.org/10.1115/1.4069122

Lumia, L., Giustra, M.G., Viviani, G., Di Bella, G., 2020. Washing Batch Test of Contaminated Sediment: The Case of Augusta Bay (SR, Italy). Appl. Sci. 10, 473. https://doi.org/10.3390/app10020473

Łyszczarz, S., Lasota, J., Szuszkiewicz, M.M., Błońska, E., 2021. Soil texture as a key driver of polycyclic aromatic hydrocarbons (PAHs) distribution in forest topsoils. Sci. Rep. 11, 14708. https://doi.org/10.1038/s41598-021-94299-x

Ma, Q., Wang, P., 2020. Underground solar energy storage via energy piles. Appl. Energy 261, 114361. https://doi.org/10.1016/j.apenergy.2019.114361

Mahon, H., O'Connor, D., Friedrich, D., Hughes, B., 2022. A review of thermal energy storage technologies for seasonal loops. Energy 239, 122207. https://doi.org/10.1016/j.energy.2021.122207

Malode, S., Mohanta, J.C., Prakash, R., 2022. A review on life cycle assessment approach on thermal power generation. Mater. Today Proc. 56, 791–798. https://doi.org/10.1016/j.matpr.2022.02.258

Manfra, L., Maggi, C., d'Errico, G., Rotini, A., Catalano, B., Maltese, S., Moltedo, G., Romanelli, G., Sesta, G., Granato, G., Lanera, P., Amici, M., Martuccio, G., Onorati, F., Di Mento, R., Berducci, M.T., Chiaretti, G., Faraponova, O., Regoli, F., Tornambè, A., 2021. A Weight of Evidence (WOE) Approach to Assess Environmental Hazard of Marine Sediments from Adriatic Offshore Platform Area. Water 13, 1691. https://doi.org/10.3390/w13121691

Maris, G., Flouros, F., 2021. The Green Deal, National Energy and Climate Plans in Europe: Member States' Compliance and Strategies. Adm. Sci. 11, 75. https://doi.org/10.3390/admsci11030075

McCartney, J., Baser, T., Zhan, N., Lu, N., Ge, S., Smits, K., 2017. Storage of Solar Thermal Energy in Borehole Thermal Energy Storage Systems. Oklahoma State University Library. https://doi.org/10.22488/okstate.17.000512

Menter, F.R., 1994. Two-equation eddy-viscosity turbulence models for engineering applications. AIAA J. 32, 1598–1605. https://doi.org/10.2514/3.12149

Mhatre, P., Thakur, C., 2022. Design and analysis of solar parabolic trough collector.

Miglino, A.N., Holmes, C.M., 2023. Applying weight of evidence methods to assessing exposure in aquatic environments: Comparing lines of evidence. Integr. Environ. Assess. Manag. 19, 1207–1219. https://doi.org/10.1002/ieam.4602

Mneimneh, F., Ghazzawi, H., Ramakrishna, S., 2023. Review Study of Energy Efficiency Measures in Favor of Reducing Carbon Footprint of Electricity and Power, Buildings, and Transportation. Circ. Econ. Sustain. 3, 447–474. https://doi.org/10.1007/s43615-022-00179-5

Mohan Das A N, Sudeep Kumar T, U.H., Bhimasen Soragaon, Abdulrajak Buradi, 2024. Enhancing Parabolic Trough Solar Collector Efficiency through Absorber Tube Rotation: A Computational Study. Power Syst. Technol. 48, 285–305. https://doi.org/10.52783/pst.276

Molnár, G., Cabeza, L.F., Chatterjee, S., Ürge-Vorsatz, D., 2024. Modelling the building-related photovoltaic power production potential in the light of the EU's Solar Rooftop Initiative. Appl. Energy 360, 122708. https://doi.org/10.1016/j.apenergy.2024.122708

Moretti, E., Stamponi, E., 2023. The Renewable Energy Communities in Italy and the Role of Public Administrations: The Experience of the Municipality of Assisi between Challenges and Opportunities. Sustainability 15, 11869. https://doi.org/10.3390/su151511869

Müllejans, H., Zaaiman, W., Galleano, R., Pavanello, D., Salis, E., Sample, T., Bardizza, G., Lopez Garcia, J., Kenny, R., Shaw, D., Field, M., Castellazzi, L., Dunlop, E.D., 2020. State-of-the-art for assessment of solar energy technologies.

Munawwar Khalil, 2023. Analysis and Optimization of Heat Transfer in Receiver on Line Focusing Concentrating Solar Thermal System.

O'Brien, P.L., DeSutter, T.M., Casey, F.X.M., Khan, E., Wick, A.F., 2018. Thermal remediation alters soil properties – a review. J. Environ. Manage. 206, 826–835. https://doi.org/10.1016/j.jenvman.2017.11.052

Oketola, T., Mwesigye, A., 2024. Numerical investigation of the overall thermal and thermodynamic performance of a high concentration ratio parabolic trough solar collector with a novel modified twisted tape insert using supercritical CO2 as the working fluid. Therm. Sci. Eng. Prog. 51, 102592. https://doi.org/10.1016/j.tsep.2024.102592

Olia, H., Torabi, M., Bahiraei, M., Ahmadi, M.H., Goodarzi, M., Safaei, M.R., 2019. Application of Nanofluids in Thermal Performance Enhancement of Parabolic Trough Solar Collector: State-of-the-Art. Appl. Sci. 9, 463. https://doi.org/10.3390/app9030463

OSPAR Commission, 2024. OSPAR Annual Report (No. n 1048/2024).

Pagnozzi, G., Carroll, S., Reible, D.D., Millerick, K., 2020. Biological Natural Attenuation and Contaminant Oxidation in Sediment Caps: Recent Advances and Future Opportunities. Curr. Pollut. Rep. 6, 281–294. https://doi.org/10.1007/s40726-020-00153-5

Panagos, P., Jones, A., Lugato, E., Ballabio, C., 2025. A Soil Monitoring Law for Europe. Glob. Chall. 9, 2400336. https://doi.org/10.1002/gch2.202400336

Panagos, P., Van Liedekerke, M., Yigini, Y., Montanarella, L., 2013. Contaminated Sites in Europe: Review of the Current Situation Based on Data Collected through a European Network. J. Environ. Public Health 2013, 1–11. https://doi.org/10.1155/2013/158764

Park, M., Panthi, G., Park, J.-H., Bajagain, R., Lee, K.Y., Hong, Y., 2025. Molecular Weight-Dependent Desorption of Alkanes in Low Temperature Thermal Treatment of Total Petroleum Hydrocarbon-Contaminated Soils. Water. Air. Soil Pollut. 236, 103. https://doi.org/10.1007/s11270-025-07738-0

Parliament, E., Council, 2006. Directive 2006/12/EC of the European Parliament and of the Council of 5 April 2006 on waste.

Pasciucco, F., Pecorini, I., Di Gregorio, S., Pilato, F., Iannelli, R., 2021. Recovery Strategies of Contaminated Marine Sediments: A Life Cycle Assessment. Sustainability 13, 8520. https://doi.org/10.3390/su13158520

Payá Pérez, A., Rodríguez Eugenio, N., 2018. Status of local soil contamination in Europe: revision of the indicator "Progress in the management contaminated sites in Europe," EUR. Publications Office of the European Union, Luxembourg. https://doi.org/10.2760/093804

Petrollese, M., Arena, S., Cascetta, M., Casti, E., Cau, G., 2019. Techno-economic comparison of different thermal energy storage technologies for medium-scale CSP plants. Presented at the SECOND INTERNATIONAL CONFERENCE ON MATERIAL SCIENCE, SMART STRUCTURES AND APPLICATIONS: ICMSS-2019, Erode, India, p. 020128. https://doi.org/10.1063/1.5138861

Piccardo, M., Vellani, V., Anselmi, S., Grazioli, E., Renzi, M., Terlizzi, A., Pittura, L., D'Errico, G., Regoli, F., Bevilacqua, S., 2024. The application of the Weight-Of-Evidence approach for an integrated ecological risk assessment of marine protected sites. Ecol. Indic. 159, 111676. https://doi.org/10.1016/j.ecolind.2024.111676

Pino-Herrera, D.O., Pechaud, Y., Huguenot, D., Esposito, G., Hullebusch, E.D. van, Oturan, M.A., 2017. Removal mechanisms in aerobic slurry bioreactors for remediation of soils and sediments polluted with hydrophobic organic compounds: An overview. J. Hazard. Mater. https://doi.org/10.1016/j.jhazmat.2017.06.013

Pourasl, H.H., Barenji, R.V., Khojastehnezhad, V.M., 2023. Solar energy status in the world: A comprehensive review. Energy Rep. 10, 3474–3493. https://doi.org/10.1016/j.egyr.2023.10.022

Prestigiacomo, C., Giaconia, A., Proietto, F., Caputo, G., Balog, I., Ollà, E., Terranova, C.F., Scialdone, O., Galia, A., 2024. Concentrated solar heat for the decarbonization of industrial chemical processes: a case study on crude oil distillation. Energy 293, 130718. https://doi.org/10.1016/j.energy.2024.130718

Rapti, D., Tinti, F., Caputo, C.A., 2024. Integrated Underground Analyses as a Key for Seasonal Heat Storage and Smart Urban Areas. Energies 17, 2533. https://doi.org/10.3390/en17112533

Re, I., Bosco, D., Henzen, E., 2019. Soil Contamination from Hydrocarbons in Italy. A mapping of progress in the remediation of Sites of National and Regional Interest. https://doi.org/10.13140/RG.2.2.33104.53764

Ren, J., Song, X., Ding, D., 2020. Sustainable remediation of diesel-contaminated soil by low temperature thermal treatment: Improved energy efficiency and soil reusability. Chemosphere 241, 124952. https://doi.org/10.1016/j.chemosphere.2019.124952

Ribeiro, A.B., others, 2020. Reuse of treated soils and sediments in the context of circular economy: European policies and technological trends. J. Environ. Manage. 262, 110–129.

Rodríguez Rodrigo, R., Díaz Martín, R., Baranda Fernández, M., Román Gallego, J.Á., Mayo Del Río, C., 2024. Technical and economic study of solar energy concentration technologies (linear Fresnel and parabolic trough collectors) to generate process heat at medium temperature for the dairy industry of Spain. Sol. Energy 271, 112420. https://doi.org/10.1016/j.solener.2024.112420

Roumpedakis, T.C., Fostieris, N., Braimakis, K., Monokrousou, E., Charalampidis, A., Karellas, S., 2021. Techno-Economic Optimization of Medium Temperature Solar-Driven Subcritical Organic Rankine Cycle. Thermo 1, 77–105. https://doi.org/10.3390/thermo1010007

S Mathew, G Visavale, V Mali, 2010. CFD Analysis of a Heat Collector Element in a Solar Parabolic Trough Collector. https://doi.org/10.13140/2.1.3247.4241

Sadeghi, H., Jalali, R., Singh, R.M., 2024. A review of borehole thermal energy storage and its integration into district heating systems. Renew. Sustain. Energy Rev. 192, 114236. https://doi.org/10.1016/j.rser.2023.114236

Salaudeen, S.A., 2019. Investigation on the performance and environmental impact of a latent heat thermal energy storage system. J. King Saud Univ. - Eng. Sci. 31, 368–374. https://doi.org/10.1016/j.jksues.2018.03.004

Sandá, A., Moya, S.L., Valenzuela, L., 2019. Modelling and simulation tools for direct steam generation in parabolic-trough solar collectors: A review. Renew. Sustain. Energy Rev. 113, 109226. https://doi.org/10.1016/j.rser.2019.06.033

Sang, Y., Yu, W., He, L., Wang, Z., Ma, F., Jiao, W., Gu, Q., 2021. Sustainable remediation of lube oil-contaminated soil by low temperature indirect thermal desorption: Removal behaviors of contaminants, physicochemical properties change and microbial community recolonization in soils. Environ. Pollut. 287, 117599. https://doi.org/10.1016/j.envpol.2021.117599

Sarshar, S., Gharali, K., Saffaripour, M., Nathwani, J., Dusseault, M.B., 2024. Multi-objective optimization and long-time simulation of a multi-borehole ground heat exchanger system. Geotherm. Energy 12, 31. https://doi.org/10.1186/s40517-024-00310-9

Sathish, T., Sivakumar, D.B., Sivasankar, G.A., Thilagham, K.T., Kaliappan, S., Saravanan, R., Ubaidullah, M., Tamboli, M.S., Gupta, M., 2024. Building heating by solar parabolic through collector with metallic fined PCM for net zero energy/emission buildings. Case Stud. Therm. Eng. 53, 103862. https://doi.org/10.1016/j.csite.2023.103862

Shepard, F.P., 1954. Nomenclature based on sand-silt-clay ratios. J. Sediment. Res. 24, 151–158. https://doi.org/10.1306/D4269774-2B26-11D7-8648000102C1865D

Shokrnia, M., Cagnoli, M., Grena, R., D'Angelo, A., Lanchi, M., Zanino, R., 2024. Comparative Techno-Economic Analysis of Parabolic Trough and Linear Fresnel Collectors with Evacuated and Non-Evacuated Receiver Tubes in Different Geographical Regions. Processes 12, 2376. https://doi.org/10.3390/pr12112376

Sierra, M.J., Millán, R., López, F.A., Alguacil, F.J., Cañadas, I., 2016. Sustainable remediation of mercury contaminated soils by thermal desorption. Environ. Sci. Pollut. Res. 23, 4898–4907. https://doi.org/10.1007/s11356-015-5688-8

Singh, P., Vitone, C., Baudet, B.A., Cotecchia, F., Notarnicola, M., Plötze, M., Puzrin, A.M., Goli, V.S.N.S., Mali, M., Petti, R., Sollecito, F., Todaro, F., Muththalib, A., Mohammad, A., Bokade, M.S., Singh, D.N., 2025. Characterisation, remediation and valorisation of contaminated sediments: a critical review. Environ. Geotech. 12, 60–75. https://doi.org/10.1680/jenge.22.00201

Singh, R.K., Chandra, P., 2023. Parabolic trough solar collector: A review on geometrical interpretation, mathematical model, and thermal performance augmentation. Eng. Res. Express 5, 012003. https://doi.org/10.1088/2631-8695/acc00a

Song, Y.H., Kim, G.Y., Kim, D.Y., Hwang, Y.W., 2024. Life Cycle Assessment of Crude Oil-Contaminated Soil Treated by Low-Temperature Thermal Desorption and Its Beneficial Reuse for Soil Amendment. Sustainability 16, 10900. https://doi.org/10.3390/su162410900

Soomro, M., Mengal, A., Shafiq, Q., Ur Rehman, S., Soomro, S., Harijan, K., 2019. Performance Improvement and Energy Cost Reduction under Different Scenarios for a Parabolic Trough Solar Power Plant in the Middle-East Region. Processes 7, 429. https://doi.org/10.3390/pr7070429

Sun, X., Zhao, L., Hai, J., Liang, X., Chen, D., Liu, J., Kang, P., 2024. Mechanisms and extended kinetic model of thermal desorption in organic-contaminated soil. J. Environ. Manage. 361, 121169. https://doi.org/10.1016/j.jenvman.2024.121169

Thuillier, G., Zhu, P., Snow, M., Zhang, P., Ye, X., 2022. Characteristics of solar-irradiance spectra from measurements, modeling, and theoretical approach. Light Sci. Appl. 11, 79. https://doi.org/10.1038/s41377-022-00750-7

Tinti, F., Tassinari, P., Rapti, D., Benni, S., 2023. Development of a Pilot Borehole Storage System of Solar Thermal Energy: Modeling, Design, and Installation. Sustain. Switz. 15. https://doi.org/10.3390/su15097432

US EPA, O. of S.R., Innovation, T., 2022. Thermal Desorption Technology Resource Guide.

US-EPA, 2025. Superfund Remedy Report -18th edition.

Vanaga, R., Narbuts, J., Freimanis, R., Zundāns, Z., Blumberga, A., 2023. Performance Assessment of Two Different Phase Change Materials for Thermal Energy Storage in Building Envelopes. Energies 16, 5236. https://doi.org/10.3390/en16135236

Velraj, R., 2016. Sensible heat storage for solar heating and cooling systems, in: Advances in Solar Heating and Cooling. Elsevier, pp. 399–428. https://doi.org/10.1016/B978-0-08-100301-5.00015-1

Vidonish, J.E., Zygourakis, K., Masiello, C.A., Sabadell, G., Alvarez, P.J.J., 2016. Thermal Treatment of Hydrocarbon-Impacted Soils: A Review of Technology Innovation for Sustainable Remediation. Engineering 2, 426–437. https://doi.org/10.1016/J.ENG.2016.04.005

Wang, B., Wu, A., Li, X., Ji, L., Sun, C., Shen, Z., Chen, T., Chi, Z., 2021. Progress in fundamental research on thermal desorption remediation of organic compound-contaminated soil. Waste Dispos. Sustain. Energy 3, 83–95. https://doi.org/10.1007/s42768-021-00071-2

Wang, S., Cheng, F., Shao, Z., Wu, B., Guo, S., 2023. Effects of thermal desorption on ecotoxicological characteristics of heavy petroleum-contaminated soil. Sci. Total Environ. 857, 159405. https://doi.org/10.1016/j.scitotenv.2022.159405

Welsch, M., Bentsen, S., Henning, M., 2025. Focused review of recent advances of sediment treatment technologies. Integr. Environ. Assess. Manag. vjaf046. https://doi.org/10.1093/inteam/vjaf046

Xu, H., Bi, Y., Gao, L., Ma, D., 2024. Thermodynamic Modeling and Heat-Moisture Transfer Characteristic Analysis of in Situ Thermal Desorption System for Polluted Soil. Am. J. Biochem. Biotechnol. 20, 279–291. https://doi.org/10.3844/ajbbsp.2024.279.291

Yaws C.L., 2008. Thermophysical Properties of Chemicals and Hydrocarbons. William Andrew Inc. https://doi.org/10.1016/C2013-0-12615-3

Yılmaz, İ.H., Mwesigye, A., 2018. Modeling, simulation and performance analysis of parabolic trough solar collectors: A comprehensive review. Appl. Energy 225, 135–174. https://doi.org/10.1016/j.apenergy.2018.05.014

Zecca, E., Pronti, A., Chioatto, E., 2023. Environmental policies, waste and circular convergence in the European context. Insights Reg. Dev. 5, 95–121. https://doi.org/10.9770/IRD.2023.5.3(6)

Zhang, J., Wang, S., Wang, X., Jiao, W., Zhang, M., Ma, F., 2025. A review of functions and mechanisms of clay soil conditioners and catalysts in thermal remediation compared to emerging photo-thermal catalysis. J. Environ. Sci. 147, 22–35. https://doi.org/10.1016/j.jes.2023.11.006

Zhang, X., Li, K., Yao, A., 2022. Thermal Desorption Process Simulation and Effect Prediction of Oil-Based Cuttings. ACS Omega 7, 21675–21683. https://doi.org/10.1021/acsomega.2c01597

Zhang, X., Li, L., Shi, X., Chen, S., Liang, W., Zhu, Y., Li, H., 2024. Influence of Thermal Desorption Technology on Removal Effects and Properties of PAH-Contaminated Soil Based on Engineering Experiments. Agronomy 14, 1117. https://doi.org/10.3390/agronomy14061117

Zhao, C., Dong, Yan, Feng, Y., Li, Y., Dong, Yong, 2019. Thermal desorption for remediation of contaminated soil: A review. Chemosphere 221, 841–855. https://doi.org/10.1016/j.chemosphere.2019.01.079

Zhao, Z., Ni, M., Li, X., Buekens, A., 2016. Thermal desorption for remediating PCB-contaminated soil.

Zhou, A., Huang, X., Wang, W., Jiang, P., Li, X., 2021. Thermo-Hydraulic Performance of U-Tube Borehole Heat Exchanger with Different Cross-Sections. Sustainability 13, 3255. https://doi.org/10.3390/su13063255

Zivdar, Z., Heidarzadeh, N., Asadollahfardi, G., 2019. Remediation of diesel-contaminated soil by low-temperature thermal desorption. Int. J. Environ. Sci. Technol. 16, 6113–6124. https://doi.org/10.1007/s13762-018-2020-4